# DESIGN AND SYNTHESIS OF STIMULI RESPONSIVE POLYMERIC NANOSTRUCTURES FOR DRUG DELIVERY APPLICATIONS

by

#### Abdurrahim Can EGIL

Submitted to the Graduate School of Engineering and Natural Sciences in partial fulfillment of the requirements for the degree of Master of Science

Sabancı University

June 2021

# DESIGN AND SYNTHESIS OF STIMULI RESPONSIVE POLYMERIC NANOSTRUCTURES FOR DRUG DELIVERY APPLICATIONS

APPROVED BY:		

© Abdurrahim Can Egil 2021 All Rights Reserved

# DESIGN AND SYNTHESIS OF STIMULI RESPONSIVE POLYMERIC NANOSTRUCTURES FOR DRUG DELIVERY APPLICATIONS

#### Abdurrahim Can Egil

Materials Science and Nano Engineering, Master of Science, 2021

Thesis Supervisor: Assoc. Prof. Dr. Gözde Özaydın İnce

Keywords: Nanomedicine, stimuli responsive drug delivery, nanoparticles, nanofibers, controlled drug release

#### **ABSTRACT**

In recent years, advances in nanotechnology have pioneered new fields of research in biomedical applications. Nanostructures in different sizes, shapes, and surface charges have provided various advantages in controlled and targeted drug delivery systems with enhanced therapeutic efficiency. Moreover, nanostructures made from stimuli responsive materials provide more control on drug release kinetics as the stimuli they respond to, i.e temperature, pH, or concentration of a biomolecule, are commonly altered in targeted areas. This thesis focuses on design and synthesis of stimuli-responsive polymeric nanostructures for drug delivery applications. In the scope of this thesis, different nanostructures having stimuliresponsive properties were prepared via different synthesis techniques. Chitosan/poly (acrylic acid)/poly (N-vinyl caprolactam) core-shell nanoparticles (<100nm) were synthesized via surfactant-free batch emulsion polymerization, for pH&Temperature responsive controlled release of rose bengal. Niosome-ChitosangPNVCL composite nanoparticles (~80nm) were prepared via thin-film hydration method and polymeric coating for encapsulation of both a hydrophilic drug, rose bengal, and a hydrophobic drug, curcumin. Here, pH and temperatureresponsive drug release of these two therapeutic agents were enabled by the grafted polymer. Self-assembly albumin nanoparticles(<100nm) were synthesized via reducing agent-assisted desolvation method and glutathione responsive curcumin release was achieved thanks to the presence of intermolecular disulfide bonds at the structure. Finally, nanoparticles associated with electrospun drug delivery patches were prepared using rose bengal loaded chitosan nanoparticles(~50nm) synthesized via ionic gelation method and curcumin loaded poly(εcaprolactone) PCL nanofibers(<200nm) via electrospinning technique. Deposition of the nanoparticles onto the nanofibers was achieved via spray drying technique using a commercial airbrush. This study can pave the way for a facile fabrication route for dual drug-loaded implantable drug delivery patches and combining the advantages of nanoparticles and nanofibers in a single structure. All nanostructures fabricated have homogenous size dispersions and great encapsulation efficiencies (<80%). Drug loading and release studies about all these nanostructures were followed by using UV-Vis spectroscopy. Besides, release kinetic analyses were performed in order to compare our experimental release profiles with the current drug release kinetic models. These studies confirmed that these smart nanostructures have the potential to display triggered release profiles for a specific stimulus.

#### İLAÇ TAŞINIM SİSTEMLERİNDE KULLANILMAK ÜZERE UYARIYA DUYARLI POLİMERİK NANOYAPILARIN TASARIMI VE ÜRETİMİ

#### Abdurrahim Can Egil

Malzeme Bilimi ve Nano Mühendislik, Yüksek Lisans Tezi, 2021

Tez Danışmanı: Doç. Dr. Gözde Özaydın İnce

Anahtar kelimeler: Nanotıp, uyarıya duyarlı ilaç taşınımı, nanopartiküller, nanolifler, kontrollü ilaç salımı

### ÖZET

Son yıllarda nanoteknolojideki gelişmeler biyomedikal uygulamalarda yeni araştırma alanlarına öncülük etmiştir. Nanoyapılar, ilaç moleküllerinin belirli bir alana taşınımı ve kontrollü salımı için ilaç taşıyıcı sistemler olarak tercih edilir ve böylece yüksek terapötik verimlilik elde edilir. Ayrıca uyarıya duyarlı malzemelerden yapılan nanoyapılar, farklı ilaç salım profilleri gösterebilmektedir. Bu durum ilaç salım kinetiği üzerinde daha fazla kontrole olanak tanır. Bu tez, ilaç taşıma uygulamaları için uyarana duyarlı polimerik nano yapıların tasarımı ve sentezi üzerine odaklanmaktadır. Bu tez kapsamında, farklı sentez teknikleri ile birtakım uyaranlara tepki verme özelliklerine sahip farklı nanoyapılar hazırlanmıştır. Kitosan/Poli(akrilik asit)/Poli(n-vinil kaprolaktam) çekirdek kabuk nanoparçacıkları, pH ve sıcaklık duyarlı ilaç salımı elde etmek için yüzey aktif madde içermeyen emülsiyon polimerizasyonu yoluyla sentezlendi. Niyozom-KitosangPNVCL kompozit nanopartiküller, hem hidrofilik bir ilacın hem de hidrofobik bir ilacın kapsüllenmesi için ince film hidrasyon yöntemi ve polimerik kaplama yoluyla hazırlandı. Burada, aşılanmış polimer tarafından bu iki terapötik ilacın pH ve sıcaklığa duyarlı salımı sağlanmıştır. Albümin nanoparçacıkları, indirgeyici madde destekli desolvasyon yöntemiyle sentezlendi. Yapıda moleküller arası disülfid bağlarının varlığı sayesinde glutatyona duyarlı ilaç salınımı sağlandı. Son olarak, nanopartikül/nanofiber yapılı ilaç dağıtım yamaları, iyonik jelleşme yöntemi ile sentezlenen kitosan nanopartikülleri ve elektrospinning tekniği ile elde edilmiş PCL nanofiberleri kullanılarak hazırlandı. Nanopartiküllerin nanofiberler üzerinde biriktirilmesi, ticari bir airbrush kullanılarak püskürtmeli kurutma tekniği ile sağlandı. Bu çalışma, iki ilaç yüklü implante edilebilir ilaç dağıtım yamaları için kolay bir üretim yolunun önünü açabilir ve nanopartiküllerin ve nanofiberlerin avantajlarını tek bir yapıda bir araya getirebilir. Bu nanoyapılarla ilgili tüm ilaç yükleme ve salım çalışmaları UV-Vis spektroskopisi kullanılarak takip edilmiştir. Ayrıca deneysel salım profillerimizi mevcut ilaç salım kinetik modelleri ile karşılaştırmak için salım kinetik analizi yapılmıştır. Bu çalışmalarla, bu akıllı nanoyapıların belirli bir uyaran için tetiklenmiş salım profillerini gösterme potansiyeline sahip olduğu sonucuna varıldı.

#### **ACKNOWLEDGEMENTS**

I would like to express my sincere gratitude to my advisor Assoc. Prof. Dr. Gözde INCE for her continuous support of my MSc study and related research, for her patience, motivation, and immense knowledge. Her guidance helped me in all the time of research and writing of this thesis.

I must thank the faculty members of department of Materials Science and Nanoengineering for their valuable and educative lectures throughout my MSc. which help me shape my profession in materials science. I thank to Prof. Dr. Mehmet Ali GULGUN, Prof. Dr. İbrahim Burç MISIRLIOGLU, and Daniel Lee CALVEY for their guidance.

I would like to express my deepest thanks to my friends Milad TORABFAM, Dr. Adnan TASDEMIR and Melike BARAK for their limitless support and friendships. I learned so many useful things from them and they supported me as true friends. Without them, I am sure that I would not survive.

I am also grateful to Egemen ACAR, Omid MORADI, Tuğçe Akkas MORADI, Ece OZDEMIR, Sepideh SHEMSHAD and Faruk CAN for being the best teammates.

I feel very lucky to know my previous lab mates Burak OZDEMIR and Bahar GOK. They will be my friend to the end of my life for making life bearable and enjoyable. Also, I want to thank to my friends from Y.T.U, Abuzer Alp YETISGIN and Hale KESIM for their friendship and support. Besides, I would like to delivery my thanks to Monireh Esmaeili Rad for her collaboration and friendship in Chapter 4.

I have to deliver my regards to our lab specialist Mrs. Nursel KARAKAYA whose advice and kind supervision have always been with us in characterization labs. Without her, we would not be able to gain experience in characterization instruments in Sabanci University.

Mrs. Sibel PURÇUKLU is the most supportive and kind person I could meet in our university. She helped us more than anyone. I sincerely appreciate her support.

I would like to thank my thesis jury committee members, Assoc Prof. Dr. Ali ZARRABI and Assoc.Prof. Dr. Yasemin Budama KILINC for their time and guidance to review my thesis and comment which would help me on a better draft of my thesis.

Thanks to all my friends in MAT grads and undergrads.

I would like to express my special thanks to Elif Şevval TEMUCIN. I am very fortunate that she is in my life.

Lastly, I want to thank my family all their support they could give to me.

## **TABLE OF CONTENTS**

ABSTR.	ACT	· · · · · · · · · · · · · · · · · · ·	iii
ÖZET	•••••		V
ACKNC	OWL	EDGEMENTS	vii
TABLE	OF	CONTENTS	ix
LIST O	F FIG	GURES	xii
LIST OI	F TA	BLES	XV
LIST OI	F SY	MBOLS AND ABBREVIATIONS	xvi
Chapter	1:	INTRODUCTION	1
1.1	Dru	ng Delivery Systems	1
1.2	Rel	ease Kinetic Models	4
1.2.	1	Zero Order Kinetic Model	5
1.2.	2	First Order Kinetic Model	5
1.2.	3	Hixson-Crowell Kinetic Model	5
1.2.	4	Higuchi Kinetic Model	5
1.2.	5	Korsmeyer-Peppas Kinetic Model	6
1.3	Pol	ymeric Nanoparticles and Nanofibers	7
Chapter	2:	EXPERIMENTAL PROCEDURE	12
2.1	Naı	noparticle Synthesis Methods	12
2.2	Ele	ctrospinning	13
Chapter	3:	TEMPERATURE AND pH DUAL RESPONSIVE NANOPARTICLES AS	S
POTEN'	TIA	L COLON SPECIFIC DRUG DELIVERY SYSTEMS	19
3.1	Intr	oduction	19
3.2	Ma	terials and Methods	21
3.2.	1	Materials	21

3	.2.2	Methods	21
3.3	F	Results and Discussion	23
3	.3.1	Characterization of the CS/PAA/PNVCL Nanoparticles	23
3	.3.2	Drug Release Profile and Kinetic Analysis	31
3.4	(	Conclusion	34
Chapt	ter 4	CO-DELIVERY OF HYDROPHILIC AND HYDROPHOBIC DRUGS BY	
DUA]	L RE	SPONSIVE NIOSOME/POLYMER NANOCARRIERS	35
4.1	I	ntroduction	35
4.2	N	Materials And Methods	36
4	.2.1	Materials	36
4	.2.2	Methods	36
4.3	F	Results and Discussion	38
4	.3.1	Characterization of the Niosomes	38
4	.3.2	Drug Release Profile and Kinetic Analysis	44
4.4	(	Conclusion	48
Chapt	ter 5	SELF ASSEMBLY ALBUMIN NANOPARTICLES FOR GLUTATHIONE	3
RESP	ONS	SIVE RELEASE OF CURCUMIN	49
5.1	I	ntroduction	49
5.2	N	Materials and Methods	50
5	.2.1	Materials	50
5	.2.2	Methods	51
5.3	F	Results and Discussion	52
5	.3.1	Characterization of the Albumin Nanoparticles	52
5	.3.2	Drug Release Studies and Kinetic Analysis	57
5 4	(	Conclusion	59

Chapter 6:	A FACILE ROUTE FOR NANOPARTICLES-ASSOCIATED	
ELECTROS	SPUN PATCHES AS IMPLANTABLE DRUG DELIVERY SYSTEMS	60
6.1 Int	roduction	60
6.2 Ma	terials and Methods	62
6.2.1	Materials	62
6.2.2 Methods		62
6.3 Res	sults and Discussion	64
6.3.1	Characterization of the Chitosan Nanoparticles and PCL Nanofibers	64
6.3.2	Drug Release Studies and Kinetic Analysis	71
6.4 Co	nclusion	74
Chapter 7:	CONCLUSION	75
REFERENC	CES	76

# LIST OF FIGURES

Figure 1-1: A Timeline of FDA Approved Current Nanomedicine Products developed by
Nanotechnology. Market Name, Composition and Year [6]1
Figure 1-2: An Illustration of Different Types of Stimulants for Triggered Drug Release3
Figure 2-1: Spectrophotometric Analysis of Rose Bengal
Figure 2-2 : Spectrophotometric Analysis of Curcumin
Figure 2-3: Spectrophotometric Analysis of Rose Bengal and Curcumin Mixture15
Figure 2-4: Spectrophotometric Analysis of Rose Bengal, Curcumin, and the Mixture in One
Spectrum
Figure 2-5 : Standard Curve of Rose Bengal
Figure 2-6 : Standard Curve of Curcumin
Figure 2-7: Standard Curve of Curcumin in the Presence of Rose Bengal
Figure 2-8 : Standard Curve of Rose Bengal in the Presence of Curcumin
Figure 3-1: Average Size of Blank Nanoparticles at Different pH Levels24
Figure 3-2: Zeta Potential Values of Blank Nanoparticles at Different pH Levels25
Figure 3-3: Average Size of Blank Nanoparticles at Different Temperature Levels (pH=4.5)
Figure 3-4: DLS Size Analysis of RB Loaded Nanoparticles at Room Temperature26
Figure 3-5 : DLS Size Analysis of RB Loaded Nanoparticles at 45°C
Figure 3-6: Zeta Potential Analysis of Loaded Nanoparticles(pH=4.5)27
Figure 3-7: SEM (A, B) and TEM Image(C) of Blank Nanoparticles
Figure 3-8: TEM (A, B) and SEM(C) Images of Loaded Nanoparticles29
Figure 3-9: FTIR Spectrum of Rose Bengal, Blank Nanoparticles and Rose Bengal Loaded
Nanoparticles
Figure 3-10: Release Profiles of Nanoparticles in different temperature and pH levels32
Figure 3-11: The photograph of drug release capsules at pH=7.4(left) and pH=5.0 (right)
after 72h at 40°C
Figure 4-1: TEM images of Bare Niosomes
Figure 4-2: TEM images of RB-CUR Loaded Niosomes, at High Magnifications(A,B) and
Lower Magnifications(C,D)41
Figure 4-4: SEM images of RB-CUR Loaded Niosomes
Figure 4-5 : FTIR Spectrum of Grafted Polymer 42

Figure 4-6: FTIR Spectrum of Bare Niosome, CUR Niosome and RB/CUR
Niosome/Polymer
Figure 4-7: Release profile of RB(A) and CUR(B) at different pH levels and temperatures45
Figure 5-1 : DLS Average Size Analysis of Bare Albumin Nanoparticles53
Figure 5-2: DLS Average Size Analysis of Loaded Albumin Nanoparticles53
Figure 5-3: Zeta Potential Distribution of Bare Albumin Nanoparticles54
Figure 5-4 : Zeta Potential Distribution of Loaded Albumin Nanoparticles54
Figure 5-5 : SEM Images of Bare Albumin Nanoparticles
Figure 5-6 : SEM Images of Curcumin Loaded Albumin Nanoparticles
Figure 5-7: FTIR Spectrum of Bare Albumin Nanoparticles, Curcumin Loaded Albumin
Nanoparticles and Curcumin
Figure 5-8: Drug Release Profiles of Curcumin in Physiological Environment and GSH
environment
Figure 6-1: Experimental Processes for the Fabrication of Nanoparticles Associated
Electrospun Patches
Figure 6-2 : DLS Average Size Analysis of Bare Chitosan Nanoparticles (A) and RB Loaded
Chitosan Nanoparticles (B)65
Figure 6-3: Zeta Potential Analysis of Bare Chitosan Nanoparticles (C) and Loaded Chitosan
Nanoparticles (D)66
Figure 6-4 : SEM Images of Bare PCL Nanofibers
Figure 6-5 : SEM Images of Curcumin Loaded PCL Nanofibers
Figure 6-6 : SEM Image of Rose Bengal Loaded Chitosan Nanoparticles
Figure 6-7: SEM Images of Curcumin Loaded PCL Nanofibers Decorated with RB loaded
Chitosan Nanoparticles
Figure 6-8: FTIR Spectrum of Curcumin, PCL Nanofibers and Curcumin Loaded PCL
Nanofibers70
Figure 6-9: FTIR spectrum of Rose Bengal, Chitosan Nanoparticles and Rose Bengal Loaded
Chitosan Nanoparticles
Figure 6-10 : Drug Release Profile of Curcumin Loaded PCL Nanofibers71
Figure 6-11: Drug Release Profiles of CUR Loaded PCL Nanofibers with RB Loaded
Chitosan Nanoparticles72

Figure 6-12 : Curve Fitting Analysis for Curcumin Release from CUR-PCL (R <sup>2</sup> =0.99,	
n=0.32)	73
Figure 6-13 : Curve Fitting Analysis for Curcumin Release from CUR-PCL/RB-CS (R <sup>2</sup> =0	).99
n=0.36)	73
Figure 6-14 : Curve Fitting Analysis for Rose Bengal Release from CUR-PCL/RB-CS	
(R <sup>2</sup> =0.99, n=0.42)	74

# LIST OF TABLES

Table 1-1: Explanation of Release Exponent in Korsmeyer Peppas Model	6
Table 3-1: Kinetic Model Analysis of the drug release profiles	.33
Table 4-1: DLS and Zeta Potential Analysis of Blank and Cur Loaded Niosomes	.39
Table 4-2: Kinetic Model Analysis of the drug release profiles.	.47
Table 5-1: Table of Release Kinetic Analysis of CUR Loaded Albumin Nanoparticles	.59

#### LIST OF SYMBOLS AND ABBREVIATIONS

RB Rose Bengal

CUR Curcumin

CS Chitosan

TPP Tripolyphosphate

PCL Poly(e-caprolactone)

PLGA Poly (lactic-co-glycolic acid)

NVCL N vinylcaprolactam

PNVCL Poly N vinylcaprolactam

KPS Potassium per sulfate

MBA N, N'-Methylenebisacrylamide

AA Acetic Acid

BSA Bovine serum albumin

HSA Human Serum Albumin

PBS Phosphate Buffered Saline

PEG Polyethylene glycol

GSH Glutathione

LCST Lower Critical Solution Temperature

UCST Upper Critical Solution Temperature

#### **Chapter 1: INTRODUCTION**

#### 1.1 Drug Delivery Systems

In recent years, studies have shown that the traditional approaches used for delivering the drugs to specific areas of the body result in some adverse effects such as poor therapeutic and biological effectiveness and lack of selectivity and stability of the active agents, in the treatments of diseases [1]. In order to avoid these problems, it is urgent to find advanced solutions to reduce the dosage, provide sustained release, remove the side and/or toxic effects of some drugs such as chemotherapeutics, and deliver the active substances to the target sites in body [2][3]. Drug delivery systems (DDSs) were created as a solution for these problems. These systems require interdisciplinary work including pharmacy, materials science, nanotechnology, and biology [4]. DDSs have been gained much more attention in the pharmaceutical and medical industry. The milestone for DDSs was the application of liposomes as nanocarriers for the controlled release of doxorubicin (DOX) [5]. These liposomes provided enhanced therapeutic efficiency for doxorubicin. Although this system has several advantages, it was lacking targeting molecules. Thus, this drug delivery system can be considered the first DDS based on a passive targeting approach. Following the Doxil, a series of nano formulation was approved by U.S. Food and Drug Administration (FDA) as nanomedicine products. These are presented in Figure 1-1.

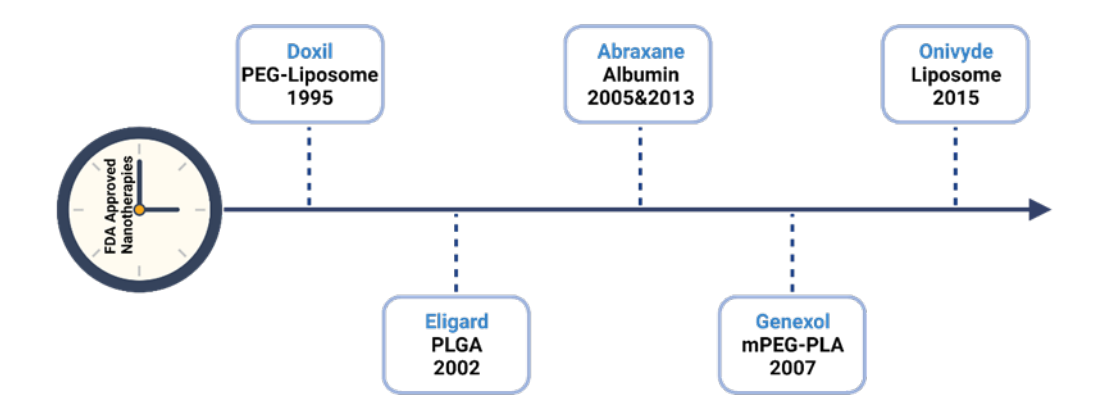


**Figure 1-1:** A Timeline of FDA Approved Current Nanomedicine Products developed by Nanotechnology. Market Name, Composition and Year [6]

The usage of drug delivery systems provides several advantages such as increased the circulation time of the drugs, accumulation of the nanostructures in tumor tissue because of enhanced retention and permeability (EPR) effect and overcoming specific barriers like a blood-brain barrier (BBB).

Polymers are widely used in drug delivery system applications for designing suitable carriers in the form of nanoparticles, and nanofibers for the drug molecules [7]. Several types of drugs can be encapsulated/entrapped with these polymeric structures. Besides, surface modifications through the functional groups on the polymer chains enable the targeting of the carriers to the intended area. For instance, specific biological compounds such as antibodies or peptides can be attached to the nanostructures for this purpose [8] [9].

#### Stimuli Responsive Polymers for Drug Delivery Applications

Stimuli responsive polymers are the polymers that change their physical or chemical behavior as a response to an external stimulus such as pH, temperature, or the presence of a biochemical agents [10]. This situation enabled for them to be used in different applications including drug delivery systems in the field of nanomedicine. Here, environmental sensitive drug delivery nanoplatforms become prominent since the differences such as different pH and temperature levels at the different sites in the body provide new therapeutic strategies for the scientists. Stimuli-responsive drug delivery systems can be examined in two different classes based on the source of the stimulus, and these are called externally regulated systems and internally regulated systems [11]. In externally regulated systems, the response of the drug delivery system is triggered by an external stimulus such as a magnetic field. On the other hand, in internally regulated systems the drug delivery system is exposed to a stimulus in the body such as pH change, the presence of a specific enzyme, or a biomolecule like glutathione. These internal and external stimuli are presented in Figure 1-2.

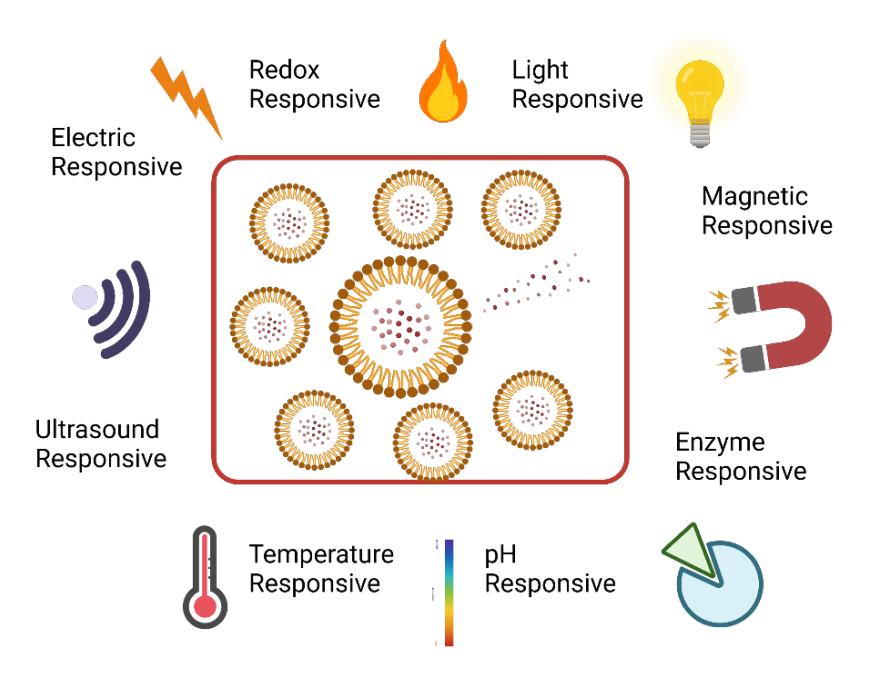


Figure 1-2: An Illustration of Different Types of Stimulants for Triggered Drug Release

In pH responsive polymers, the change in structure is based on the ionizable groups on the polymer backbone. Swelling or deswelling of the polymer is occurred due to the protonation or deprotonation of these groups at different pH levels [12]. These polymers can be examined in two different classes, polyacids and polybases. In polyacids such as polyacrylic acid, the polymer will swell when the pH level is above the pKa value of the polymer. On the other hand, the polymer will collapse when the pH level is below its pKa value. On the contrary, in polybases such as chitosan, the polymer will swell when the pH level is below its pKa and collapse when the environment where the pH level is above its pKa value. In the case of drug delivery systems, this alteration in the structure results in different release profiles in different pH levels such as faster drug release at acidic pH level and prolonged drug release in alkali environment or vice versa [13]. In general, polyacids are used in colon targeted drug delivery applications via oral administration route since the pH level in the colon environment is slightly alkali and the administration route is quite acidic [14]. This results in minimum drug release during the path where the polymer is shrunk phase and faster drug release in alkali environment. On the other hand, polybases are preferred to obtain faster drug release in the acidic environment by a proper administration route such as subcutaneous or implantable patches [15]. It is known that tumor site is slightly acidic than healthy areas and faster drug release at tumor site can be considered promising strategy in therapeutic applications.

In temperature responsive polymers, the polymeric structure undergoes a hydrophilic to hydrophobic transition through its temperature sensitive functional moieties. They have characteristic temperature levels called lower critical solution temperature (LCST) level and upper critical solution temperature (UCST) level. Polymers that are insoluble with increasing the temperature have LCST level, whereas polymers becoming soluble with increasing the temperature have UCST level [16]. PNIPAM is the most popular temperature responsive polymer [17]. Although it has been commonly used and well investigated, it is known that it poses toxicity risk because of the formation of small amide derivatives in an acidic environment [18]. PNVCL can be considered more safe alternative temperature responsive polymers. In drug delivery applications, these type of temperature sensitive polymers are commonly used alone or combined with other polymers because the tumor site has higher temperature level than healthy tissue and intended release profile would be achieved utilizing these conformational changes occurred in the temperature sensitive polymers.

The presence of an enzyme or change in concentration of a biomolecule in the targeted area can also be useful as an internal stimulus. Here, the presence of an enzyme that can digest the polymer used for the nanocarrier will lead to a burst release of the loaded drug molecules. For instance, some colonic enzymes that can disrupt the glycosidic linkage of the chitosan structure make chitosan-based drug delivery systems advantageous from this point of view [19]. On the other hand, concentration difference of glutathione (GSH) between cellular cytosol and extracellular sections brings with utilizing these reducing agent concentration difference as a drug delivery strategy [20]. For instance, materials that have disulfide bonds in their composition are susceptible to redox reactions. This can be useful since it results in faster release of the drug molecules in the presence of reducing agent.

#### 1.2 Release Kinetic Models

In drug delivery systems, the release profile of the drug from the carrier matrix has great importance in order to check the response of the carrier in the environment and analyze the drug release mechanisms that govern the system. For this purpose, the empirical release profiles obtained from the drug release tests, are compared with the current mathematical models through curve fitting analysis, and the correlation coefficients are analyzed [21]. The best suitable model is used to interpret the release kinetics. Although there are numerous models in the literature, Zero Order Kinetic Model, First Order Kinetic Model, Hixson-Crowell Kinetic

Model, Higuchi Kinetic Model and Korsmeyer-Peppas Kinetic Model can be considered as main ones.

#### 1.2.1 Zero Order Kinetic Model

In Zero Order Kinetic Model, drug release from the carrier matrix is occurred at a constant rate. The equation of this model is the following:

$$W_0 - W_t = Kt$$

where the t is the time (hour) and  $W_0$  and  $W_t$  are the initial drug amount (mg) and the drug amount at time t (mg), respectively. Besides, K is the constant. These types of drug release profiles are mostly applicable for the coated tablets containing low soluble drugs [22].

#### 1.2.2 First Order Kinetic Model

In this model, the drug release rate from the carrier matrix is concentration dependent and the equation of this model includes a simple ratio of the concentration over time. In general, a porous carrier matrix loaded with water soluble drugs can follow this profile [23].

$$\frac{dC}{dt} = K(C_x - C)$$

In this equation  $C_x$  is the equilibrium solubility(mg/ml), K is the constant and C is the solute concentration(mg/ml) in time t (hour).

#### 1.2.3 Hixson-Crowell Kinetic Model

In this model, it is assumed that the drug release is related to dissolution. Drug transportation is independent of diffusion. Here, erosion of the carrier matrix without any change in initial geometry is the driving force for the drug release [22]. The equation of Hixson Crowell Kinetic Model is

$$W_0^{1/3} - W_t^{1/3} = K_S t$$

where, the initial drug amount (mg), remaining drug amount(mg) at time t(hour) are expressed as  $W_0$  and  $W_t$  and the  $K_s$  is the diffusion constant.

#### 1.2.4 Higuchi Kinetic Model

Higuchi Kinetic Model states that dissolution and diffusion are both important in drug transportation from the carrier matrix. However, this model is valid with the following assumptions: (I) perfect sink conditions, (II) unidirectional release, (III) negligible swelling/dissolution of the matrix, (IV) larger thickness of the dosage form than the size of the drug

molecules, and (V) higher initial drug concentration in the matrix than the solubility of the drug molecules [24].

The equation of this model is,

$$Q = \sqrt{D(2C - C_s)C_s t}$$

Here, Q is the amount of released drug in time t (hour). D is the diffusivity( $m^2/s$ ) of the drug. C and  $C_s$  are the symbols of that the initial concentration(mg/ml) and the drug solubility(mg/ml) in the carrier matrix, respectively.

This model is applicable for hydrophilic and hydrophobic drugs incorporated with a carrier matrix.

#### 1.2.5 Korsmeyer-Peppas Kinetic Model

This model analyzes the release mechanism in terms of Fick's diffusion law. According to the release exponent, it is possible to understand that if drug transportation is governed by Fickian diffusion or non-Fickian diffusion mechanisms. This model should be applied for the analysis on a maximum of 60% of the drug release. Besides, the geometry of the carrier matrix is also important for the interpretation of the data. The importance of the release exponent and geometry can be seen in Table 1-1. The main equation below includes  $f_t$  as a fraction of drug released at time t, k is the release constant and n is the exponential value of the release [24].

$$f_t = at^n$$

Table 1-1: Explanation of Release Exponent in Korsmeyer Peppas Model

Release Exponent (n)		Release Mechanism
Cylindirical	Spherical	Drug Transportation
Shape	Shape	Principle
0.45	0.43	Fickian diffusion
0.45 <n<0.89< td=""><td>0.43<n<0.85< td=""><td>Anomalous transport</td></n<0.85<></td></n<0.89<>	0.43 <n<0.85< td=""><td>Anomalous transport</td></n<0.85<>	Anomalous transport
0.89	0.85	Case-II transport
0.89 <n< td=""><td>0.85<n< td=""><td>Super Case-II transport</td></n<></td></n<>	0.85 <n< td=""><td>Super Case-II transport</td></n<>	Super Case-II transport

#### 1.3 Polymeric Nanoparticles and Nanofibers

Nanoparticles and nanofibers are the commonly used nanostructures as carriers for specific drugs and active agents. Their biocompatible nature, high drug loading capabilities and ability to release the drug molecules in a sustained manner make them advantageous tools in drug delivery systems. Furthermore, their fabrication methods have the potentials for large scale production for the industrial needs [25][26]. Polymeric nanoparticles can be prepared using several synthesis methods. Among them, ionic gelation, nanoprecipitation, emulsification, thin film hydration, desolvation and batch emulsion polymerization are commonly preferred ones [27][28].

Chitosan is one of the most abundant polymers in the nature and ionic gelation method is utilized to prepare its nanoparticle form. Here, the polycationic nature of the chitosan chains are ionically crosslinked with an anionic molecule called tripolyphosphate (TPP). Addition of TPP molecules into chitosan solution results in formation of chitosan nanoparticles in spherical morphology. The size, surface charge and stability of the nanoparticles can be tuned by using different mixing ratios for the polymer and the crosslinker. Besides, experimental conditions such as reaction temperature, stirring speed, and incubation time are also important in this regard.

The stimuli responsive nature of chitosan nanoparticles is one of the reasons for their wide range of applications in biomedical field. The ionizable amino groups on the polymeric backbone leads to conformational change in the structure at different pH levels (pKa=6.0). Therefore the release profile of the drug loaded chitosan nanoparticles differs at different pH levels such as faster drug release in acidic environment and minimum drug release under alkali conditions [29]. Besides, its functional groups allow several surface modifications such as conjugation of a growth factor or decorating with folic acid groups for targeting applications [30], [31]. Also, the mucoadhesive feature of chitosan is another key property for its usage in drug delivery applications. Chitosan nanoparticles can easily interact with the mucus membrane and provide sustained release of the drug molecules [32].

Polymers like poly(e-caprolactone) (PCL) and poly (lactic-co-glycolic acid) (PLGA) are also preferred for drug delivery applications. Although they are synthetic polymers, they are biocompatible. Nanoprecipitation is the most popular technique in order to obtain either PCL or PLGA nanoparticles. Here, the polymer solution in an organic solvent is mixed with an aqueous solution containing a stabilizer such as poly (vinyl alcohol) (PVA). Nanoparticles start

to precipitate as a result of solvent diffusion between the aqueous and non-aqueous phases. Emulsification techniques such as single emulsion and double emulsion are also applicable to obtain PCL or PLGA nanoparticles [33]. Here, an oil and aqueous phases were emulsified using specific equipment such as homogenizer or probe sonicator. Then this mixture is added to another phase and double emulsion is occurred. Angel et al. prepared a biodegradable and biocompatible nanocarriers using PCL nanoparticles for the delivery of a chemotherapeutic agent, carboplatin [34]. They revealed that their nanoparticles have strong potential to be used in brain drug delivery. Shu et al. on the other hand, prepared PLGA nanoparticles around 150 nm in average size, against prostate cancer [35]. They used capecitabine as a model drug and they found that the nanoparticles favor the cellular uptake of the drug molecules and cytotoxic effect was observed on cancer cells.

PLGA and PCL nanoparticles are mostly combined with Poly (ethylene glycol) (PEG) since PEG molecules provide longer circulation time and avoiding of the clearance for the nanoparticles by the immune system [36], [37]. In fact, PEG have gained great interest due to the above-mentioned properties and incorporation of PEG with drug delivery systems became an important strategy in nanomedicine [38], [39].

The desolvation method is similar to the nanoprecipitation technique. This principle is also based on the mixing of an organic phase and aqueous phase in a proper ratio. In general, Albumin nanoparticles are prepared by this technique. A proper amount of bovine serum albumin (BSA) or human serum albumin (HSA) is mixed with ethanol and albumin proteins start to aggregate. Following the incubation of this solution with an appropriate time, stabile nanoparticles are formed either by crosslinking with specific agents such as glutaraldehyde (GA) or self-assembly through intermolecular disulfide bounding. They can be administrated with various routes and several bioactive molecules with different nature, hydrophilic or hydrophobic, can be encapsulated within these nanocarriers.

Albumin nanoparticles have intensely preferred for encapsulation of drugs or active molecules [40]. Their biocompatibility and ease in surface modification on their structure can be considered important reasons for preference. Tingting et al. prepared albumin nanoparticles for brain drug delivery applications. They achieved to encapsulate two different drugs and performed surface modifications on the albumin nanoparticles using specific peptide molecules. Finally, they demonstrated the potential of their surface modified albumin nanocarriers by cell culture and animal model experiments [41].

Batch emulsion polymerization technique is preferred for the usage of the monomers to obtain a polymeric nanostructure [42][43]. In this case, a reaction mixture contains proper amounts of monomer(s), crosslinker and initiator, is exposed to nitrogen atmosphere and specific temperature. Thus, temperature-sensitive initiator can be activated in order to start the reaction through the formation of the free radicals. During the reaction, the monomers start to bind each other, and polymeric structures are obtained. Thereafter, intense dialysis and/or centrifugation are performed in order to remove the excess molecules such as initiator residues.

PNIPAM nanoparticles are commonly prepared based on this technique. The temperature responsive property of PNIPAM enable to obtain of different drug release profiles at different temperature levels. PNIPAM can be used either alone or combined with other polymeric/inorganic materials for different purposes such as dual responsive nanocarriers in the presence of a pH responsive polymer, some therapies based on hyperthermia or imaging applications [44]–[46]. However, the potential cytotoxicity risk due to the degradation of PNIPAM caused to seeking of some alternatives for the same purpose. Thus, PNVCL nanoparticles have gain great attention for drug delivery applications [47]. For instance, Adriana et al. prepared PNVCL-magnetite nanocomposite drug delivery systems for the delivery of doxorubicin. They proved the potential of their nanocarriers for nanomedicine applications thorough several characterizations and experiments [48].

The thin-film hydration method is another popular fabrication technique for the nanoparticles. Lipid based nanoparticles such as liposomes and niosomes, can be prepared via this technique [49]. Firstly, a thin film is obtained from the organic solution that contains surfactants and other molecules such as cholesterol. This film is then hydrated with water and nanovesicles are formed. The changes in the mixing ratios, concentration, and experimental conditions such as hydration time and temperature with/without sonication, affect the size, stability, and dispersity of the resulting nanoparticles. Niosomes are the self-assembly nanovesicles obtained from nonionic surfactants in an aqueous media. They are able to carry both hydrophobic drugs and hydrophilic drugs due to their structures. They have an aqueous core that is suitable for hydrophobic drugs and the lipid bilayer around the aqueous core is suitable for the encapsulation of hydrophobic drug molecules [50]. They are biocompatible and highly stable vesicles [51].

Nanofibers are also outstanding nanostructures among the drug delivery systems. The ease in their production, high drug loading capacities and ability to surface modifications through the functional groups on the polymeric backbone make them advantageous in nanomedicine applications. In drug delivery applications, they are mostly preferred as implantable drug

delivery systems for several purposes such as avoidance of the cancer recurrence after the tumor ablation and multiple drug release in a controlled manner. Liu et al. prepared poly (lactic acid) (PLA) nanofibers as local drug delivery patches for doxorubicin [52]. Their motivation was based on an easy and simple treatment of cancerous tissue by direct usage of drug loaded electrospun mats. After several in vitro and in vivo experiments, they observed a significant antitumor effect in doxorubicin loaded PLA nanofibers against liver cancer cells. However, they pointed out the necessity for the controlling of drug release from the nanofibers. For this purpose, Sayin et al. utilized initiated chemical vapor deposition(iCVD) system in order to create a thin film coating of poly(4-vinylpyridine-co-ethylene glycol dimethacrylate) p(4VP-co-EGDMA) on the surface of the PVA nanofibers [53]. They used rose bengal as a model therapeutic agent and the polymeric coating also enabled to have a pH responsive drug release profile because of the presence of poly(4VP). Furthermore, they performed kinetic analysis on their empirical release profiles and revealed that drug release from their nanofibers have great correlation with Korsmeyer Peppas Model.

It is also possible to incorporate nanoparticles with nanofibers in order to combine the advantageous properties of both nanoparticles and nanofibers. Wang et al. prepared drug loaded PCL nanofibers containing chitosan nanoparticles loaded with another drug. This approach can be considered a promising strategy for combinational therapy applications [54]. Jalvandi et al. used the same approach with drug conjugated silica nanoparticles and PCL nanofibers. However, they did not include a second drug in the system. They used the nanofibers as a second control on the release of the drug from the nanoparticles [55]. Long et al. prepared PCL-co-PEG nanofibers containing albumin nanoparticles for the co-delivery of dexamethasone (DEX) and bone morphogenetic protein-2 (BMP-2) [56]. Here, BMP-2 was encapsulated within albumin nanoparticles and nanofibers were used for the delivery of DEX molecules. The incorporation of the loaded nanoparticles with the nanofibers was achieved by simple addition of nanoparticles into the polymer solution which will be used in the electrospinning process. Their advanced nanoplatform acted as both a scaffold and a drug delivery system.

All these efforts indicate a strong need for the development of smart drug delivery systems for nanomedicine applications. This thesis focuses on the preparation and characterization of stimuli-responsive nanostructures as drug delivery systems. Several synthesis techniques and characterization methods were used for the analysis of the potential of these nanostructures as drug delivery platforms. Temperature, pH, and redox responsiveness were chosen as

environmental stimuli that can trigger the drug release. Rose bengal and curcumin were preferred as a hydrophilic model drug and a hydrophobic model drug, respectively. In Chapter 3, we analyzed the potential of the pH and temperature-responsive core-shell nanoparticles for colon-specific drug delivery application. Chitosan/Poly (acrylic acid)/Poly (N-vinyl caprolactam) core-shell nanoparticles were synthesized via surfactant-free batch emulsion polymerization technique and rose bengal was used as a model hydrophilic drug. Chapter 4 is about the fabrication of pH and temperature-responsive nanostructures for both a hydrophilic drug and a hydrophobic drug. Temperature and pH-responsive drug release of two different therapeutic agents were enabled by the grafted polymer, chitosangPNVCL. Curcumin was used as a model hydrophobic drug and encapsulated with niosomes. Following the synthesis of curcumin-loaded niosomes, a polymeric coating process was performed with chitosangPNVCL solution containing rose bengal. In this way, the ultimate composite nanoparticles were obtained as niosome-chitosangPNVCL nanoparticles loaded with 2 therapeutic agents that are curcumin and rose bengal. In Chapter 5, redox responsive nanostructures were prepared using protein-based nanoparticles and the controlled release of curcumin was investigated. Selfassembly albumin nanoparticles were synthesized via reducing agent-assisted desolvation method and glutathione, a reducing agent, responsive curcumin release was achieved thanks to the presence of intermolecular disulfide bonds at the structure. Finally, Chapter 6 is about a facile route for the fabrication of nanoparticles associated with electrospun drug delivery patches. Chitosan nanoparticles were synthesized via the ionic gelation method for the encapsulation of rose bengal. In the meantime, curcumin-loaded poly(ε-caprolactone) (PCL) nanofibers were produced via electrospinning technique. Here, deposition of the nanoparticles onto the nanofibers was achieved via spray drying technique using a commercial airbrush. This study can pave the way for a facile fabrication route for dual drug loaded implantable drug delivery patches, combining the advantages of nanoparticles and nanofibers in a single structure. Drug loading and release studies about all these nanostructures were followed by using UV-Vis spectroscopy. Besides, release kinetic analyses were performed in order to compare our experimental release profiles with the current drug release kinetic models. These studies were concluded that these smart nanostructures have the potential to display triggered release profiles for a specific stimulus and can be preferred as drug delivery systems.

## **Chapter 2: EXPERIMENTAL PROCEDURE**

Nanostructures can be prepared with numerous methods. In this thesis, several synthesis methods were performed in order to obtain nanostructures for controlled drug release applications. These are the ionic gelation method, thin-film hydration method, batch emulsion polymerization method, desolvation method, and electrospinning. On the other hand, rose bengal and curcumin were preferred as model therapeutic agents for the drug delivery systems. Following the fabrication of the nanostructures, various characterization techniques were utilized. These are dynamic light Scattering for the hydrodynamic average size of the nanoparticles, scanning electron microscopy and transmission electron microscopy for morphology analysis of the nanostructures, Fourier transform infrared spectroscopy for the chemical makeup analysis of the resulting nanostructures. Finally, UV-Vis spectroscopy was utilized for the standard curve of the model drugs for the determination of encapsulation efficiency, loading capacity, and drug release profiles. Here, the characteristic wavelengths for rose bengal and curcumin were determined as 560nm and 425nm, respectively. Here, it is obvious to see that these two molecules do not have any adverse effect on their characteristic peaks. When they are mixed and analyzed, two distinguished peaks were obtained at identical wavelengths. This allowed us to determine the amount of each drug using UV-Vis spectroscopy. The spectroscopic analyses are shown in Figure 2-1 to Figure 2-4, and the standard curves are shown in Figure 2-5 to Figure 2-8. After the determination of the main peak values, standard curves were obtained by absorbance measurements at a single wavelength for each drug. Then, these standard curves were used for the calculation of encapsulation efficiency via Equation 1 and drug release via Equation 3.

#### 2.1 Nanoparticle Synthesis Methods

The ionic gelation method was used to prepare chitosan nanoparticles. The principle of this method is based on the interaction between the polycationic nature of the chitosan structure with a polyanionic agent, TPP.

The batch emulsion polymerization method was used in preparation of chitosan/polyacrylic acid/poly (N-vinyl caprolactam) core shell nanoparticles. Here, free radical polymerization occurs using potassium persulfate as an initiator of the polymerization of acrylic acid and n-vinyl caprolactam monomers in the presence of chitosan.

The thin film hydration method was preferred for the preparation of niosomes. In this method, a thin film is obtained from the mixture of nonionic surfactants with cholesterol in an organic solvent using a rotary evaporator and this film is hydrated with water in order to allow the formation of the niosomes.

The desolvation method was the synthesis method to produce albumin nanoparticles. Briefly, an organic solvent like ethanol is dropped into the aqueous bovine serum albumin (BSA) solution in order to trigger the aggregation of the albumin proteins to form nanoparticles. Dropwise addition of the desolvating agent was preferred to obtain the nanoparticles in the homogeneous size dispersion. In this study, the BSA solution was treated with glutathione (GSH) for 1h to reduce the disulfide bonds in order to create intermolecular disulfide bonds between the albumin proteins during the aggregation. Thus, the stability of the nanoparticles was provided.

#### 2.2 Electrospinning

Electrospinning is one of the most common methods for producing nanofibers for several purposes. In the electrospinning technique, firstly the polymer solution in a volatile solvent is transferred into the syringe. Following the placing of the syringe in the pump mechanism with adjustable flow rate, the system is made ready by adjusting the distance between the collector and needle tip. The process is started by applying a voltage between 5-30 kV to the metal needle at the tip of the syringe. Here, the high voltage applied by the power source to the solution drop hanging on the tip of the syringe needle remains in a spherical form up to a certain limit value because of the forces caused by the surface tension of the solution drop. As soon as the high voltage applied to the solution drop reaches a certain limit value, the electrical forces equalize the surface tension forces and the system comes to equilibrium. In this case, the solution droplet changes its shape from spherical to conical form. This cone shape is called Taylor Cone [57].

Increasing in the high voltage applied to the solution from the metal syringe needle, the balance between the surface tensions of the cone-shaped droplet and the electrostatic forces acting on it changes in favor of electrical forces. Therefore, the conical droplet hanging on the tip of the syringe needle changes its shape again and starts moving towards the collector. Ultimately, the nanofibers emerging from the tip of the syringe needle in the form of jet begin to accumulate on the surface of the collector plate randomly with unstable twisting movements due to electrostatic repulsive forces and solvent evaporation. Then, the nanofibers formed on the collector plate surface are taken from the collector [58].

The morphology and thickness of the nanofibers are related with several parameters. These can be classified in polymer-based, solution-based and experimental system-based parameters. For instance, the molecular weight and the solubility of the polymer are polymer-based parameters. Concentration, conductivity, and viscosity of the polymer solution can be considered solution-based parameters. On the other hand, the flow rate of the polymer solution, humidity, applied voltage level, distance are the experimental based parameters that effect the fiber properties [59], [60]. In general, higher polymer concentrations and lower voltage levels lead to an increase in fiber diameter and lower flow rate with appropriate viscosity levels and higher molecular weight result in a decrease in fiber diameter. Besides, bead formation on the fibrous structure can be prevented by the increase in the molecular weight of the polymer and the viscosity.

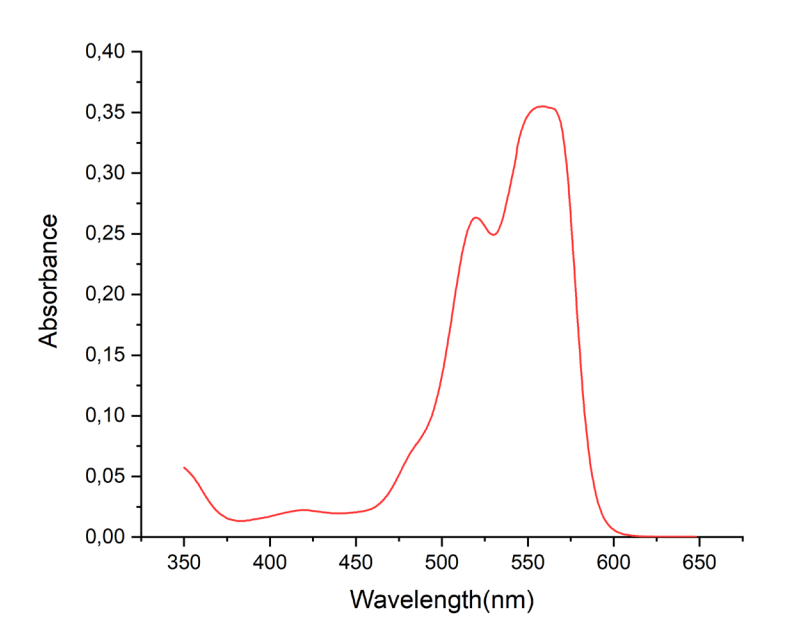


Figure 2-1: Spectrophotometric Analysis of Rose Bengal

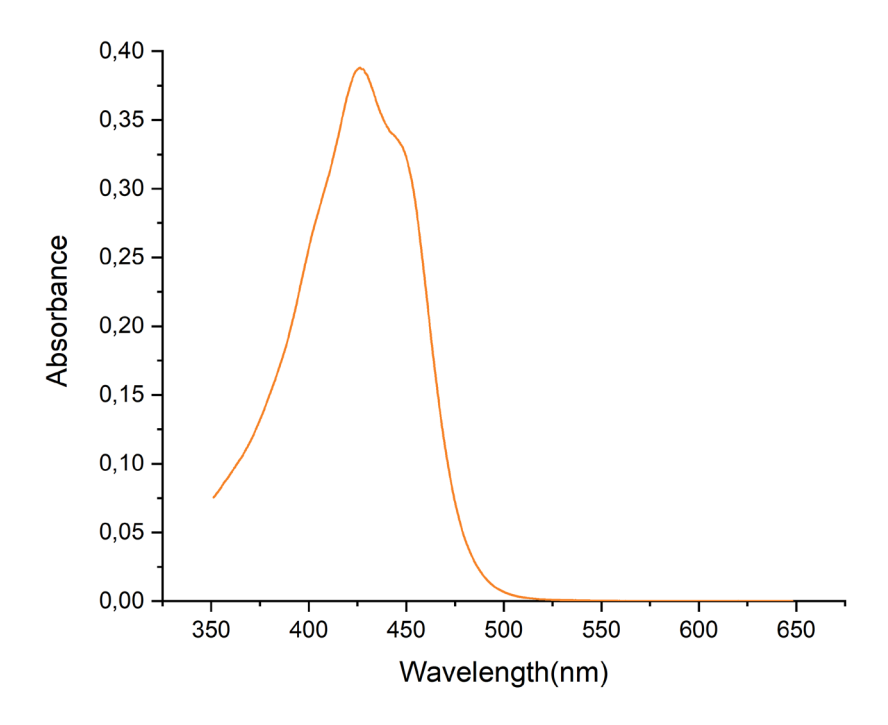


Figure 2-2: Spectrophotometric Analysis of Curcumin

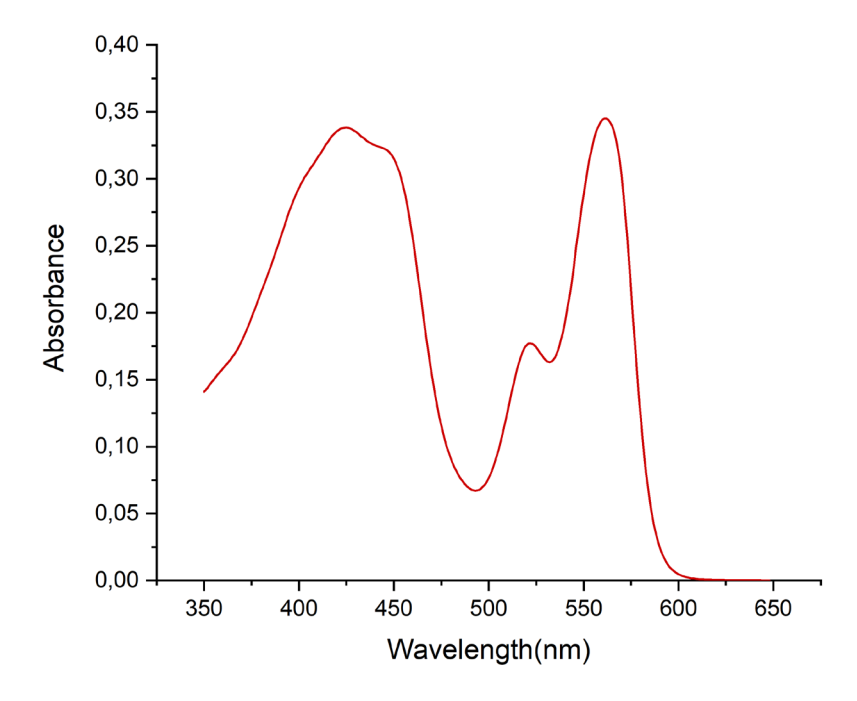
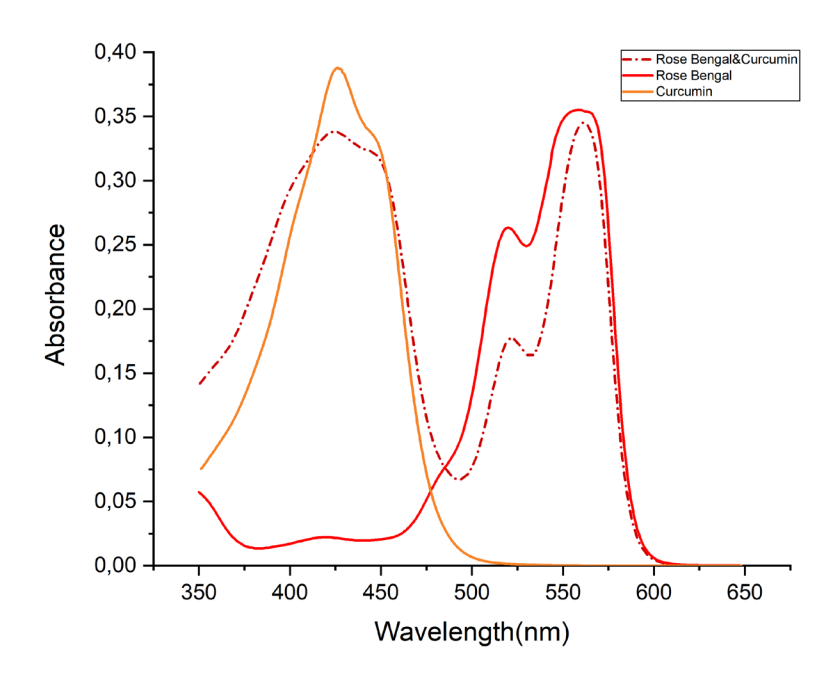


Figure 2-3: Spectrophotometric Analysis of Rose Bengal and Curcumin Mixture



**Figure 2-4 :** Spectrophotometric Analysis of Rose Bengal, Curcumin, and the Mixture in One Spectrum

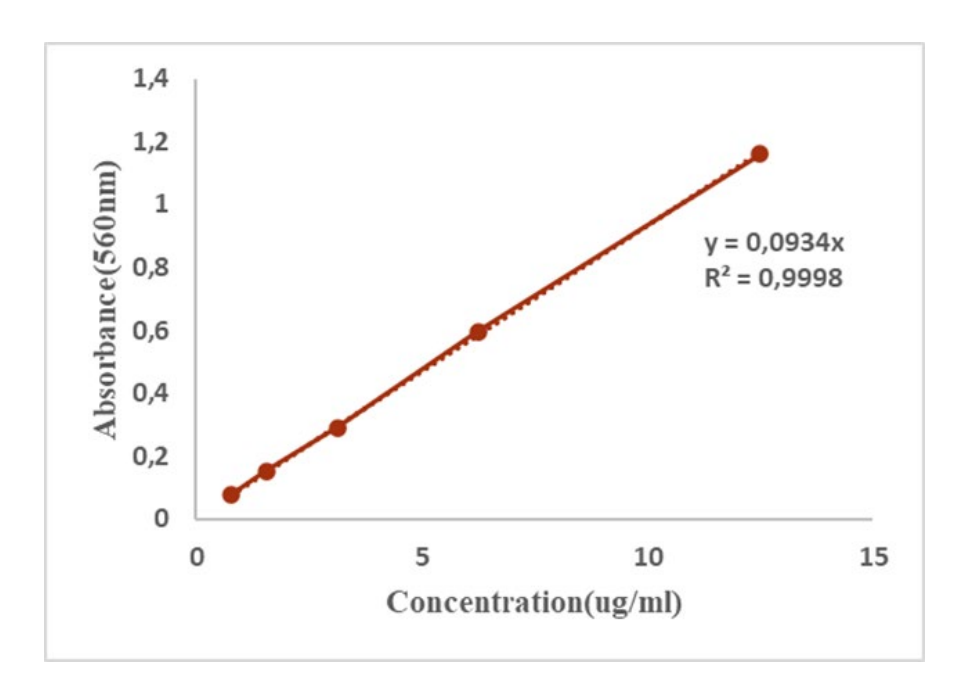


Figure 2-5: Standard Curve of Rose Bengal

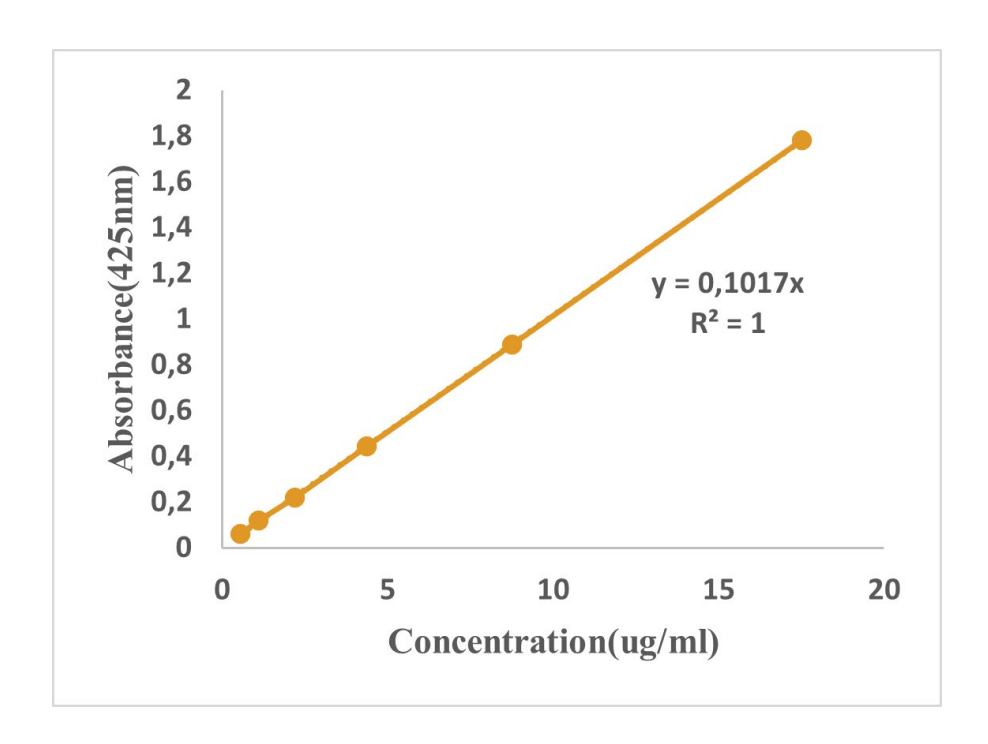


Figure 2-6: Standard Curve of Curcumin

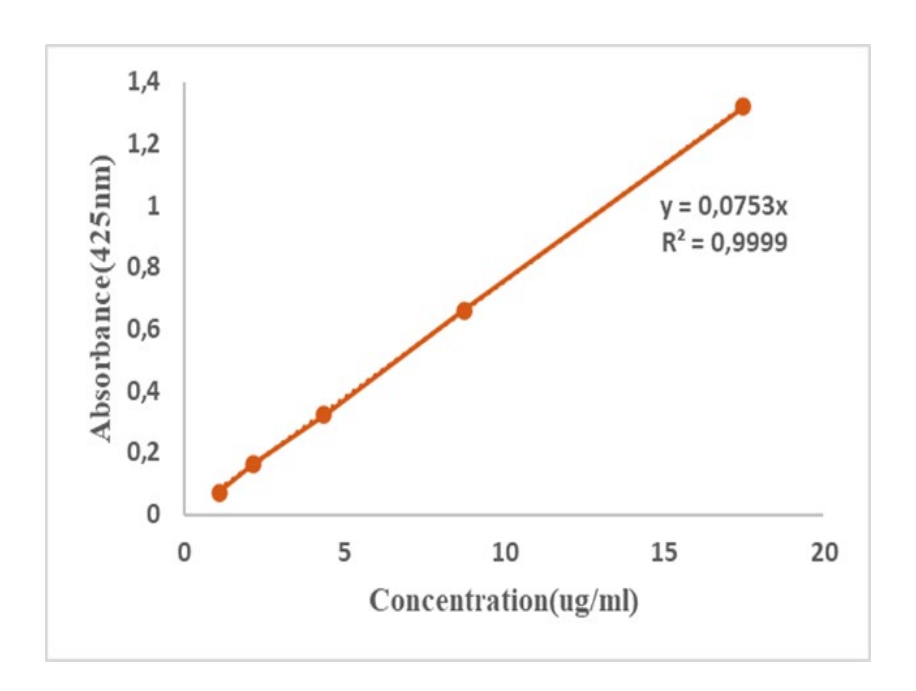


Figure 2-7: Standard Curve of Curcumin in the Presence of Rose Bengal

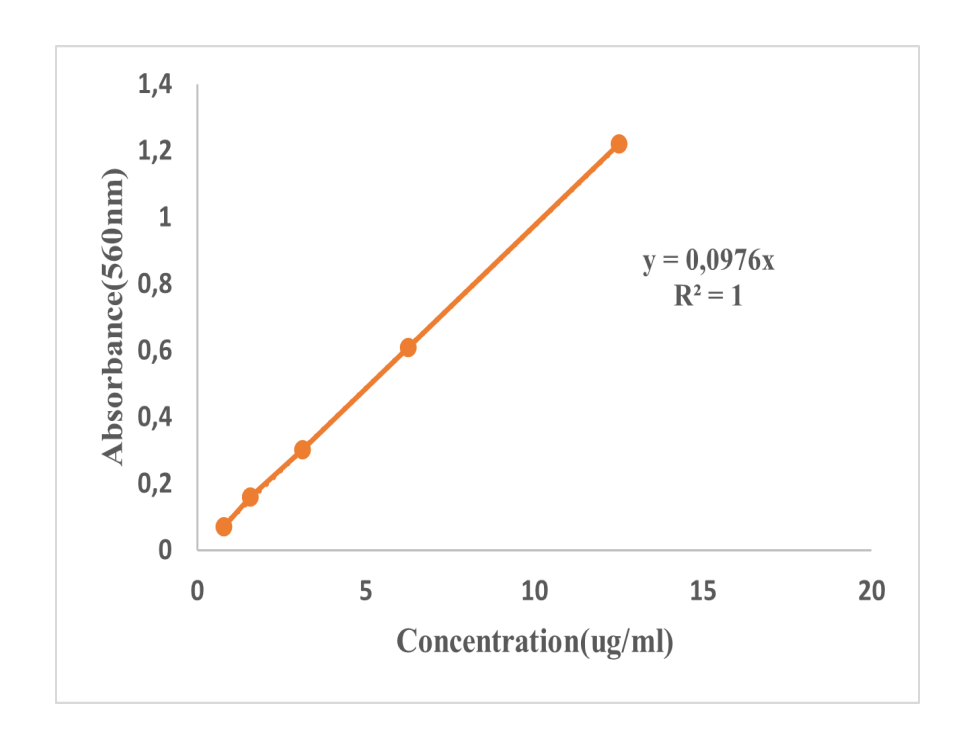


Figure 2-8: Standard Curve of Rose Bengal in the Presence of Curcumin

# Chapter 3: TEMPERATURE AND pH DUAL RESPONSIVE NANOPARTICLES AS POTENTIAL COLON SPECIFIC DRUG DELIVERY SYSTEMS

#### 3.1 Introduction

Drug administration via the oral route is one of the most promising strategies due to its simplicity and suitability as being a non-invasive method. However, the gastrointestinal (GI) tract has harmful conditions. For example, the pH range in the stomach is highly acidic (pH=2-3) and this situation would cause the loss and deformation of the drug during the passage of this route. These conditions are relieved after the stomach and turn to slightly alkaline levels varying between pH=6-7.5 in the small intestine and colon [61]. In consideration of these types of limitations, designing controlled drug delivery systems(CDDS) for specific drugs against colonic diseases requires the utilization of environmentally sensitive materials in order to regulate the release rate and preserve the drugs [62].

Smart nanocarriers can be considered outstanding vehicles to protect the drug molecules, on the GI tract, and to release their cargo at the desired rate, in the colon environment. In accordance with this purpose, pH-responsive nanoparticles can be utilized for a higher amount of drug release at alkali pH levels and minimizing the drug release in the acidic environment. Usually, poly(methylmethacrylate)-based copolymers are commercially used for this purpose. They are applied as coating materials for tablets and named Eudragit in the market [63]. Li et al. prepared several nanoparticle formulations including a combination of Eudragit polymers with chitosan. They observed that these oppositely charged polymers can form stable nanosized polyelectrolyte complexes providing intended pH-responsive release profiles for oral drug delivery applications. Also, they demonstrated that these formulations did not cause any adverse effect on the structural conformation of the drug [64]. On the other hand, Chau et al. used succinylated ε-polylysine (SPL) as a pH-responsive polymer to coat mesoporous silica nanoparticles loaded with prednisolone. They demonstrated that usage of these pH-responsive nanoparticles can prevent the release of the drug through the GI tract and provide maximum drug release in the colonic site [65]. Yun et al. prepared polyacrylic acid and chitosan-coated hydroxyapatite nanoparticles which include 5-FU as a model drug and gadolinium ion as an imaging agent [66]. They revealed that the chitosan-polyacrylic acid complex can protect the drug from the possible adverse effects of the GI environment and provide the intended release profile in the colon site. However, the resulting structure was sensitive to only pH changes whereas enhanced drug release can be accomplished via the presence of a temperature-responsive polymer [67]. In this way, the drug release will be modulated by changes in pH on the GI tract and also by changes in temperature [68]. This approach would be useful since the temperature level at the diseased area is slightly higher than in healthy tissues [69].

Yang et al. produced chitosan-polyacrylic acid micelles and they included PNIPAM as a thermoresponsive polymer. This complex nanocarrier has the capability to display responsiveness to both temperature and pH changes [70]. Kim et al. synthesized copolymeric nanocarriers that possess pH/temperature dual responses, including N-isopropyl acrylamide (NIPAAm) and acrylic acid as temperature-responsive and pH-responsive moieties, respectively [71]. Thus they observed a higher amount of  $\beta$ -lapachone ( $\beta$ -LP) release with increasing temperature. Although intended release profiles were obtained at different pH and temperature levels, a considerable amount of drug was released in the acidic environment and this might be a disadvantage regarding therapeutic efficiency. More importantly, PNIPAM becomes cytotoxic after degradation into small amide derivatives in the acidic environment [72]. Poly(n-vinyl-caprolactam (PNVCL) as another popular thermoresponsive polymer can be replaced with PNIPAM in the case of oral drug delivery applications since there is no such type of risk in PNVCL [73]. For this reason, PNVCL can be considered safer material than PNIPAM for the administration of drugs via oral route where the nanoparticles are exposed to highly acidic conditions.

All these efforts indicate a strong need for safe and biocompatible nanocarriers that are sensitive to both pH and temperature for oral drug delivery in the treatments of colonic diseases. Herein, chitosan polyacrylic acid polyelectrolyte complex shell and poly(n-vinyl caprolactam) core nanoparticles were synthesized. Rose bengal was chosen as a photosensitizer model drug. To the best of our knowledge, first time in literature NVCL was polymerized within the chitosan polyacrylic acid complex, and rose bengal was used as a model drug. Following the fabrication of nanoparticles, several characterization studies were performed such as size and zeta potential measurements by DLS, analysis of morphology and chemical makeup by SEM and FTIR, respectively. Also, encapsulation efficiency and loading capacity of the nanoparticles and the release profiles at different pH levels and temperatures were determined through the evaluations using the data obtained from UV-Vis spectrophotometer.

#### 3.2 Materials and Methods

#### 3.2.1 Materials

Chitosan (75–85% deacetylated, low molecular weight, CAS no. 9012-76-4) was bought from Sigma-Aldrich, USA. Acetic acid (CAS no. 64-19-7) was purchased from Merck, USA. Acrylic Acid (CAS Number: 79-10-7), N- vinyl-caprolactam (CAS Number 2235-00-9) and N, N'-Methylenebisacrylamide (CAS Number 110-26-9) were purchased from Sigma-Adrich, USA.

#### 3.2.2 Methods

#### Preparation of Chitosan/Poly(acrylic acid)/Poly(n-vinylcaprolactam) Nanoparticles

Surfactant free batch emulsion polymerization technique was used in the synthesis of the CS/PAA/PNVCL nanoparticles [74]. A proper amount of n-vinyl caprolactam (0.11g) was dissolved in 20ml ultrapure double distilled water. After complete dissolution, 0.11g acrylic acid and 0.25g chitosan were added to this solution. Sodium bicarbonate buffer (0.065g) was used to maintain a constant pH value of the reaction mixture preventing hydrolysis of n-vinyl-caprolactam under acidic conditions.[16] The reaction mixture was placed in reflux system and purged with nitrogen for 30 minutes. The temperature was adjusted to 80°C after purging and KPS solution (0.041g in 5ml) was injected to the system as the initiator for surfactant-free polymerization of n-vinyl-caprolactam (NVCL) and acrylic acid (AA) in the presence of chitosan. The solution became milky after 10 minutes of initiation. Polymerization was carried for 5 hours, and the resulting solution was filtered(0.45um) then centrifugated at 40.000 rpm, 4°C for 45 minutes.

#### Preparation of Rose Bengal Loaded CS/PAA/PNVCL Nanoparticles

A diffusion-based drug loading technique was used to obtain drug loaded nanoparticles. Briefly, a stock solution of blank nanoparticles was diluted 10 times and incubated in aqueous rose bengal solution(0.25mg/ml) for 72h at room temperature then centrifugated for 45 min at 40 000 rpm and 4°C in order to remove the free rose bengal molecules and calculate the encapsulation efficiency through the supernatant.

#### Characterization of the CS/PAA/PNVCL Nanoparticles

Hydrodynamic size, dispersity, and zeta potential values were measured using ZetaSizer Nano ZS (Malvern Instruments, UK) instrument, which contains a 4.0 mV Helium-Neon laser (633 nm). Size analysis was performed at varying temperature and pH levels at 25 °C to 45°C and

pH=3.5 to pH=6.5, respectively. The size and morphology of the synthesized nanoparticles were assessed by a field-emission scanning electron microscope (Zeiss Leo Supra 35VP SEM-FEG, Germany) at a 3 kV operating voltage. 10ul of the nanoparticles were dropped on a piece of the silicon wafer and dried for 5 hours at room temperature. The dried samples were coated with Au-Pd using a sputter coater (Cressington 108, UK) at 40 mA for 120 s. The SEM images were obtained by the secondary electron (SE) detector. On the other hand, 3 ul of stock solution was dropped on a transmission electron microscopy (TEM) grid, and analysis was performed at 200 kV using the device (JEMARM200, JEOL, Japan). Chemical makeup analysis was performed by using Fourier-Transform Infrared Spectroscopy (Thermo Scientific, Nicolet, iS10, USA). The scanning range for the analysis was 4,000–400 cm<sup>-1</sup>.

#### Drug Release Studies of the CS/PAA/PNVCL Nanoparticles

Encapsulation efficiency and loading capacity were evaluated using UV- Vis spectrophotometer. The amounts of rose bengal in the supernatant were determined using the calibration curve with Equation 1 [9].

$$Encapsulation \ Effficiency \ (\%) = \frac{\textit{Total Drug Amount-Free Drug Amount}}{\textit{Total Drug Amount}} \times 100$$
(1)

Furthermore, the solution of rose bengal loaded nanoparticles was freeze-dried and weighed. The loading capacity of dual drug-loaded nanoparticles was determined via Equation 2 [10].

Loading Capacity(%) = 
$$\frac{Encapsulated Drug Amount}{Total Nanoparticle Weight} \times 100$$
 (2)

Rose bengal loaded nanoparticles were poured into dialysis capsules with a cellulose membrane of 12-14 kDa. Thus, drug molecules can diffuse through the pores easily while the nanoparticles stay inside the dialysis capsules. The capsules were placed in beakers containing 50 ml of PBS at pH=5.0 and pH=7.4. They incubated in shaking incubators at 25°C and 40°C. The samples were taken at several time intervals as 1-3-6-12-24-48-72-96-120 hours. Rose bengal amounts in the samples were determined via UV-Vis analysis. Calibration curves were used to calculate the amount of drug released with Eq.3. The drug release profile was plotted as cumulative drug release (%) versus time. The resulting release profiles were analyzed by curve fitting studies on several kinetic models in the literature and the results were compared through their R<sup>2</sup> values.

$$Release (\%) = \frac{Released Amount of Drug}{Total Amount of Drug} \times 100$$
(3)

#### 3.3 Results and Discussion

# 3.3.1 Characterization of the CS/PAA/PNVCL Nanoparticles

#### DLS Analysis of the CS/PAA/PNVCL Nanoparticles

The hydrodynamic average size and zeta potential values were determined by the dynamic light scattering technique. The particle size and the surface charge of the nanoparticles changed at different pH and temperature levels. This behavior can be attributed to the pH and temperaturesensitive composition of the nanoparticles. The ionization degree of chitosan and polyacrylic acid at several pH levels leads to alteration in the polyelectrolyte complex. In some extreme points, one of these polymers starts to dominate the size due to the changes in the interaction between the protonated amino groups of chitosan (pKa=6.0) and the carboxylic acid groups of polyacrylic acid (pKa=4.5). At pH =5.5 where two polymers are charged, the most compact complex was formed. However, the size of the nanoparticles starts to increase when one of the polymers begins losing its charge such as when pH value is closing to 4.5 or 6.0. In that scenario, lower interactions between the charged groups result in less strength polyelectrolyte complex, thus larger average size are observed. The different size values obtained at different pH levels can be seen in Figure 3-1. This phenomenon can also be explained through the zeta potential values of the nanoparticles at different pH levels. The nanoparticles have 22.6 mV zeta potential at pH=5.5. This positive surface charge is due to the cationic nature of the chitosan. Furthermore, this value becomes more positive when the pH values approach highly acidic pH levels, since chitosan chains become more ionized and carboxylic groups of the PAA are almost neutral. On the contrary, the zeta potential value starts to decrease when the pH level is approaching 6.5. In this case, the chitosan structure loses its charge while PAA becomes highly ionized. The different zeta potential values at different pH levels can be seen in Figure 3-2.

On the other hand, the nanoparticles are also sensitive to the temperature due to the presence of poly (n vinyl caprolactam) (PNVCL) moieties. Around 30 °C which is around the LCST value of PNVCL, a sharp decrease in average size is observed. This can be explained through the shrinking behavior of the PNVCL, expelling the water molecules from the structure due to

the hydrophobic hydrophilic transition. The size values obtained by temperature-dependent measurements can be seen in Figure 3-3.

Following the rose bengal loading, the nanoparticles were around 217nm in hydrodynamic diameter with 24.0 mV zeta potential at pH=4.5 conditions. They also preserved their monodispersed feature. The size distribution of the loaded nanoparticles at 25 °C and 45 °C and the zeta potential analysis are presented in Figure 3-4, Figure 3-5, and Figure 3-6, respectively.

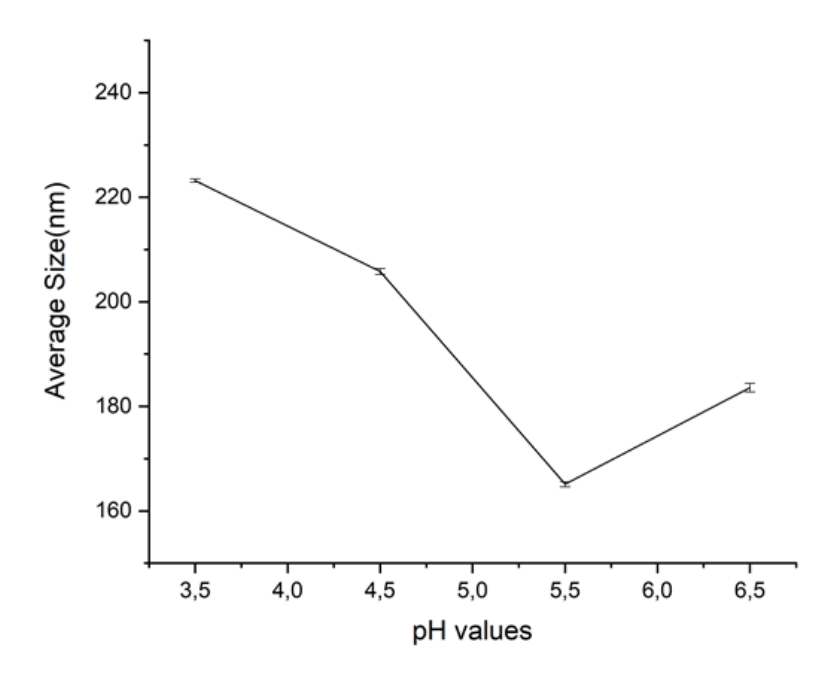


Figure 3-1: Average Size of Blank Nanoparticles at Different pH Levels

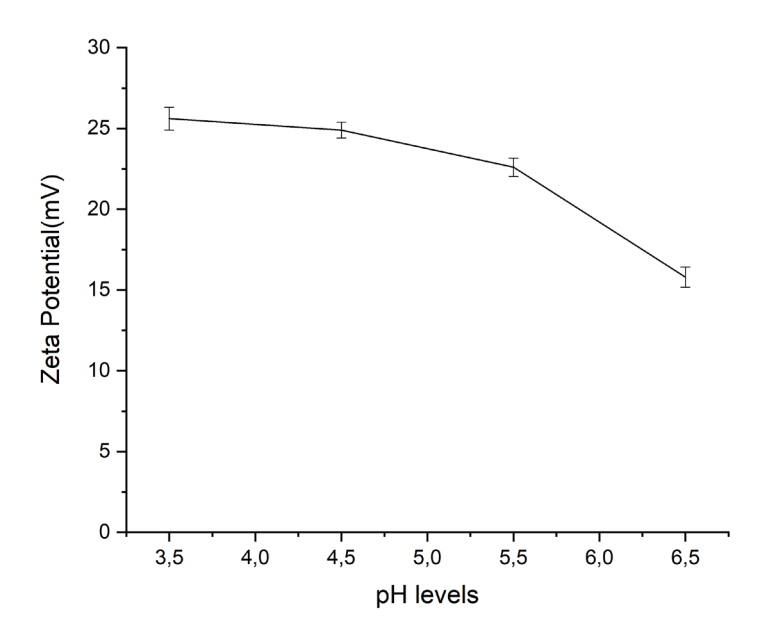


Figure 3-2: Zeta Potential Values of Blank Nanoparticles at Different pH Levels

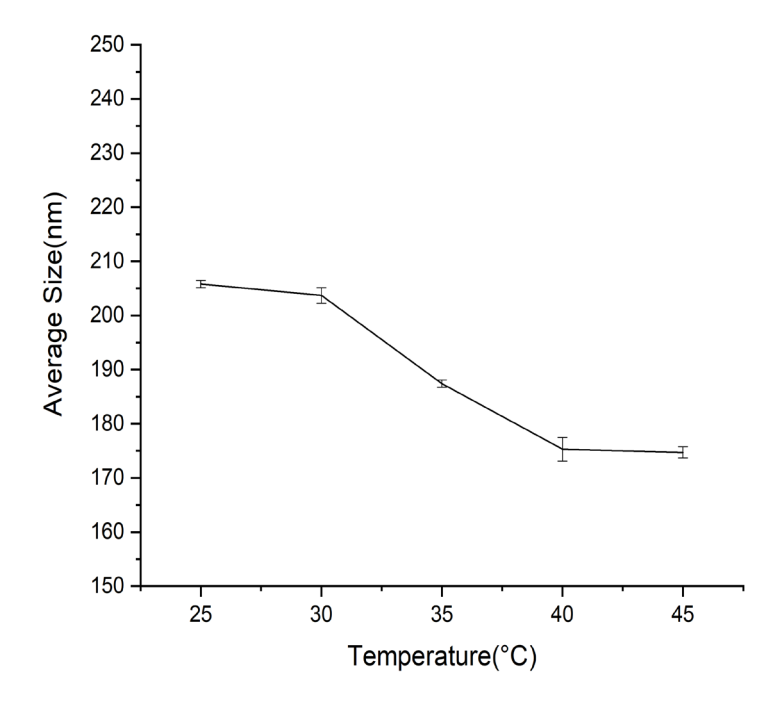


Figure 3-3: Average Size of Blank Nanoparticles at Different Temperature Levels (pH=4.5)

			Size (d.nm):	% Intensity:	St Dev (d.nm):
Z-Average (d.nm):	217,1	Peak 1:	239,3	100,0	76,80
Pdl:	0,081	Peak 2:	0,000	0,0	0,000
Intercept:	0,943	Peak 3:	0,000	0,0	0,000
Result quality :	Good				

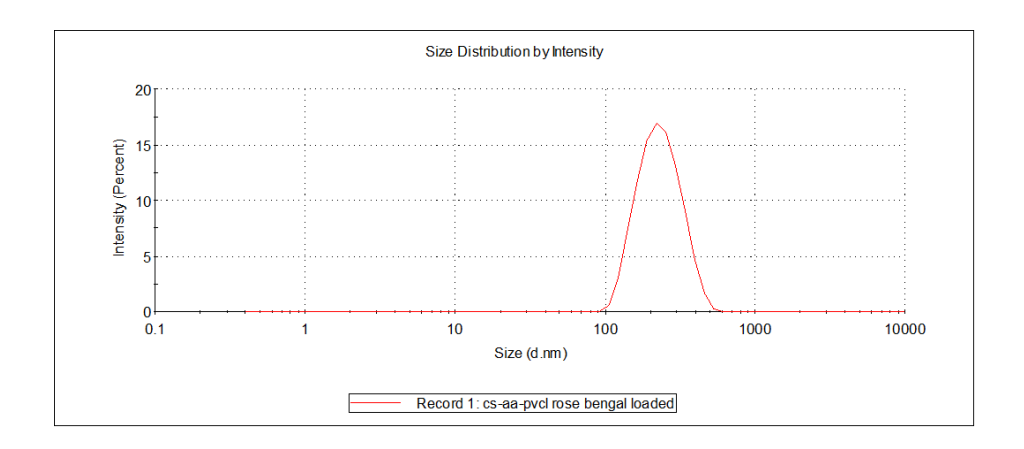


Figure 3-4: DLS Size Analysis of RB Loaded Nanoparticles at Room Temperature

			Size (d.nm):	% Intensity:	St Dev (d.nm):
Z-Average (d.nm):	189,3	Peak 1:	207,2	100,0	64,25
Pdl:	0,077	Peak 2:	0,000	0,0	0,000
Intercept:	0,944	Peak 3:	0,000	0,0	0,000
Result quality :	Good				

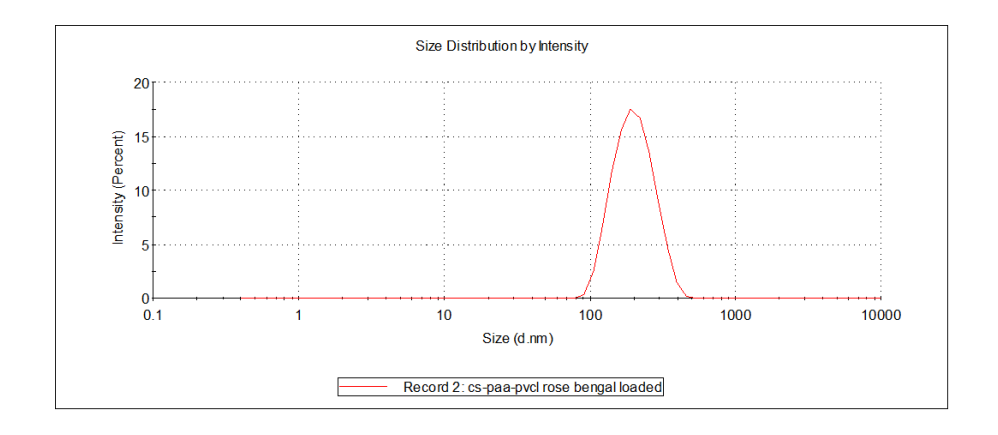
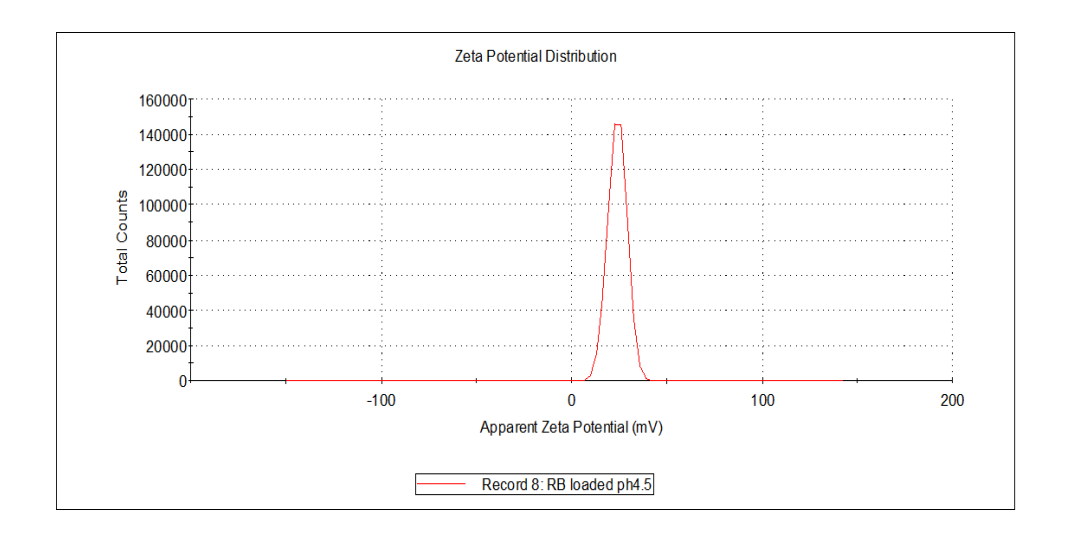


Figure 3-5: DLS Size Analysis of RB Loaded Nanoparticles at 45°C

			Mean (mV)	Area (%)	St Dev (mV)
Zeta Potential (mV):	24,0	Peak 1:	24,1	100,0	4,97
Zeta Deviation (mV):	4,73	Peak 2:	0,00	0,0	0,00
Conductivity (mS/cm):	0,0991	Peak 3:	0,00	0,0	0,00
Result quality :	Good				



**Figure 3-6:** Zeta Potential Analysis of Loaded Nanoparticles(pH=4.5)

# Electron Microscopy Imaging of the CS/PAA/PNVCL Nanoparticles

The spherical morphology of bare and drug-loaded nanoparticles was confirmed using transmission electron microscopy (TEM) and scanning electron microscopy (SEM). It is observed that the size of the nanoparticles is smaller than those measured by the DLS analysis. This can be explained through the differences in measurement principles of DLS and electron microscopy analysis. Dynamic light scattering is a technique that is based on a mathematical modeling study about the diffusion rate of the nanoparticles that undergo Brownian motion. Besides this model includes the solvent ions around the nanoparticles and the measured size is called hydrodynamic size because of this situation. However, in electron microscopy, the nanoparticles are completely dried, and the images obtained are results from electron beam matter interaction. Therefore, it is reasonable to observe smaller size values in electron microscopy, compared to the dynamic light scattering.

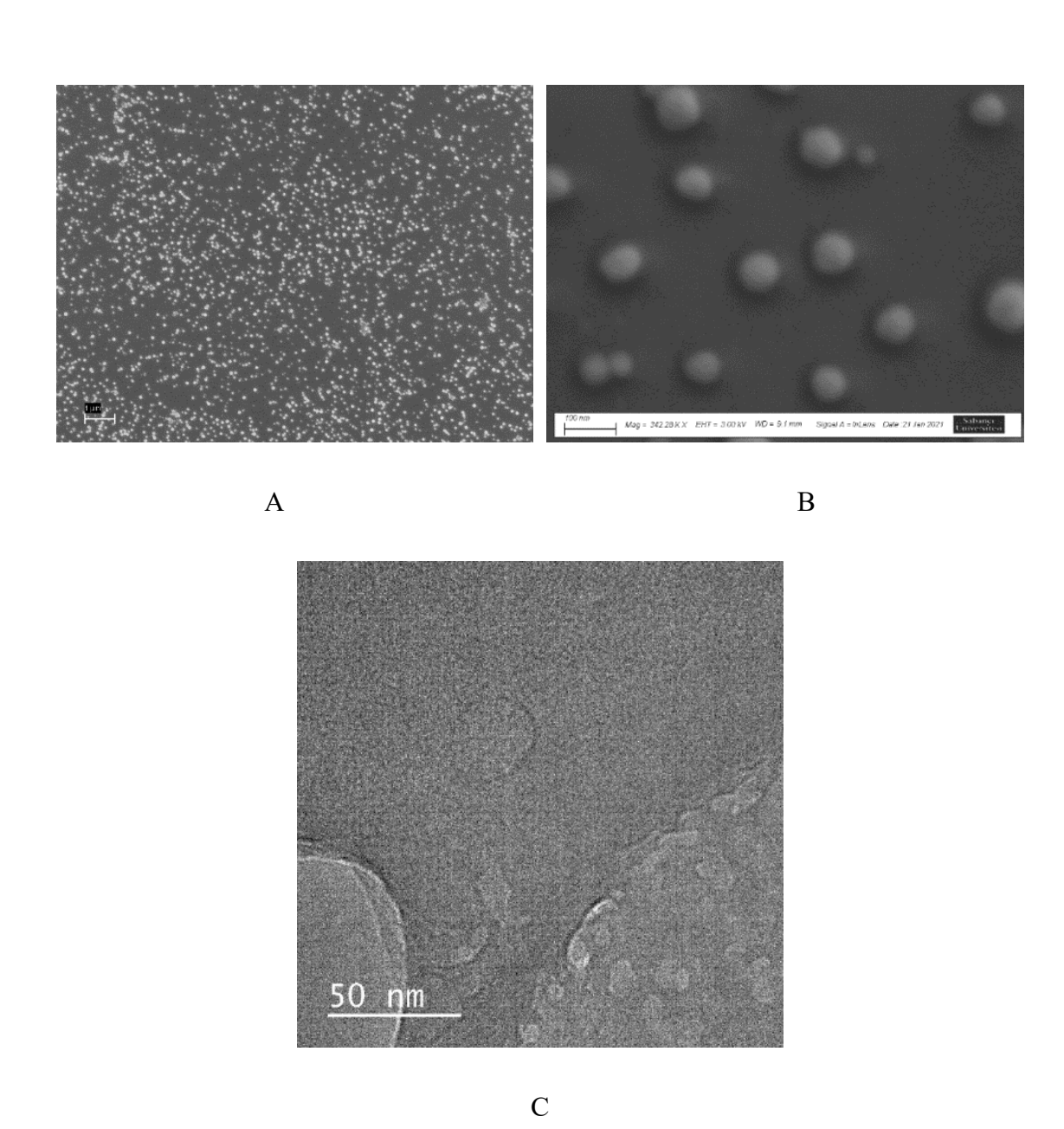
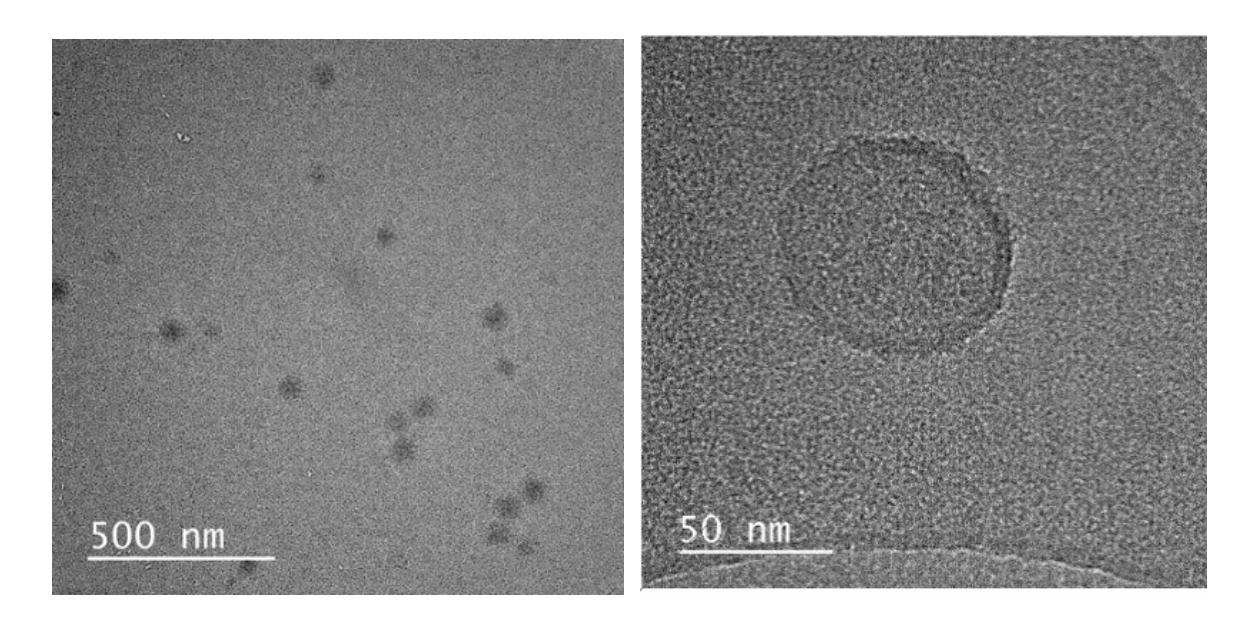
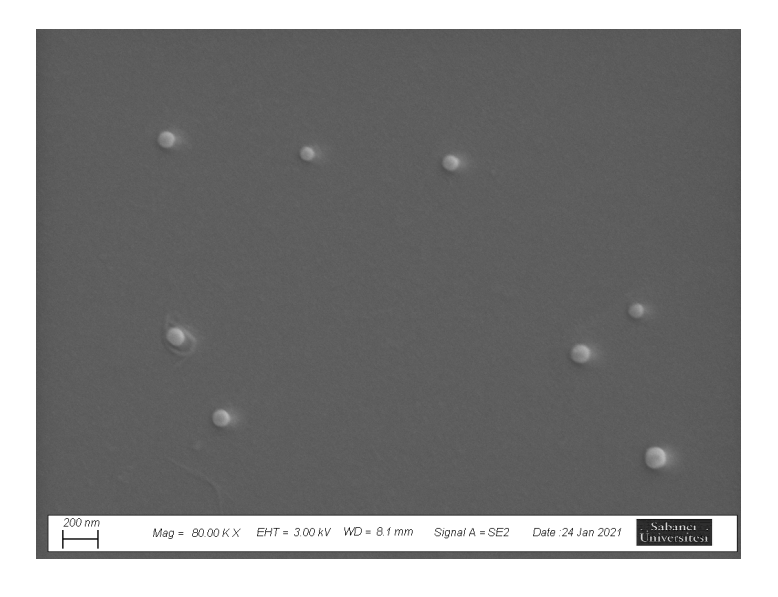


Figure 3-7: SEM (A, B) and TEM Image(C) of Blank Nanoparticles



A B



C

Figure 3-8: TEM (A, B) and SEM(C) Images of Loaded Nanoparticles

# FTIR Analysis of the CS/PAA/PNVCL Nanoparticles

FTIR spectroscopy was performed to analyze the chemical makeup of the nanoparticles. In the spectrum, carboxylic acid peaks were observed at 3241.05cm<sup>-1</sup> and 1262.77 cm<sup>-1</sup> as O-H stretch and C-O stretch, respectively [75]. Aliphatic C-H stretch was detected at 2926.84 cm<sup>-1</sup> and the absorption bands that indicate C-N and C-C stretching in the aromatic ring were observed at 1485.61 cm<sup>-1</sup> and 1418.08 cm<sup>-1</sup> [76]. On the other hand, N-H bending belongs to amino compounds in the chitosan structure was observed at 1635.81cm<sup>-1</sup>. The peaks observed at 1556.06 cm<sup>-1</sup> and 1030.5 cm<sup>-1</sup> were ascribed to N-O stretching and C6-OH of chitosan [77]. After rose bengal loading, the peak at 1635 cm<sup>-1</sup> disappeared, the peak at 1262 cm<sup>-1</sup> diminished and the peak at 1030 cm<sup>-1</sup> shifted. These changes can be attributed to the possible interactions between the carboxylic group of the rose bengal and amino groups in the nanoparticle structure.

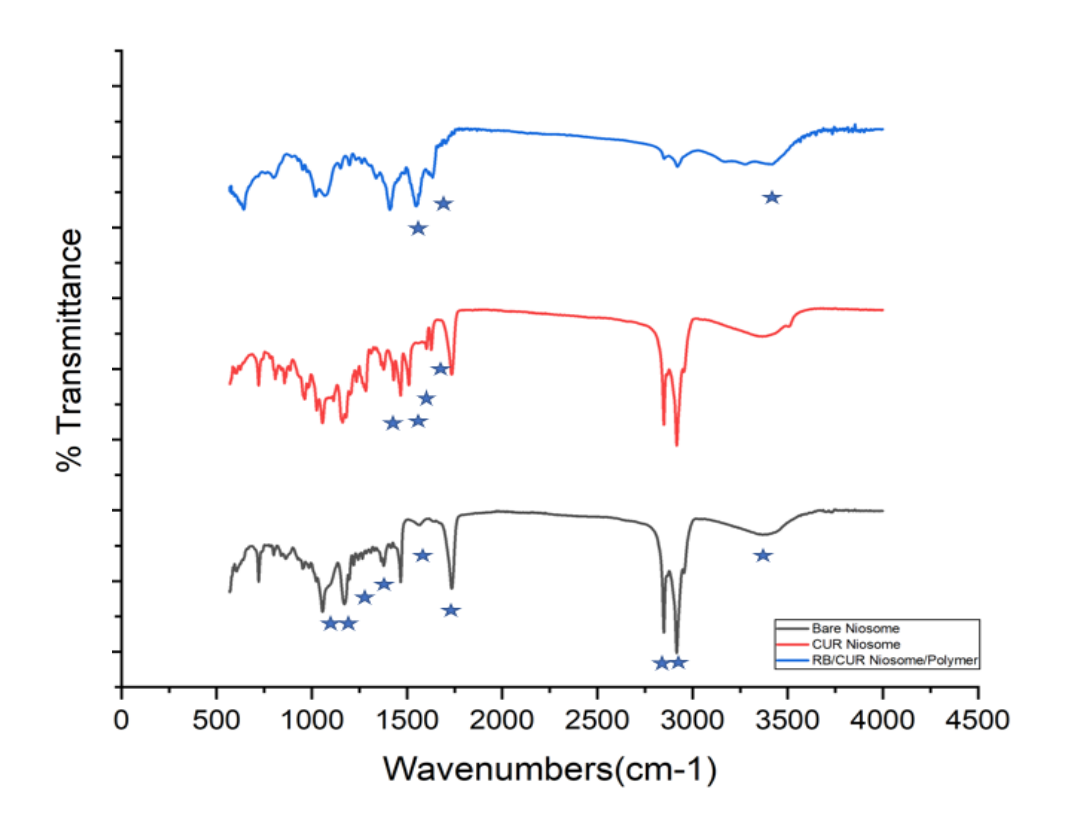


**Figure 3-9 :** FTIR Spectrum of Rose Bengal, Blank Nanoparticles and Rose Bengal Loaded Nanoparticles

# 3.3.2 Drug Release Profile and Kinetic Analysis

Following the obtaining of standard curves for rose bengal, encapsulation efficiency was calculated as 93.57% by using Eq (1), and loading capacity was calculated as 4,93% by using Eq (2).

Rose bengal release at different pH and temperature levels is presented in Figure 3-10. The release profiles of rose bengal from the nanoparticles are strongly affected by pH and temperature changes. This behavior can be attributed to the presence of both pH-responsive and temperature-responsive moieties in the complex nanostructure. The nanoparticles are able to allow faster drug release at physiological/alkali pH level whereas only a small amount of drug release was observed under acidic conditions. This behavior can be explained through the swelling of the polymeric structure in the alkali pH environment due to the presence of polyacrylic acid. This swelling phenomenon results in an increase in the transportation rate of the drug molecules from the nanostructure. Besides, the release rate is also able to be triggered by an increase in the temperature. This stimulus leads to the conformational change in the PNVCL structure. The transition between the hydrophilic to hydrophobic states results in a shrinking of the polymer matrix, thus an acceleration in the drug release rate. This behavior was observed both at alkali and acidic pH levels. Ultimately, the consequence of the stimuliresponsive release of rose bengal can be seen in the photograph of dialysis capsules after 72h at 40°C, in Figure 3-11.

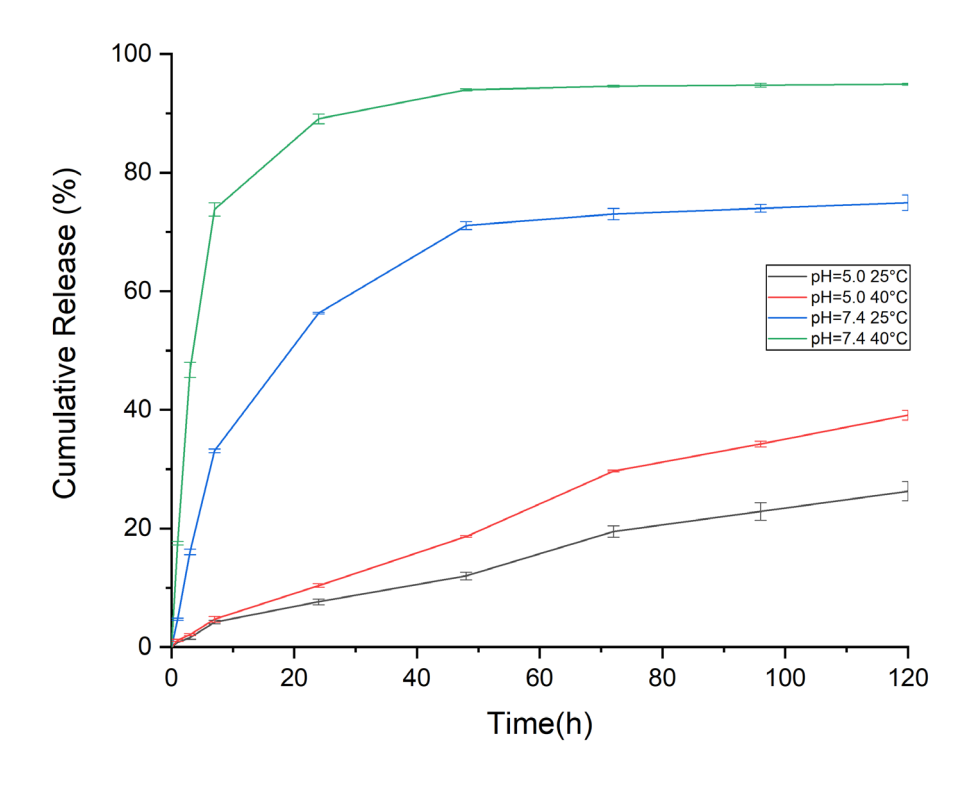


Figure 3-10: Release Profiles of Nanoparticles in different temperature and pH levels



Figure 3-11 : The photograph of drug release capsules at pH=7.4(left) and pH=5.0 (right) after 72h at  $40^{\circ}$ C

**Table 3-1:** Kinetic Model Analysis of the drug release profiles.

Formulation/Model	Korsmayer- Peppas			Higuchi	Zero order	First order	Hixson- Crowell
Rose Bengal (RB)	(R <sup>2</sup> )	(n)		(R <sup>2</sup> )	(R <sup>2</sup> )	(R <sup>2</sup> )	(R <sup>2</sup> )
RB1	0.99	0.72		0.75	0.98	0.78	0.88
RB2	0.99	0.76		0.68	0.98	0.80	0.89
RB3	0.99	0.90		0.83	0.90	0.20	0.58
RB4	0.99	0.95		0.59	0.99	0.60	0.81

**RB1**: Rose Bengal release profile at pH=5.0 and 25°C RB2: Rose Bengal release profile at pH=5.0 and 40°C **RB3**: Rose Bengal release profile at pH=7.4 and 25°C **RB4**: Rose Bengal release profile at pH=7.4 and 40°C

Table 3-1 shows the correlation factors of each kinetic model to our experimental release profiles. According to our results from curve fitting processes on the empirical drug release profiles, it is possible to explain our release kinetics through two kinetic models, Korsmeyer Peppas Model and Zero Order Model. The obtained n values in Korsmeyer Peppas Model are important to determine the governing forces on drug transportation between the carrier and the release media. In spherical geometries, the n value below 0.43 indicates that the Fickian diffusion is dominating the system. In the case of n is higher than 0.85, swelling or relaxation of polymeric structure governs the drug transportation. This phenomenon is also correlated with zero-order kinetics. Also, the non-Fickian, or in other words the anomalous model is another case where the n value is between 0.43 and 0.85. In this situation, the drug release mechanism is governed by both diffusion and swelling.

In our case, non-Fickian diffusion is valid at acidic conditions. Besides, an increase in temperature affected the system and increase the n value a fair amount. On the other hand, our release profiles are in extreme behavior in Korsmeyer Peppas Model, and they displayed almost zero order kinetics at the alkali environment. This can be explained by both the n values of

each Korsmeyer Peppas Model and the correlation coefficients with zero order kinetics. Here, the stimuli responsive property of the nanocarriers can be confirmed through the release profiles and curve fitting results.

#### 3.4 Conclusion

CS/PAA/PVCL nanoparticles were successfully prepared by surfactant-free polymerization of NVCL and AA in the presence of chitosan. The synthesized nanoparticles were exposed to several characterizations to determine their hydrodynamic size, zeta potential, morphology, and chemical composition. The nanoparticles displayed different release profiles at different pH and temperature levels corresponding to the conditions at the GI tract. According to our results, a faster drug release profile was obtained at alkali pH levels and elevated temperature and slower drug release was observed at acidic pH levels and room temperature. This type of nano formulation can be considered a promising candidate for oral drug delivery applications.

# Chapter 4: CO-DELIVERY OF HYDROPHILIC AND HYDROPHOBIC DRUGS BY DUAL RESPONSIVE NIOSOME/POLYMER NANOCARRIERS

#### 4.1 Introduction

The delivery of anticancer drugs to the tumor site at the intended rate and dosage is the most promising strategy to increase the effectiveness of the therapy and reduce the side effects of the drugs. Nanoparticle-mediated drug delivery systems are one of the key tools for this purpose [78]. In recent years, drug delivery systems based on vesicular nanoparticles such as liposomes, niosomes, and polymeric micelles have been introduced as promising carriers in the treatment of severe diseases like cancers. They show the capability to protect the drug from degradation, enhance drug efficacy, and provide controlled and sustained release [79].

The therapeutic effect of these nanocarriers can be enhanced by modulating the drug release in accordance with environmental conditions such as pH and temperature. In the case of niosome based carriers, this can be usually done using specific surfactants or their derivatives modified with stimuli responsive chemical moieties such as cholesteryl hemisuccinate (CHEMS) or tween 21 [80]. For instance, Tila et al. prepared pH responsive niosomes using cholesterol derivatives for the delivery of mitoxantrone and they investigated they investigated the release of mitoxantrone at different pH levels. Finally, they obtained a higher amount of drug release at acidic pH level corresponding to the tumor site [81]. Marzoli et al. preferred tween 20 modified with glycine to the same purpose. They used ibuprofen as a model drug and revealed the effect of their pH responsive niosomes on animal models [82]. However, those carriers were sensitive to only pH changes in the environment whereas enhanced drug release can be acquired with changes in the temperature. Tavano et al. prepared L64 surfactant and its derivative L64ox based niosomes to obtain a triggered release profile with changes in the temperature [83]. Regulation of the drug release in the above-mentioned studies is restricted by modified cholesterol and surfactants. Besides, the drug release profiles were only sensitive to one stimulus, (pH or temperature). Here, incorporation of stimuli-responsive polymers with the niosomes becomes prominent in overcoming these issues. The electrostatic interaction between polymer chains and the surface of the niosomes enables the stable core-shell nanostructures with the intended properties. Although these approaches have been widely used on liposomes, the studies on niosome based nanocarriers are rather focused on overcoming some specific issues such as lower mucoadhesivity and circulation time [84] [85] [86] [87].

Herein, we prepared pH and temperature, dual responsive, niosome nanoparticles coated with chitosan grafted poly(n-vinyl caprolactam) (CSgPVCL) polymer. Rose bengal (RB) and curcumin (CUR) were chosen as model drugs. RB was encapsulated into the polymeric shell whereas CUR was loaded into the lipid bilayer of the niosomes. Dynamic light scattering (DLS) was utilized to determine the hydrodynamic size, zeta potential, and polydispersity index of the resulting nanoparticles. The chemical makeup of the grafted polymer and niosomes were analyzed by FTIR spectroscopy. Electron microscopy analysis were performed to confirm the spherical morphology of the nanoparticles. Besides, encapsulation efficiency, loading capacity, and the release profile of the nanoparticles were determined by UV-Vis spectroscopy. Curve fitting studies were implemented to check the coherence of the empirical release profiles to the release models in the literature.

#### 4.2 Materials And Methods

#### 4.2.1 Materials

Sorbitan monostearate (Span 60) was purchased from Alfa Aesar. Cholesterol was purchased from PanReac. Chitosan (75–85% deacetylated, low molecular weight, CAS Number 9012-76-4) was from Sigma Aldrich. Chloroform, methanol, and curcumin were from Merck, all analytical grades. For all the experiments Milli-Q water was used. Sodium tripolyphosphate (TPP, CAS Number 7758-29-4), was from Sigma–Aldrich. Acetic acid (CAS Number 64-19-7) was purchased from Merck. N-vinyl caprolactam (CAS Number 2235-00-9). N, N'-Methylenebisacrylamide (CAS Number 110-26-9) were purchased from Sigma-Adrich.

#### 4.2.2 Methods

# **Preparation of the Grafted Polymer**

The grafting of chitosan onto poly(n-vinyl caprolactam) was performed by the following procedure of Duan et al. with small modifications [88]. Sodium bicarbonate buffer was used to maintain a constant pH value of the reaction mixture. Thus, hydrolysis of n-vinyl-caprolactam under acidic conditions can be avoided. [89].

Briefly, a proper amount of chitosan was dissolved in a 1% acetic acid solution and the pH value was adjusted to pH=5.0. Following the solution was heated to 70°C under nitrogen, equal moles of KPS and NaHCO<sub>3</sub>, was added to the reaction system. After 15 minutes, NVCL and

MBA were added, and the mixture was stirred for 3 hours under nitrogen. The resulting polymer solution was dialyzed against ultrapure Milli Q double distilled water for 7 days and then freeze-dried.

#### **Preparation of the Bare Niosomes**

Niosomal vesicles were prepared using the thin film hydration (TFH) method. Briefly, Span 60 and cholesterol (2:1) were homogeneously dissolved in a mixture of methanol and chloroform (3:1) in a round bottom flask. Then the organic solvents were evaporated under reduced pressure, using a rotary vacuum evaporator, to obtain a thin film inside the flask. Hydration of obtained thin film with PBS resulted in the formation of niosomes. Several trials and errors were repeated to obtain the suitable type of surfactant and solvents, surfactant to cholesterol and methanol to chloroform ratios, as well as volume and duration of hydration.

The optimum formulation of the niosomes was chosen to prepare curcumin-loaded niosomes. Span 60, cholesterol, and curcumin were dissolved in the mixture of methanol and chloroform, then solvents were removed to obtain a thin film layer containing curcumin molecules. After hydration with PBS, the niosomes with curcumin in their bilayer were gained. The produced nanoparticles were sonicated for an hour to reduce their size, then kept at 4 °C overnight to stabilize. The resulting nanoparticle solution was centrifuged at 17.000 rpm for 30 min to remove the free CUR molecules.

#### Preparation of the CSgPVCL Coated Niosomes

The coating process was performed by using a microfluidic syringe pump (KD Scientific Legato 100). An equal volume of 1%(w/v) aqueous polymer solution either alone or mixed with a predetermined amount of rose bengal was added dropwise at 25ul/sec rate, to the blank or CUR loaded niosome solutions. The polymer-niosome mixtures were stirred for 1h at room temperature and then centrifuged at 17.000 rpm for 30 min in order to remove the excess polymer and unencapsulated Rose Bengal molecules.

#### **Characterization of the Niosomes**

Hydrodynamic size, dispersity, and zeta potential values were measured using ZetaSizer Nano ZS (Malvern Instruments, UK) instrument, which contains a 4.0 mV Helium-Neon laser (633 nm). Size analysis was performed at 25 °C. The size and morphology of the synthesized nanoparticles were assessed by a field-emission scanning electron microscope (Zeiss Leo Supra 35VP SEM-FEG) at a 3 kV operating voltage. 10 ul of the nanoparticles were dropped on a

piece of the silicon wafer and dried for 5 hours at room temperature. The dried samples were coated with Au-Pd using a sputter coater (Cressington 108) at 40 mA for 120s. The SEM images were obtained by the secondary electron (SE) detector. On the other hand, 3 ul of stock solution was dropped on a transmission electron microscopy (TEM) grid, and analysis was performed at 200 kV using the device (JEM-ARM200, JEOL). Chemical makeup analysis was performed by using Fourier-Transform Infrared Spectroscopy (Thermo Scientific, Nicolet, iS10, USA). The scanning range for the analysis was 4,000–400 cm<sup>-1</sup>.

#### **Drug Release Studies of the CSgPVCL Coated Niosomes**

Encapsulation efficiency and loading capacity were evaluated using UV-Vis spectrophotometer. The amounts of rose bengal and curcumin in the supernatant were determined using the calibration curve with Equation 1. Furthermore, the solution of rose bengal and curcumin loaded nanoparticles was freeze-dried and weighed. The loading capacity of dual drug-loaded nanoparticles was determined via Equation 2.

In release studies, rose bengal and curcumin loaded nanoparticles were put in dialysis capsules with a cellulose membrane of 12-14 kDa. The capsules were placed in beakers containing 50 ml of PBS-T (5%) at pH=5.5 and pH=7.4. They incubated in shaking incubators at 25°C and 37°C. The samples were taken at several time intervals as 1-3-6-12-24-48-72-96-120 hours. Rose bengal and curcumin amounts in the samples were determined via UV-Vis analysis and the calibration curves. The drug release profile was plotted as cumulative drug release (%) versus time. The resulting release profiles were analyzed by curve fitting studies on several kinetic models in the literature and the results were compared through their R<sup>2</sup> values.

#### 4.3 Results and Discussion

#### 4.3.1 Characterization of the Niosomes

# DLS Analysis of the Bare Niosomes and CSgPVCL Coated Niosomes

The hydrodynamic size, zeta potential value, and polydispersity index of the nanoparticles were determined based on the dynamic light scattering technique. According to the results in Table 4-1, unloaded niosomes have 41.9 nm average particle size, 0.316 polydispersity index, and -43,9 mV zeta potential value. In the case of curcumin loaded niosomes, these values increase to 56.44nm, 0.327 and-46.1 mV, respectively. When these niosomes are coated with CSgPVCL

polymer associated with rose bengal, the average size of the resulting nanoparticles rises to 79.91 nm with 0.364 polydispersity index and +30mV zeta potential value. The change in zeta potential value from-46.1mV to +30mV indicates the presence of chitosan included polymer at the surface [90]. Also, these zeta potential values are not in the interval of -30 mV and +30 mV where the nanoparticles are prone to aggregate [91].

Table 4-1: DLS and Zeta Potential Analysis of Blank and Cur Loaded Niosomes

Formulation	Average Size (nm)	Polydispersity Index	Zeta Potential
		(PDI)	(mV)
Blank Niosome	41.19	0.316	-43.9
Curcumin Loaded Niosome	56.44	0.327	-46.1
Polymer RB/CUR Niosome	79.91	0.364	+30.7

#### TEM/SEM Analysis of the Niosomes and CSgPVCL Coated Niosomes

The morphology of bare niosome, CUR loaded niosome, and RB&CUR loaded niosome-polymer composite nanoparticles were analyzed using transmission electron microscopy (TEM) and scanning electron microscopy (SEM). Electron microscopy analysis confirmed the spherical morphology of the nanoparticles. Here, it is worth emphasizing that the size differences between the DLS and SEM/TEM analysis stem from the measurement principles of DLS and SEM/TEM techniques. In dynamic light scattering, the measured size is called hydrodynamic size since the technique also includes the ions around the nanoparticles and the size of the nanoparticles is measured as bigger than the actual size. Also, this technique is based on mathematical modeling of the diffusion rate of the nanoparticles that undergo Brownian motion. However, in electron microscopy, the nanoparticles should be prepared in dried form for analysis, and the micrographs are obtained through electron beam-matter interaction. Therefore, smaller size values are observed in electron microscopy [92], [93].

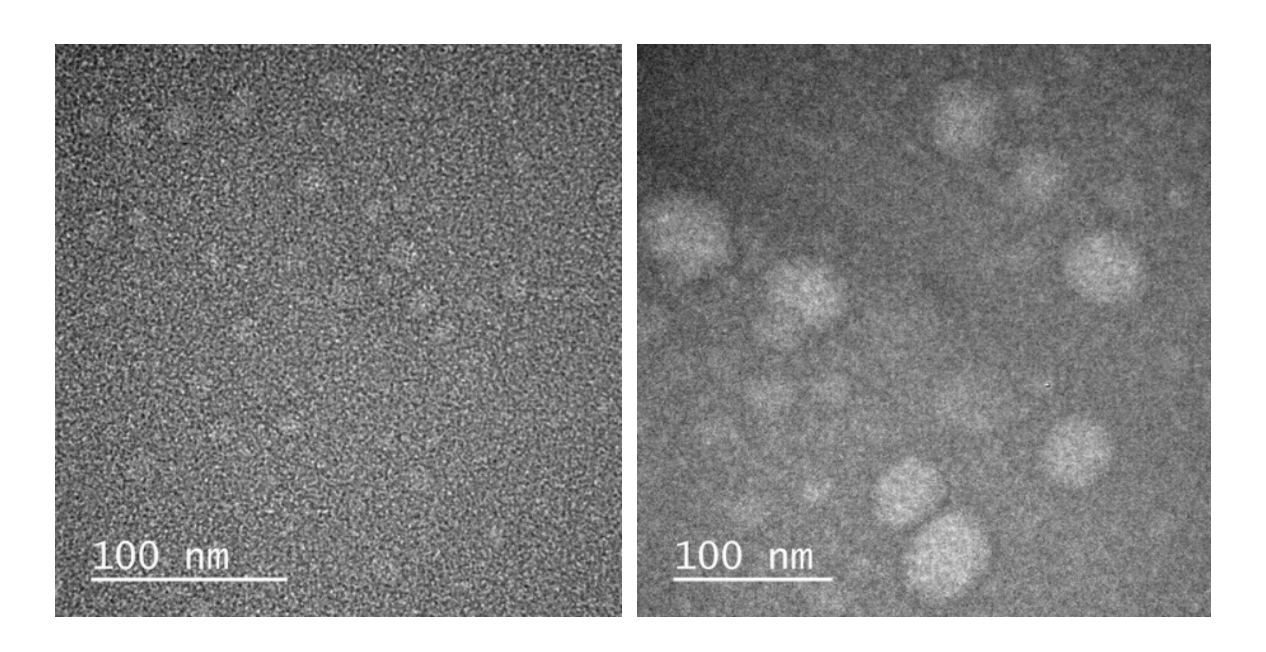
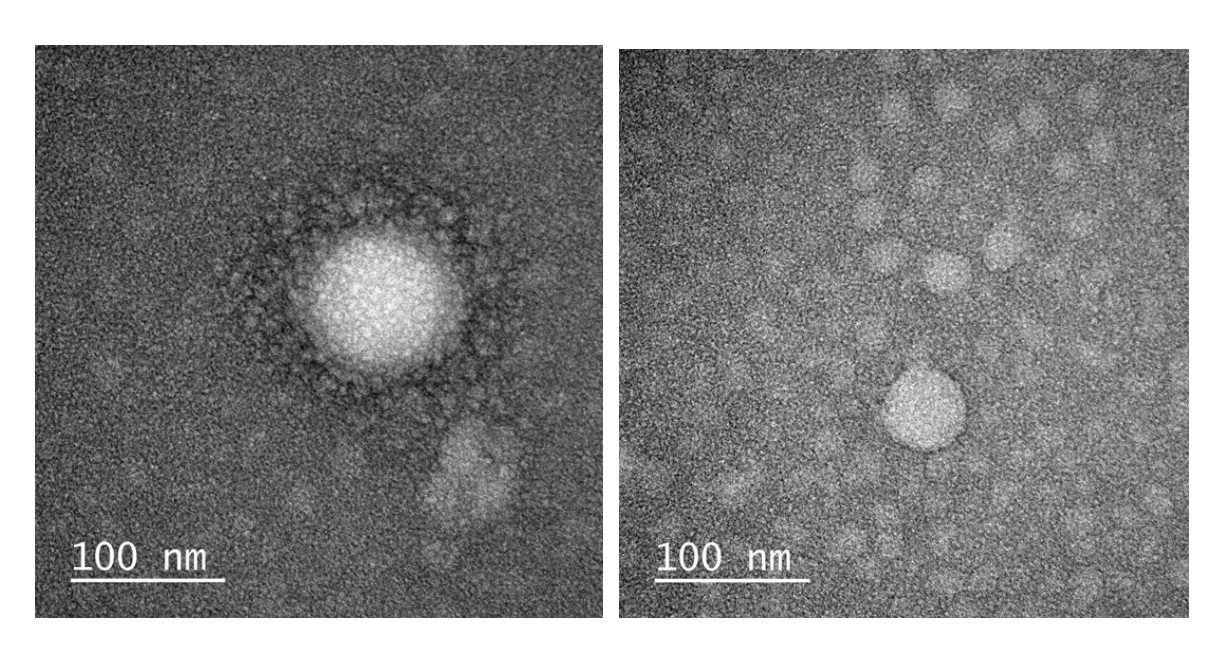
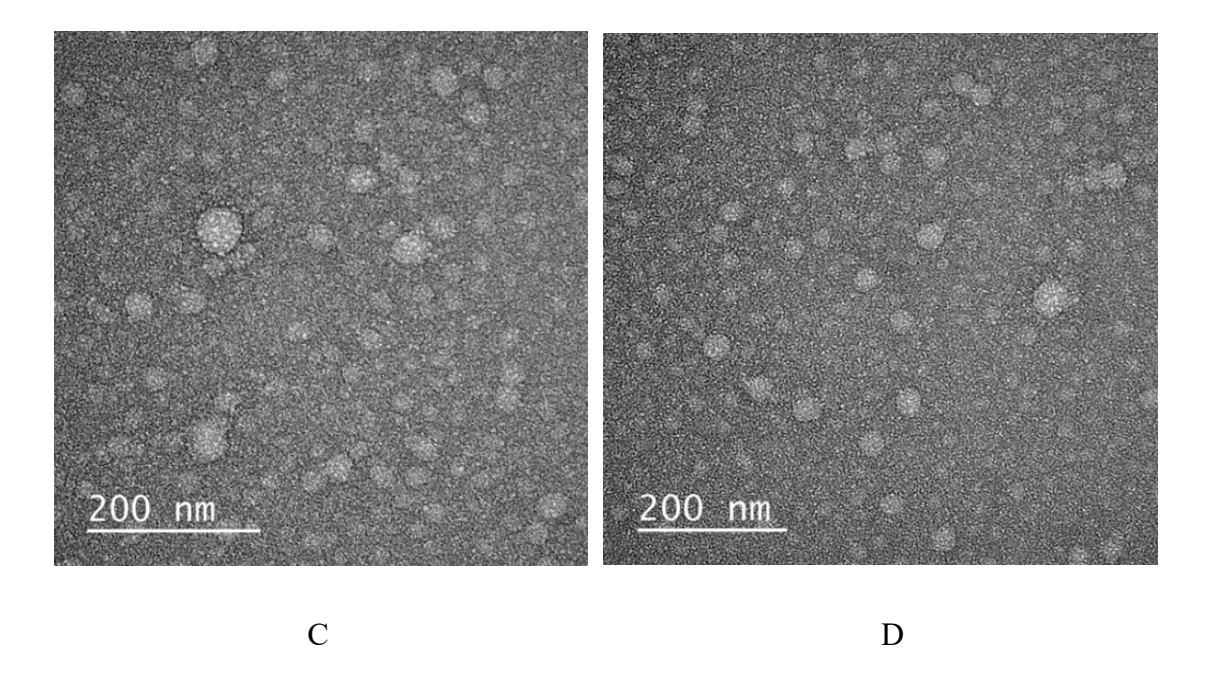


Figure 4-1: TEM images of Bare Niosomes



A B



**Figure 4-2:** TEM images of RB-CUR Loaded Niosomes, at High Magnifications(A,B) and Lower Magnifications(C,D)

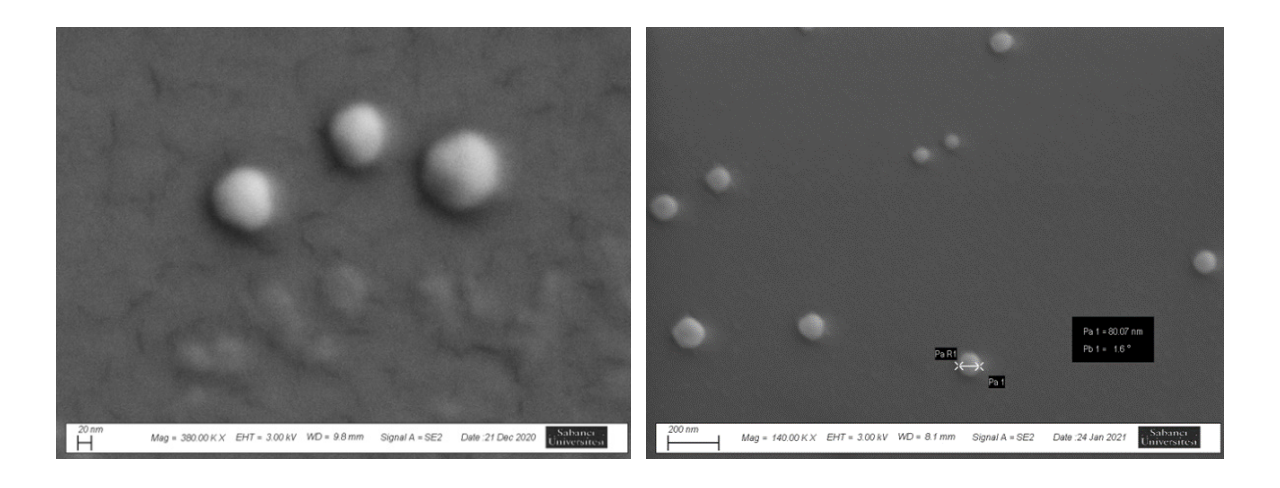


Figure 4-3: SEM images of RB-CUR Loaded Niosomes

# FTIR Analysis of the CSgPVCL and CSgPVCL Coated Niosomes

The FTIR spectra of the grafted polymer is shown in Figure 4-5. In the spectrum of grafted polymer, the presence of chitosan structure was confirmed through the peaks at 1031cm<sup>-1</sup> and 1073 cm<sup>-1</sup> indicating the C<sub>3</sub>-OH and C<sub>6</sub>-OH vibrations in the chitosan chains. Also, the peak at 3355cm<sup>-1</sup> indicate the N-H vibration and 2920cm<sup>-1</sup> and 2856cm<sup>-1</sup> are coherent with the presence of aliphatic C-H groups. The C-C and C-N bonds from the PNVCL structure was detected at 1616cm<sup>-1</sup> and 1478 cm<sup>-1</sup>.

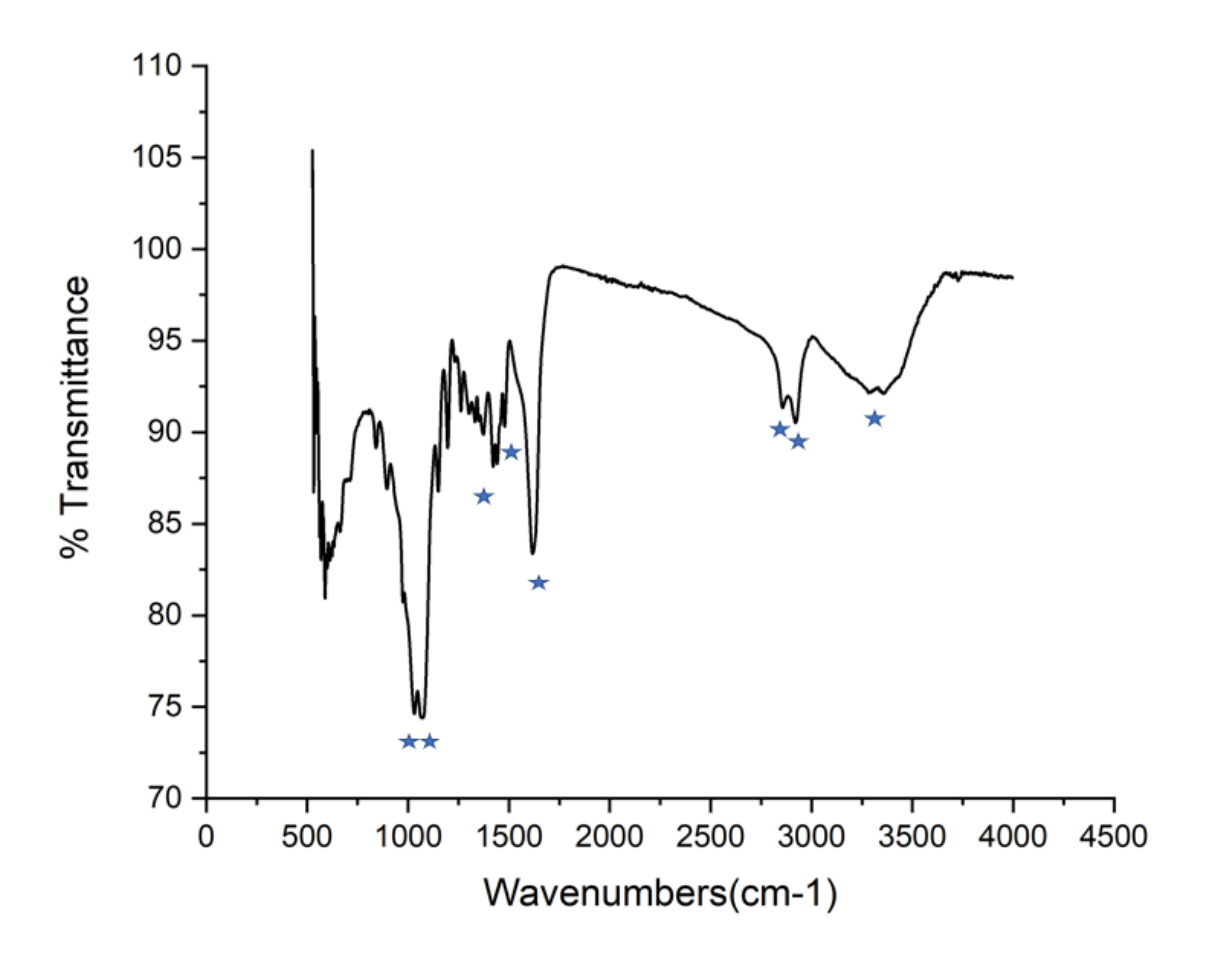
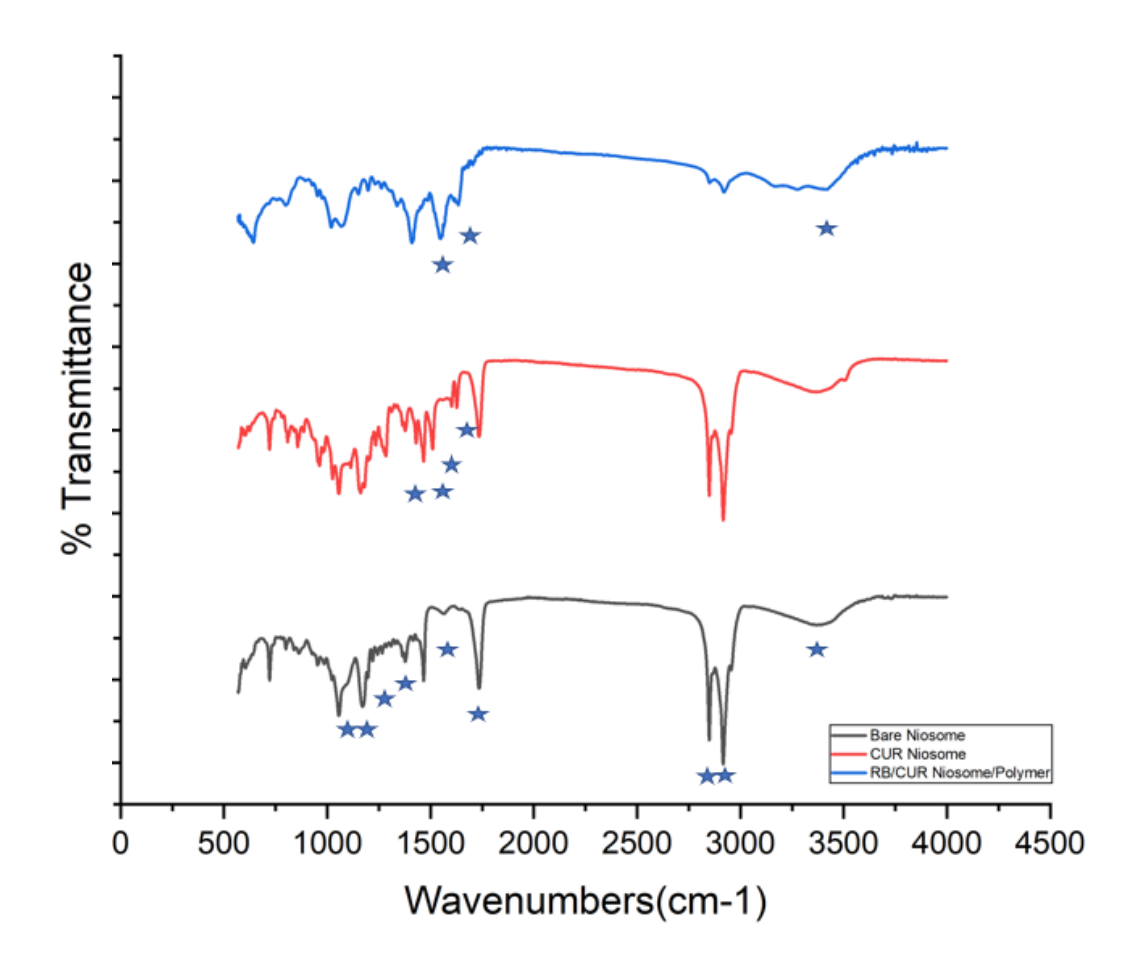


Figure 4-4: FTIR Spectrum of Grafted Polymer



**Figure 4-5:** FTIR Spectrum of Bare Niosome, CUR Niosome and RB/CUR Niosome/Polymer

In the spectrum of bare niosomes, the phenolic compounds were identified at 3368cm<sup>-1</sup>, the presence of alkane groups were detected at 2849cm<sup>-1</sup> and 1466cm<sup>-1</sup> for CH<sub>2</sub> groups, at 1265cm<sup>-1</sup> for CH<sub>3</sub> groups. Besides, the vibrational modes of alkane structure were also observed at 2916cm<sup>-1</sup> and 1377 as CH stretching. Also, C=C stretch from the cholesterol structure was identified at 1564cm<sup>-1</sup>. Besides, the existence of ester groups due to Span60 was confirmed at 1734cm<sup>-1</sup> and 1243cm<sup>-1</sup> as C=O and C-O stretching, respectively. In curcumin loaded niosomes, in addition to the characteristic peaks from the spectrum of bare niosome, new peaks were observed at 1627cm<sup>-1</sup>, 1602cm<sup>-1</sup>, 1430cm<sup>-1</sup> and 1509cm<sup>-1</sup> which are coherent with the presence of alkene group with an aromatic compound, C=C and C-C bonds in the aromatic ring, respectively. These peaks were also observed in the spectrum of curcumin, with small shifts. Following the RB-loaded polymeric coating of niosomes, the presence of nitrogen compounds was detected at 3419cm<sup>-1</sup> and 1548cm<sup>-1</sup>. Besides, the peaks at 1734cm<sup>-1</sup>, 1627cm<sup>-1</sup> and 1430cm<sup>-1</sup> shifted to 1704cm<sup>-1</sup>, 1634cm<sup>-1</sup> and 1410cm<sup>-1</sup>. The peak at 1466cm<sup>-1</sup> and 1430cm<sup>-1</sup> were disappeared and the peak at 1410cm<sup>-1</sup> emerged for indicating the C-C stretching

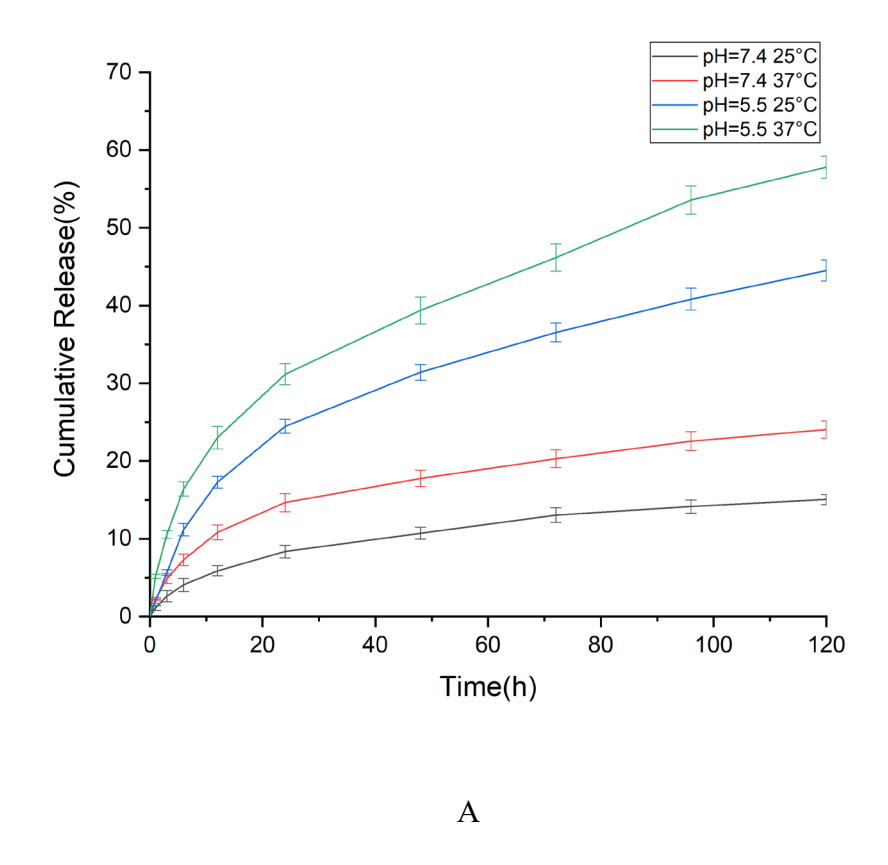
in the aromatic ring. Furthermore, the new peak at 1688 cm<sup>-1</sup> is indicating the carboxylic acid related C=O vibration originated from the rose bengal structure.

# 4.3.2 Drug Release Profile and Kinetic Analysis

Following the obtaining of standard curves for curcumin and rose bengal, encapsulation efficiencies for these 2 drug molecules were calculated as 98,21% for rose bengal and 97,19% for curcumin by using Eq (1) and loading capacities for rose bengal and curcumin were calculated as 8,61% and 7,67% by using Eq (2), respectively.

The nanoparticles were exposed to 2 different pH levels (pH=7.4 and pH=5.5) and temperature (25°C and 37°C). In Figure 4-7, the release profiles for both rose bengal and curcumin were presented. Under all different pH and temperature conditions, sustained-release profiles were observed, and thanks to the presence of temperature and pH-responsive polymeric shell, faster drug release was achieved under acidic condition (pH=5.5) and at 37°C. This phenomenon can be attributed to the protonated amine groups of chitosan. Because this ionization leads to swelling of the polymer under slightly acidic conditions and provides more space for diffusion. Besides, at elevated temperature (>LCST), the conformational change in the structure results in the shrinking of the polymer and promotes faster drug release [94][95].

According to our results, 57,79 % of rose bengal were released at pH=5.5 and at 37°C whereas this amount is 23% at pH=7.4 at and 37°C. On the other hand, these release amounts are 36,40% and 17,71% for curcumin under the same conditions. The resulting nanoparticles displayed faster drug release at acidic pH levels corresponding to the tumor environment. Besides, at 25°C the released amount of rose bengal is 44% at pH=5.5 and only 15 % at pH=7.4. Under the same conditions, these values are 26,75% and only 13% for curcumin, respectively. In addition to pH sensitiveness, temperature-responsive release profiles are related to the presence of a temperature-sensitive polymer, PNVCL in the structure.



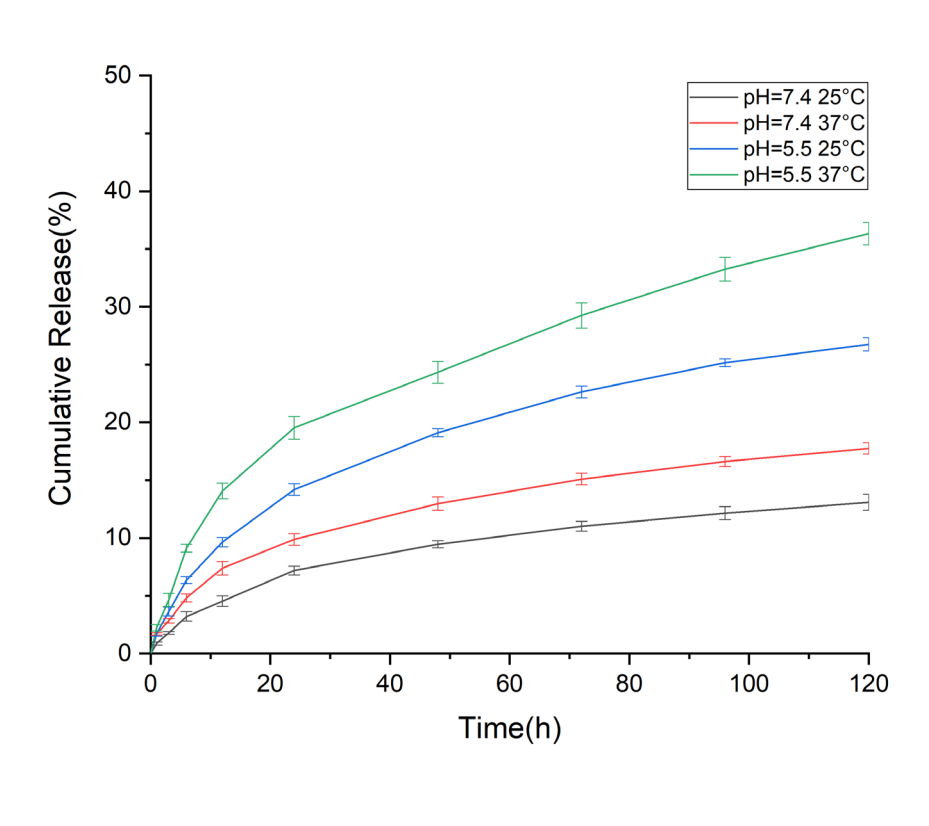


Figure 4-6: Release profile of RB(A) and CUR(B) at different pH levels and temperatures

В

Following the curve fitting processes of all release profiles, the correlation coefficients were presented in Table 4.2. The Korsmeyer Peppas Model has the highest R<sup>2</sup> values (>0.97) among the other kinetic analysis models. The n values for each release profile are above 0.43 which indicates non-Fickian diffusion. In Korsmeyer Peppas Model for spherical geometry, the drug release is coherent with Fickian diffusion in the case of the n value is below 0.43 and this means that the diffusion rate is greater than the polymeric chain relaxation process. In the other extreme condition where n is greater than 0.85, drug release is governed by swelling or relaxation of polymeric chains, and this phenomenon is also correlated with zero-order kinetics. In addition to these 2-extreme conditions, the non-Fickian or in other words the anomalous model is observed where the n value is between 0.43 and 0.85. In this case, the drug release mechanism is governed by both diffusion and swelling [96]. In addition to Korsmeyer Peppas Model, our drug release profiles have great correlation factors with Higuchi Model. However, this model can be applied if the assumptions of the Higuchi Model had been satisfied. These assumptions are the following: (I) perfect sink conditions, (II) unidirectional release, (III) negligible swelling/ dissolution of the matrix, (IV) larger thickness of the dosage form than the size of the drug molecules, and (V) higher initial drug concentration in the matrix than the solubility of the drug molecules [97]. Although we obtained high correlation factors, our release profiles cannot be explained through this model since our system does not satisfy all required assumptions for this model, such as criteria (III) and (V). On the other hand, firstorder release kinetics states that the release rate only depends on the concentration. Also, in Hixson-Crowell Model assumed that the drug release is related to dissolution velocity and is not related to diffusion [98]. In consideration of our n values for these two models, it can be clearly seen that our release profiles are not coherent with these models. They are strongly correlated with Korsmeyer Peppas Model.

**Table 4-2:** Kinetic Model Analysis of the drug release profiles.

Formulation/Model	Korsma Peppas	yer	Higuchi	Zero order	First order	Hixson- Crowell
(RB/CUR)	(R <sup>2</sup> )	(n)	(R <sup>2</sup> )	(R <sup>2</sup> )	(R <sup>2</sup> )	(R <sup>2</sup> )
RB1	0.9943	0.46	0.9615	0.8835	0.6018	0.7204
RB2	0.9806	0.48	0.9705	0.9148	0.6888	0.7816
RB3	0.9954	0.46	0.9806	0.8955	0.6581	0.7569
RB4	0.9730	0.47	0.9234	0.8685	0.6406	0.7306
CUR1	0.9962	0.49	0.9810	0.9032	0.6720	0.7683
CUR2	0.9962	0.47	0.9808	0.9053	0.6499	0.7537
CUR3	0.9954	0.46	0.9797	0.8970	0.6694	0.7635
CUR4	0.9858	0.50	0.9727	0.8909	0.6825	0.7650

RB1: Rose Bengal release profile at pH=5.5 and 25°C RB2: Rose Bengal release profile at pH=5.5 and 37°C RB3: Rose Bengal release profile at pH=7.4 and 37°C CUR1: Curcumin release profile at pH=5.5 and 25°C CUR2: Curcumin release profile at pH=5.5 and 37°C CUR3: Curcumin release profile at pH=7.4 and 37°C CUR3: Curcumin release profile at pH=7.4 and 37°C

#### 4.4 Conclusion

Rose bengal and curcumin loaded niosome polymer composite nanoparticles were prepared successfully. The thin-film hydration method was used to synthesize curcumin loaded niosomes and polymer coating in the presence of rose bengal was performed to obtain polymer-coated niosome based nanocarriers. Nanoparticles displayed sustained drug release profile under different conditions. These release profiles were also analyzed through the current kinetic models in the literature. It is found that drug release profiles are strongly correlated with Korsmeyer Peppas Model and displaying anomalous diffusion behavior. In conclusion, the motivation of this study was to contribute to the design of a novel niosome based controlled release system including both a hydrophilic drug (rose bengal) and a hydrophobic drug (curcumin) for combinational usage in cancer therapy. According to the results, it can be deduced that these nanostructures have the potential for applications in dual drug delivery-based therapies.

# Chapter 5: SELF ASSEMBLY ALBUMIN NANOPARTICLES FOR GLUTATHIONE RESPONSIVE RELEASE OF CURCUMIN

#### 5.1 Introduction

In recent years, protein-based nanoparticles have gained great interest thanks to their outstanding properties such as biocompatibility, biodegradability, and ease in surface functionalization. Albumin is one of the favorable proteins in biomedical applications. In addition to the enhanced permeability and retention (EPR) effect of nanosized materials, albumin is able to bind specific receptors that are upregulated on cancer cells, such as the 60-kDa glycoprotein (gp60) receptor [99]. Therefore, albumin nanoparticles can be considered naturally equipped for enhanced cellular internalization. Furthermore, the functional groups in its structure allow additional surface modifications to increase the therapeutic effect of the resulting nanostructures. For instance, Choi et al. revealed that albumin nanoparticles displayed extended drug release and increased therapeutic efficiency after surface modifications [100].

Albumin nanoparticles can be prepared via various techniques and they are mostly preferred for encapsulation of poorly soluble drugs in water [101]. Desolvation is the most common method among them. Briefly, the aqueous albumin solution is mixed with an organic solvent containing drug molecules. Thereafter, a crosslinker such as glutaraldehyde (GA) is added to stabilize the nanoparticles. Bansal et al. followed this route to prepare albumin nanoparticles for the encapsulation of paclitaxel [102]. This facile synthesis route was also followed with small modifications for other drugs such as curcumin and temozolomide, to overcome their solubility problems [103][104]. However, although it is used in very small amounts, GA has still the potential to pose a risk of toxicity [105][106]. Besides, this chemical crosslinking would lead to the binding of the drug molecules to the protein structure, and/or loss of the functionality of the drug molecules.

This situation has encouraged scientists to find alternative methods against GA-based crosslinking. Self-crosslinking via disulfide bonding can be considered as an alternative approach to preparing stable albumin nanostructures [107]. Utilizing the intermolecular disulfide bonds between albumin proteins enables the preparation of stable nanoparticles without the usage of any toxic chemicals or chemicals that limit the selection of therapeutic agents. Besides, these disulfide bonds make the nanoparticles responsive in a reducing agent environment. In this way, the nanoparticles can be disintegrated in the presence of reducing

agents such as the glutathione(GSH), whereas they keep their stability in blood circulation. This stimulus-responsive property has also great potential for nanomedicine applications in cancer treatment since the GSH concentration in the tumor site is higher than in normal tissue [108]. Therefore, triggered release in a reducing agent environment would be a beneficial strategy for increased therapeutic efficiency. Zhao et al. prepared paclitaxel loaded albumin nanoparticles using intermolecular disulfide bonds for stabilization. Firstly, human serum albumin (HSA) solution was treated with GSH for partially reducing disulfide bonds then tertbuthyl alcohol was used as a desolvating agent and stable albumin nanoparticles were obtained without any extra crosslinking step. Besides, they revealed that the nanoparticles displayed triggered drug release in the GSH environment [109]. Alternatively, this GSHpretreatment step can also be done using mercaptoethanol(ME) instead of GSH [110]. On the other hand, Safavi et al. developed a reducing agent free synthesis of hydrophobic drug loaded albumin nanoparticles, and used curcumin as a model drug. Although they obtained promising results, intense optimization studies such as finding the optimum ionic strength, were required to prepare the nanoparticles in desired properties. Also, they did not analyze the nanoparticles in terms of drug release profile and kinetic analysis [111].

In this study, we synthesized curcumin-loaded albumin nanoparticles stabilized via intermolecular disulfide bonds. L-Glutathione was preferred as a reducing agent. Following the preparation of the nanoparticles, several characterization studies were performed such as size and zeta potential measurements by DLS, morphology analysis by SEM, and chemical makeup analysis by FTIR. Also, encapsulation efficiency and loading capacity of the nanoparticles were determined by UV-Vis spectrophotometer analysis. Furthermore, release kinetic analyses of self assembly albumin nanoparticles were investigated in order to compare our experimental drug release profiles with the current drug release kinetic models.

#### 5.2 Materials and Methods

#### 5.2.1 Materials

Bovine serum albumin(Cas Number: 9048-46-8) and L- Glutathione(Cas Number: 70-18-8) were purchased from Sigma Aldrich.

#### 5.2.2 Methods

#### Synthesis of the Albumin Nanoparticles

Bovine serum albumin (BSA) was dissolved in distilled water at a concentration of 40 mg/mL. Glutathione (50mM) was added in order the break up the intramolecular disulfide bonds and the solution was incubated at room temperature for 1 hour. Then this solution was dialyzed against 1L distilled water at 4°C for 24 hours. After removal of excessive GSH by dialysis, a desolvation agent, ethanol, was added to the BSA solution and the resulting solution was left for 12 hours at moderate stirring for the stabilization of the nanoparticles. Finally, the nanoparticles were centrifugated 3 times at 14.000 rpm for 30 minutes and then lyophilized for 2 days for further usage.

In curcumin-loaded albumin nanoparticles, 1 mg of curcumin was dissolved in ethanol and the same procedure was followed for nanoparticle synthesis.

#### **Characterization of the Albumin Nanoparticles**

Hydrodynamic size, dispersity, and zeta potential values were measured using ZetaSizer Nano ZS (Malvern Instruments, UK) instrument, which contains a 4.0 mV Helium-Neon laser (633 nm). Size analysis was performed at varying temperature and pH levels at 25 °C. The size and morphology of the bare and curcumin loaded albumin nanoparticles were assessed by a field-emission scanning electron microscope (Zeiss Leo Supra 35VP SEM-FEG, Germany) at a 3kV operating voltage. 10ul of the nanoparticles were dropped on a piece of the silicon wafer and dried for 5h at room temperature. The dried samples were coated with Au-Pd using a sputter coater (Cressington 108, UK) at 40mA for 120s. The SEM images were obtained by the secondary electron (SE) detector. Chemical makeup analysis was performed by using Fourier-Transform Infrared Spectroscopy (Thermo Scientific, Nicolet, iS10, USA). The scanning range for the analysis was 4,000–400 cm<sup>-1</sup>.

#### **Drug Release Studies and Kinetic Analysis**

Encapsulation efficiency and loading capacity were calculated using UV-Vis spectrophotometer. The amounts of curcumin in the supernatant were determined using the calibration curve and the encapsulation efficiency was calculated Equation 1. Furthermore, the solution of curcumin loaded albumin nanoparticles was freeze-dried and weighed. The loading capacity of curcumin loaded nanoparticles was determined via Equation 2.

In release studies, curcumin loaded nanoparticles were poured into dialysis capsules with a cellulose membrane of 12-14 kDa. The capsules were placed in beakers containing 30 ml of PBS-T (1%Tween 80) at pH=7.4 with or without 10mM GSH. They incubated in shaking incubators at 37°C. The samples were taken at several time intervals as 1-3-6-12-24-48-72-96-120 hours. Curcumin amounts in the samples were determined via UV-Vis analysis and the calibration curves. The drug release profile was plotted as cumulative drug release (%) versus time. The resulting release profiles were analyzed by curve fitting studies on several kinetic models in the literature and the results were compared through their R<sup>2</sup> values.

#### 5.3 Results and Discussion

# **5.3.1** Characterization of the Albumin Nanoparticles

# **DLS Analysis of the Albumin Nanoparticles**

The average size and polydispersity index values of bare albumin nanoparticles and curcumin loaded albumin nanoparticles were shown in Figure 5-1 and Figure 5-2, respectively. According to the results, bare albumin nanoparticles have a hydrodynamic diameter of around 137 nm with 0,074 PDI. The size and dispersity of the nanoparticles are quite similar in curcumin loaded albumin nanoparticles and they are around 140 nm with 0,077 PDI. The zeta potential distributions of the nanoparticles are shown in Figure 5-3 and Figure 5-4 respectively. They have a positive surface charge of 20.6 mV and 19.2 mV for bare and loaded nanoparticles, respectively. These indicate stable nanoparticle suspensions with acceptable surface charges.

			Size (d.nm):	% Intensity:	St Dev (d.nm):
Z-Average (d.nm):	137,9	Peak 1:	148,9	100,0	41,97
Pdl:	0,074	Peak 2:	0,000	0,0	0,000
Intercept:	0,961	Peak 3:	0,000	0,0	0,000
Result quality :	Good				

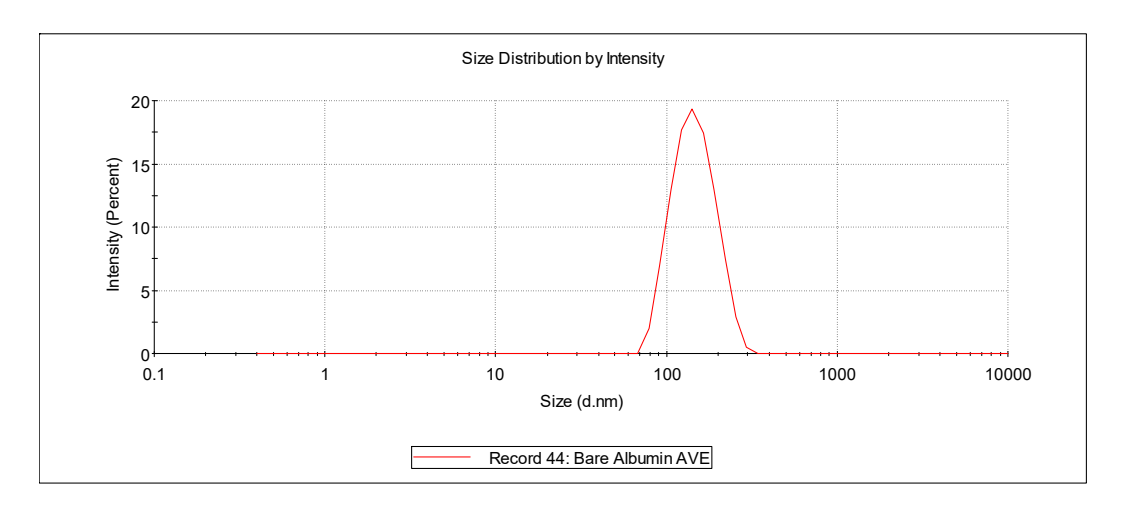


Figure 5-1: DLS Average Size Analysis of Bare Albumin Nanoparticles

			Size (d.nm):	% Intensity:	St Dev (d.nm):
Z-Average (d.nm):	140,9	Peak 1:	152,9	100,0	44,69
Pdl:	0,077	Peak 2:	0,000	0,0	0,000
Intercept:	0,956	Peak 3:	0,000	0,0	0,000
Result quality :	Good				

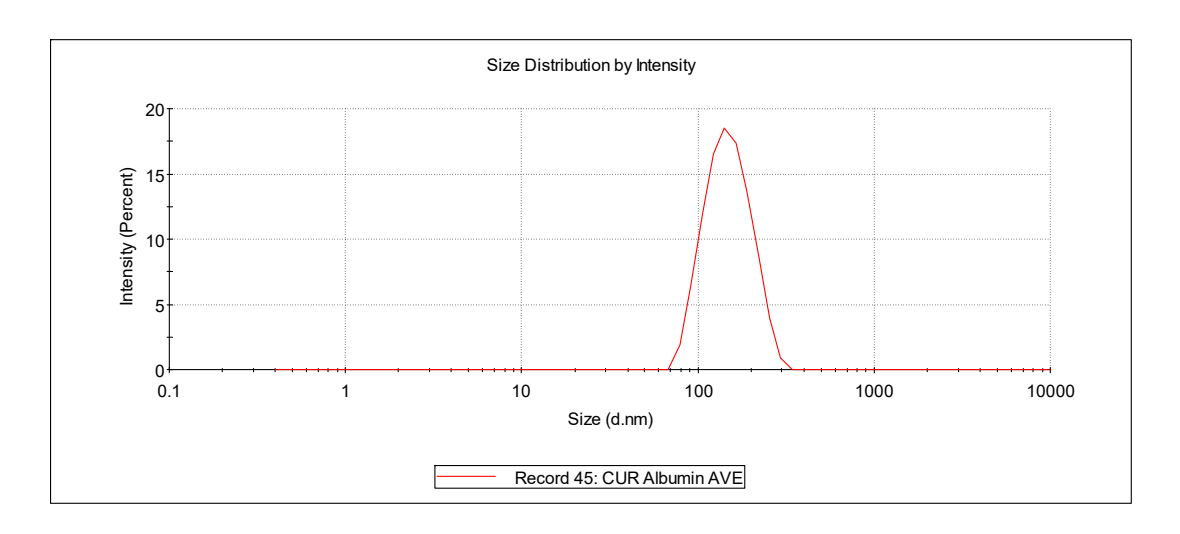


Figure 5-2: DLS Average Size Analysis of Loaded Albumin Nanoparticles

			Mean (mV)	Area (%)	St Dev (mV)
Zeta Potential (mV):	20,6	Peak 1:	20,6	100,0	4,80
Zeta Deviation (mV):	4,80	Peak 2:	0,00	0,0	0,00
Conductivity (mS/cm):	0,0768	Peak 3:	0,00	0,0	0,00

Result quality: Good

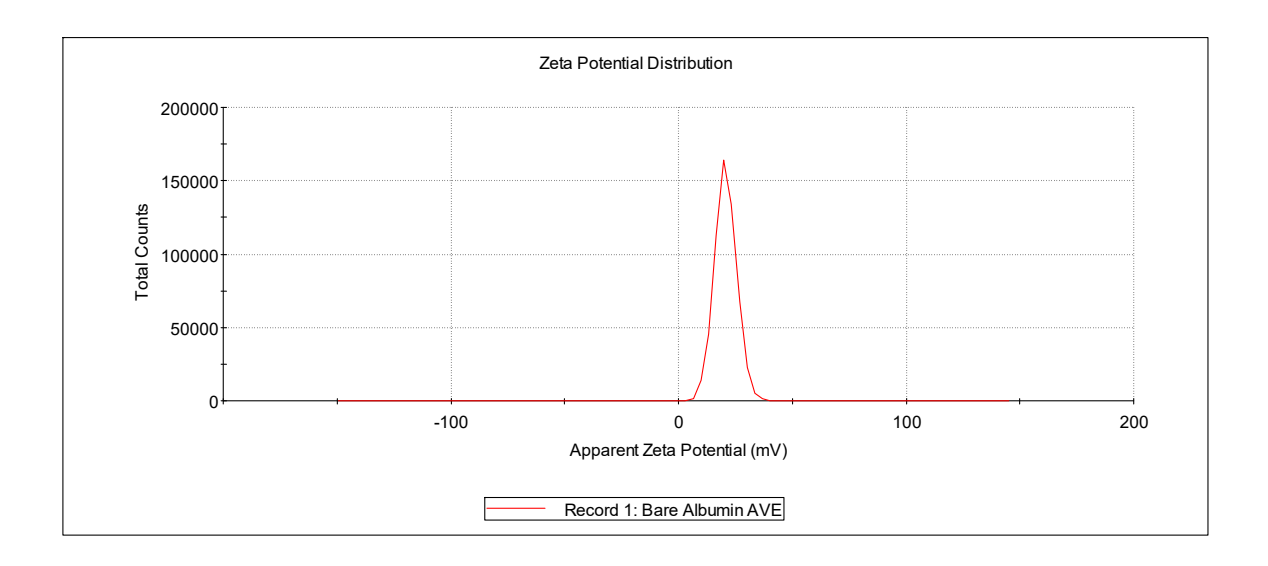


Figure 5-3: Zeta Potential Distribution of Bare Albumin Nanoparticles

			Mean (mV)	Area (%)	St Dev (mV)
Zeta Potential (mV):	19,2	Peak 1:	19,2	100,0	5,07
Zeta Deviation (mV):	5,07	Peak 2:	0,00	0,0	0,00
Conductivity (mS/cm):	0,0736	Peak 3:	0,00	0,0	0,00
Descrit accelites					

Result quality : Good

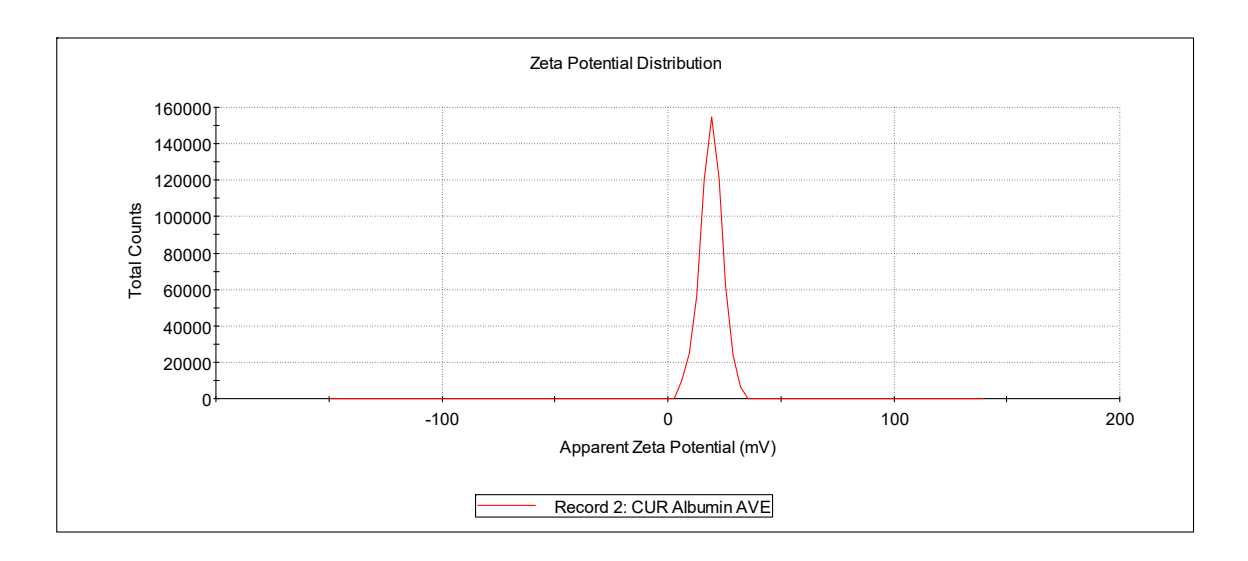


Figure 5-4: Zeta Potential Distribution of Loaded Albumin Nanoparticles

#### **SEM Analysis of the Albumin Nanoparticles**

The spherical morphology of albumin nanoparticles was confirmed using scanning electron microscopy (SEM). It is observed that albumin nanoparticles are not as spherical as polymeric nanoparticles. On the other hand, the size of the nanoparticles is around 100 nm. The difference between the size values obtained by DLS and SEM can be attributed to the measurement principles of dynamic light scattering and electron microscopy techniques. The nanoparticles are found as smaller than their hydrodynamic size measured by DLS since the DLS measurement is based on a mathematical model fitting processes considering some parameters of the nanoparticles and solvents, such as refractive index and absorption value of the material and viscosity of the solvent. Here the measured size value is called hydrodynamic size since it includes the solvent molecules around the nanoparticles. However, there is no such type of situation in the electron microscopy techniques because the sample should be prepared in dried form. Therefore, it is logical to observe different size values between two measurements and smaller size values in electron microscopy analysis.

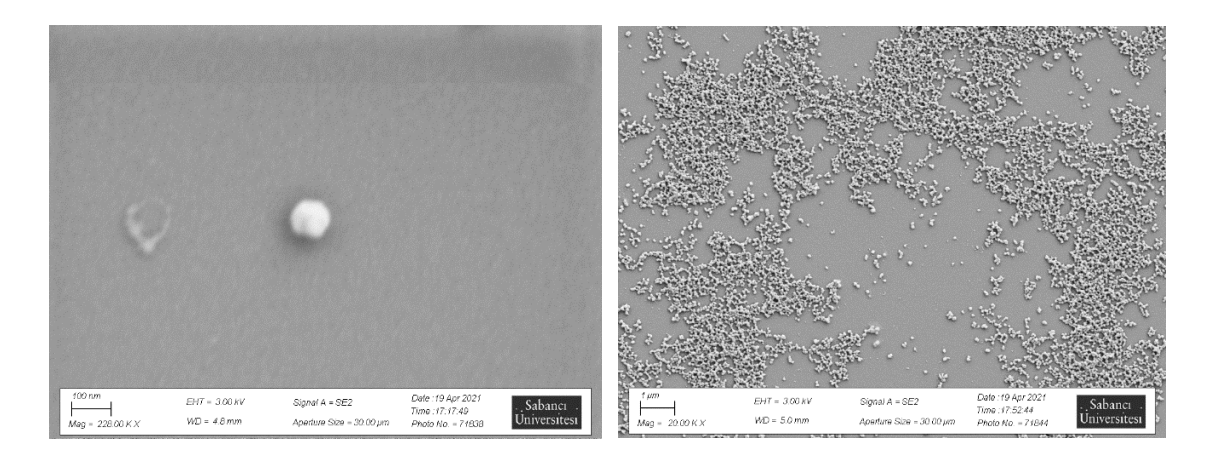


Figure 5-5: SEM Images of Bare Albumin Nanoparticles

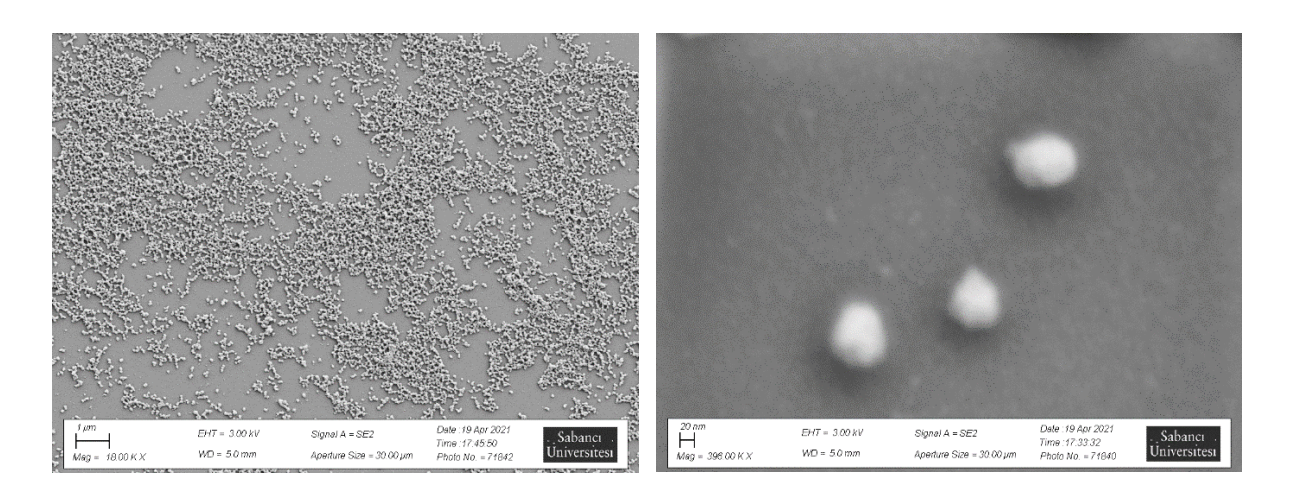
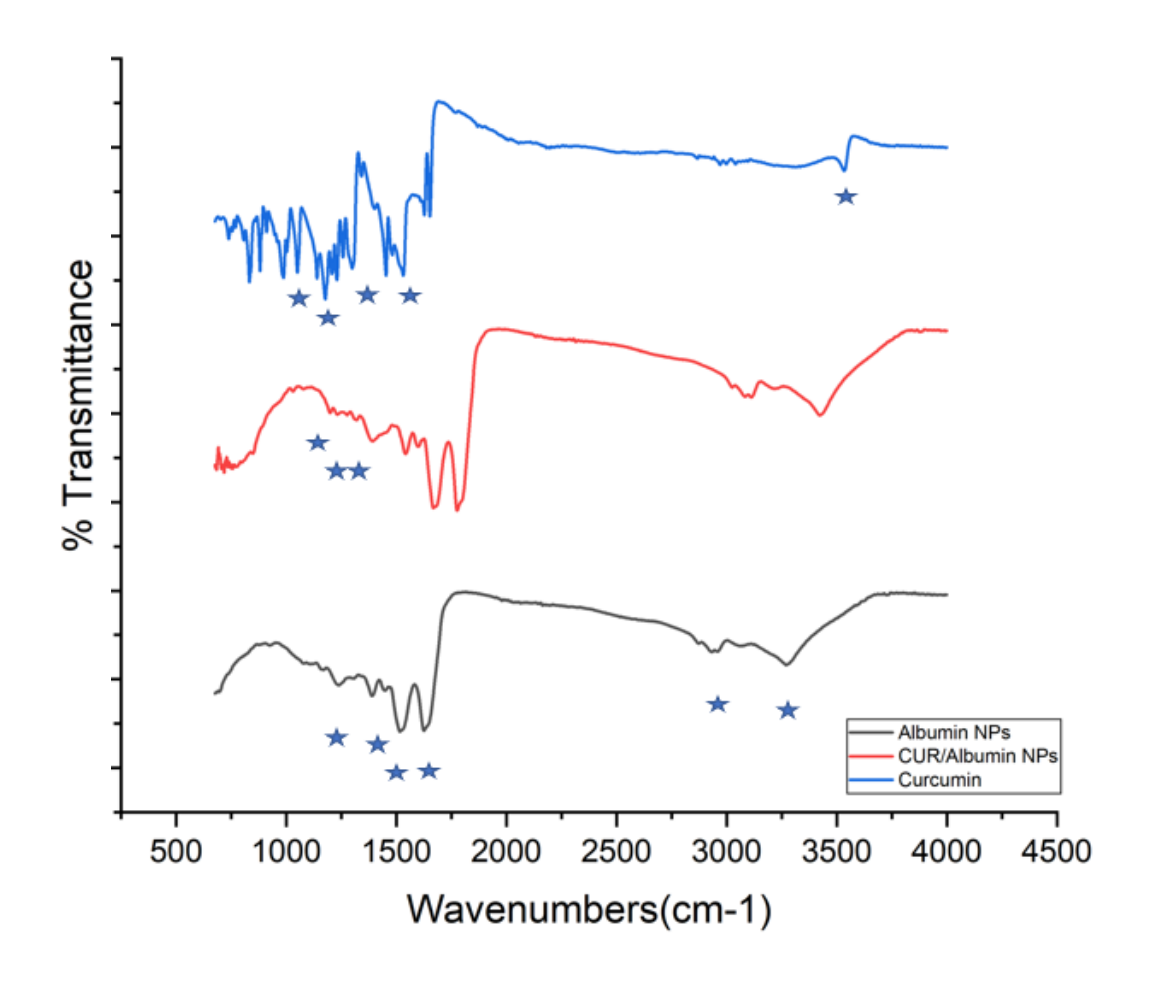


Figure 5-6: SEM Images of Curcumin Loaded Albumin Nanoparticles

#### FTIR Analysis of the Albumin Nanoparticles

The FTIR spectrum of bare albumin nanoparticles, curcumin loaded albumin nanoparticles and curcumin were shown in Figure 5-7. In the spectrum of albumin nanoparticles, the phenolic compound and the presence of carboxylic acid groups were identified at 3270 cm<sup>-1</sup> and 2933cm<sup>-1</sup>. The vibrational modes related to N-H bending and N-O stretching were detected at 1625cm<sup>-1</sup> and 1516 cm<sup>-1</sup>. Also, C-H bending in the protein structure was detected at 1390 cm<sup>-1</sup>. In addition to O-H stretching at 3270cm<sup>-1</sup>, C-O stretching belongs to the carboxylic acid groups was identified at 1237cm<sup>-1</sup>. In the case of curcumin loaded albumin nanoparticles, new peaks corresponding to the existence of curcumin molecules were observed at 1125cm<sup>-1</sup>, 1048cm<sup>-1</sup> and 879cm<sup>-1</sup>. These indicate the C-H stretching in the aromatic ring and C-O stretching in the alcohol group and C-O stretching in the ether group on the curcumin structure. Also, a small shift was observed as 1237 cm<sup>-1</sup> from the bare albumin nanoparticles to 1241 cm<sup>-1</sup> from the curcumin-loaded albumin nanoparticles.



**Figure 5-7 :** FTIR Spectrum of Bare Albumin Nanoparticles, Curcumin Loaded Albumin Nanoparticles and Curcumin

## 5.3.2 Drug Release Studies and Kinetic Analysis

According to the standard curve for curcumin, the encapsulation efficiency of albumin nanoparticles was calculated as 83,22% by using Eq. (1) and loading capacity was calculated as 8,33%. by using Eq. (2).

Figure 5-8 shows the curcumin release from the albumin nanoparticles under two different environmental conditions, as pH=7.4 and pH=7.4 with 10 mM GSH. The nanoparticles are able to perform sustained drug release profiles and curcumin release is faster in the GSH environment due to the breaking of intermolecular disulfide bonds in the presence of GSH. This leads to the disruption of the nanoparticles and results in faster diffusion of curcumin molecules. This situation can be explained through the current kinetic models in the literature. In the case of a GSH free environment, the drug release profile of the albumin nanoparticles is

correlated with Korsmeyer Peppas Model with a 0.95 R<sup>2</sup> value. Besides the n value of the model is 0.44 which indicates a non-Fickian/Anomalous drug transportation profile (0.43<n<0.89). This means that the drug release is governed by both diffusion and drug-carrier interactions. In the presence of GSH, curcumin release from the albumin-based carrier matrix was strongly affected and the n value became 0.68 with the R<sup>2</sup> as 0.99. The release profile is still anomalous but with a higher n value. It became closer to 0.85, indicating the change in the release kinetics. This increase can also be analyzed by the correlation factor of the drug release profiles in the Zero Order Kinetic Model. Because drug release starts to be coherent with Zero Order Kinetic Model when the n value approaches 0.85, for the carriers in the form of spherical morphology. The R<sup>2</sup> value of the Zero Order Kinetic Model in the GSH free environment is 0.76, it became 0.98 in the GSH environment. Also, curcumin release in the GSH environment displayed a good correlation with Hixson-Crowell Model, as R<sup>2</sup>=0.94. This can be attributed to the erosion of nanoparticles due to the disruption of disulfide bonds with GSH and the disintegration of the nanostructures. These differences in release kinetics under two different conditions demonstrate that the ability of albumin nanoparticles to display redox responsive drug release profile.

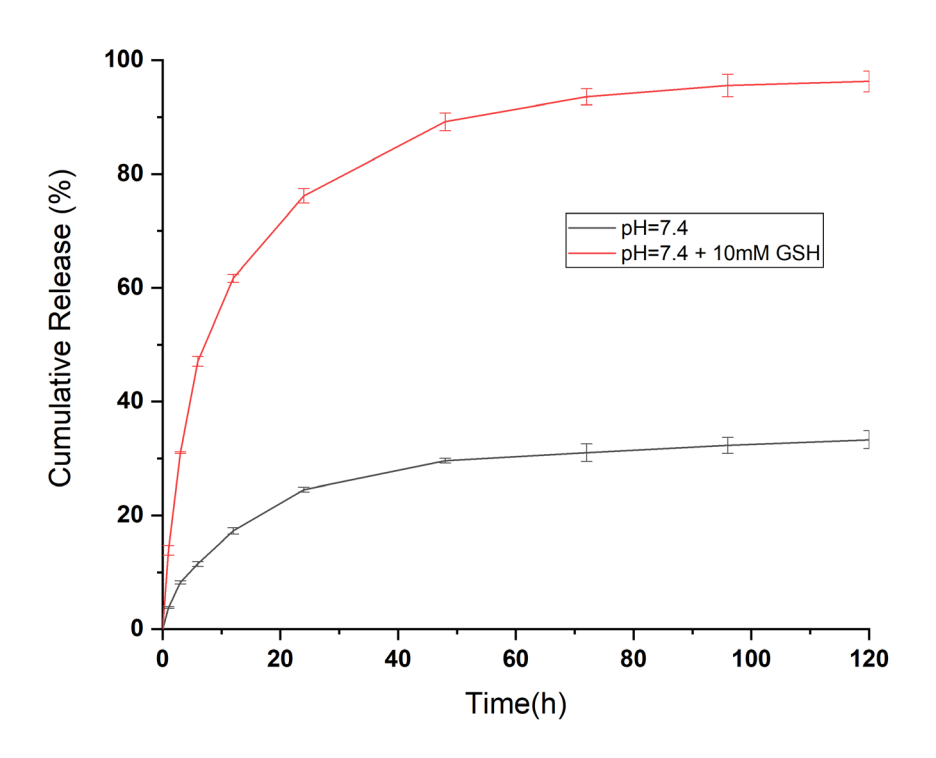


**Figure 5-8 :** Drug Release Profiles of Curcumin in Physiological Environment and GSH environment

Table 5-1: Table of Release Kinetic Analysis of CUR Loaded Albumin Nanoparticles

Formulation/Model	Korsme Peppas	yer-	Higuchi	Zero order	First order	Hixson- Crowell
CUR	(R <sup>2</sup> )	(n)	(R <sup>2</sup> )	(R <sup>2</sup> )	(R <sup>2</sup> )	(R <sup>2</sup> )
CUR1	0.95	0.44	0.75	0.76	0.58	0.65
CUR2	0.99	0.68	0.91	0.98	0.91	0.94

CUR 1: Curcumin release at PBS-T at pH=7.4

CUR 2: Curcumin release at PBS-T at pH=7.4 + 10mM GSH

## 5.4 Conclusion

Curcumin-loaded self-assembly albumin nanoparticles were successfully prepared using the intermolecular disulfide bonding assisted desolvation method. Nanoparticles were characterized in terms of size, zeta potential, dispersity index, morphology, chemical makeup, and release kinetic analysis. The redox responsiveness provided by disulfide bonds of the nano albumin particles was confirmed through the drug release tests under different conditions. Nanoparticles displayed sustained drug release profile at physiological pH level whereas they started to disintegrate in GSH environment and displayed faster drug release profile. The change in release profiles was detected by release kinetic analysis. In conclusion, curcumin release from the albumin nanoparticles under two different conditions is strongly correlated with non-Fickian diffusion in the Korsmeyer Peppas Model (R<sup>2</sup>>0.95).

# Chapter 6: A FACILE ROUTE FOR NANOPARTICLES-ASSOCIATED ELECTROSPUN PATCHES AS IMPLANTABLE DRUG DELIVERY SYSTEMS

#### 6.1 Introduction

The combinational delivery of therapeutic agents has been considered a promising strategy to overcome the limitations of traditional approaches. Administration of multiple drugs using a single platform has been reported as a strongly effective approach in preventing tumor reoccurrence and suppressing drug resistance. Also, the usage of multiple drugs can create a synergistic effect and results in enhanced toxicity in the site of action [112][113]. In recent years, there has been considerable interest in the development of polymeric nanostructures for co-delivery therapeutic drugs for advanced nanomedicine applications.

Nanoparticles synthesized from biocompatible materials are one of the promising tools as drug carriers in combinational drug delivery. They can favor cellular uptake thanks to their physicochemical properties such as size, shape, and surface charges and allow several surface modifications through their functional groups. Feng et al. designed mesoporous silica nanoparticles coated with lipid layer and observed a synergistic therapeutic effect on cell proliferation, growth, and angiogenesis in various cancer types such as liver and cervical cancers [114]. Soni et al. observed similar effects on breast cancer cells using PLGA nanoparticles for the delivery of paclitaxel and thymoquinone [115]. Although these studies demonstrate the effectiveness of the nanoparticles in multiple drug delivery applications, the administration of the nanoparticles is still an issue. They require several modifications to reach the targeted site without having a problem such as elimination by immune cells, and drug leakage during the pathway to the target area. Besides, directionless, and rapid diffusion behavior of the nanoparticles due to their smaller size is still a drawback.

On the other hand, nanofibers can be considered superior nanomaterials from this standpoint. They can be easily placed onto the diseased area, act as implantable drug delivery systems and release their cargo in a sustained manner [116]. For instance, Davani et al. prepared core-sheath electrospun nanofibers containing two different drug molecules in the core and sheath separately. Their results indicated that co-delivery of multiple drugs from a single carrier provided excellent toxicity against diabetic foot ulcer disease [117]. However, the main disadvantage of this technique is the requirement of intense effort for the optimization of the

electrohydrodynamic behavior of the core-sheath electrospinning process [118]. This brings additional equipment, complex systems, and finding proper polymer solutions in order to optimize all experimental parameters for the fine core-sheath nanofibers. Besides, the drug molecules lack carriers that can favor their cellular uptake, and the release kinetics of therapeutic agents is limited with only a fibrous structure.

All these efforts indicate that there is a growing demand for combinational drug delivery via facile route. The association of nanoparticles with electrospun patches can be considered a promising strategy to overcome the limitations and to combine the advantages of each approach. Electrospinning of a polymer solution including nanoparticles is one of the most common methods for this purpose. There are numerous studies on electrospinning of nanoparticle-containing polymer solution or co-electrospinning/electrospraying process to obtain nanoparticle incorporated fibrous patches [119]–[121]. However, nanoparticles become embedded position in this approach. Therefore, detachment of the nanoparticles from the nanofibers and drug release from the nanoparticles will also be affected by the presence of fibrous structures. Furthermore, mixing nanoparticles with the polymer solution affects the electrospinning conditions and leads to additional experimental optimizations. Sydow et al. used a layer by layer (LBL) deposition technique and obtained multilayer electrospun polycaprolactone (PCL) patches incorporated with chitosan nanoparticles [122]. Due to the principles of LBL deposition, they had to prepare an additional polymeric layer that will act as a polyanionic surface against polycationic nanoparticles, and the nanoparticles were attached by the dip coating method. Tsao et al. preferred surface functionalization through 1-ethyl-3-(3dimethylaminopropyl) carbodiimide /N-hydroxysuccinimide (EDC/NHS) coupling in order to immobilize silica nanoparticles onto poly(DLlactide-co-glycolide) acid (PLGA) electrospun patches [123]. Although chemical coupling showed promising results, creating chemical bonds between the functional groups of the nanoparticle and nanofiber structures would not be applicable for all types of polymeric materials and drugs. This type of chemical coupling requires appropriate functional groups and can lead to undesirable consequences such as loss of functionality of the polymer or drugs used.

In this study, we focused on the deposition of rose bengal (RB) loaded chitosan nanoparticles on curcumin (CUR) loaded polycaprolactone (PCL) electrospun patches for multiple drug delivery applications via a facile route. Firstly, curcumin, a hydrophobic model drug, loaded polycaprolactone nanofibers were fabricated. In the meantime, rose bengal, a hydrophilic model drug, loaded chitosan nanoparticles were synthesized via the ionic gelation method.

Finally, nanoparticles were sprayed onto the electrospun patch using a commercial airbrush. Scanning electron microscopy (SEM) was used to analyze the morphology of the resulting nanoplatforms, and fourier-transform infrared spectroscopy (FTIR) was utilized for the chemical makeup analysis. The average size and zeta potential of the nanoparticles were measured using dynamic light scattering (DLS). The ultraviolet-visible (UV-Vis) spectrophotometer was used for the calculation of encapsulation efficiency of the nanoparticles, and the release profile of the resulting complex structure. Presented data provides novel scientific evidence for fulfilling the requirements of multiple drug delivery systems with the ability to provide dual release of rose bengal and curcumin in different profiles.

#### **6.2** Materials and Methods

#### 6.2.1 Materials

Chitosan (75–85% deacetylated, low molecular weight, CAS no. 9012-76-4), PCL (Mn = 80,000) and sodium tripolyphosphate (TPP, CAS no. 7758-29-4), were from Sigma–Aldrich. Acetic acid (CAS no. 64-19-7) were purchased from Merck.

#### 6.2.2 Methods

#### Fabrication of the Polycaprolactone (PCL) Nanofibers

20% PCL solution(w/v) was prepared using acetic acid and then stirred for 24 h to obtain a homogenous polymer solution. Nanofibers were collected onto a 10 cm x 10 cm collector covered with aluminum foil, using a high voltage supply, syringe pump, stainless steel spinneret needle, and 2 ml syringe. The process parameters were 13 cm distance, 10 kV applied voltage and 0.3 ml/h flow rate. Curcumin-loaded PCL nanofibers were fabricated dissolving 1mg of curcumin in PCL solution and mixed for 1h to obtain homogenous dispersion and the same electrospinning route was followed.

## **Synthesis of the Chitosan Nanoparticles**

Chitosan (CS) nanoparticles were prepared using the ionic gelation method. 10 mg of chitosan was dissolved in 50 ml, 1%(v/v) aqueous acetic acid solution then stirred overnight. 5 mg of sodium tripolyphosphate (TPP) was dissolved in 10ml distilled water. This solution was then added to the chitosan solution in a 1:3 ratio and the final solution mixed at 500 rpm for 15 minutes. In rose bengal loaded nanoparticles, 50 ul of rose bengal stock solution(10mg/ml)

were mixed with TPP solution and then the same procedure was followed. Following the synthesis, nanoparticles were centrifugated at 30.000 rpm, 4°C for 45 minutes, and freezedried.

#### Deposition of the Chitosan Nanoparticles onto the PCL Nanofibers

Freeze-dried nanoparticles were dispersed in 2 ml distilled water and sprayed onto nanofibers using a commercial airbrush. The distance between the airbrush and electrospun samples was kept as 15 cm. Nanoparticles decorated electrospun patches were incubated in a vacuum oven at 40 °C for 24 h. The overall experimental steps were illustrated in Figure 6-1.

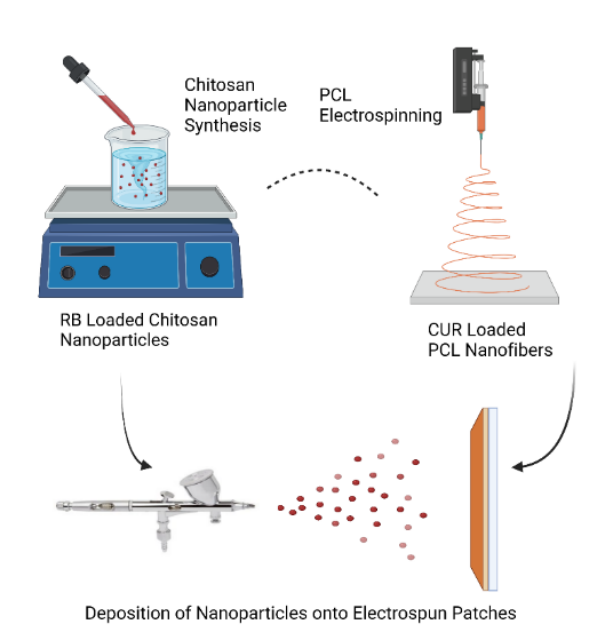


**Figure 6-1 :** Experimental Processes for the Fabrication of Nanoparticles Associated Electrospun Patches

#### Characterization of the Chitosan Nanoparticles and PCL Nanofibers

Hydrodynamic size, dispersity, and zeta potential values were measured using ZetaSizer Nano ZS (Malvern Instruments, UK) instrument, which contains a 4.0 mV Helium-Neon laser (633 nm). Nanoparticles and nanofibers were imaged by field emission scanning electron microscopy (Zeiss, Leo Supra VP35) with an accelerating voltage of 3 kV. Briefly, 3 ul of the nanoparticles were dropped on a piece of the silicon wafer and dried for 5 hours at room temperature. In the meantime, nanofibers were placed onto carbon tape adhered to a silicon wafer. The samples were coated with Au-Pd using a sputter coater (Cressington 108) at 40 mA for 120 s. The SEM images were obtained by the secondary electron (SE) and In-Lens

detectors. Chemical makeup analysis was performed by using Fourier-Transform Infrared Spectroscopy (Thermo Scientific, Nicolet, iS10, USA). The scanning range for the analysis was 4,000–400 cm<sup>-1</sup>.

#### **Drug Release Studies and Kinetic Analysis**

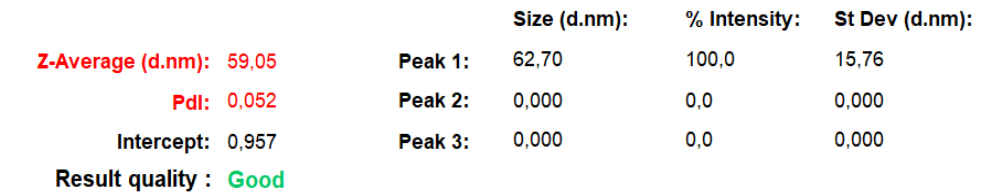
Encapsulation efficiency and loading capacity were evaluated using UV-Vis spectrophotometer. The amount of rose bengal in the supernatant was determined using the calibration curve and the encapsulation efficiency was calculated with Equation 1. Furthermore, following the freeze-drying process, RB loaded chitosan nanoparticles were weighed. The loading capacity of dual drug-loaded nanoparticles was determined via Equation 2.

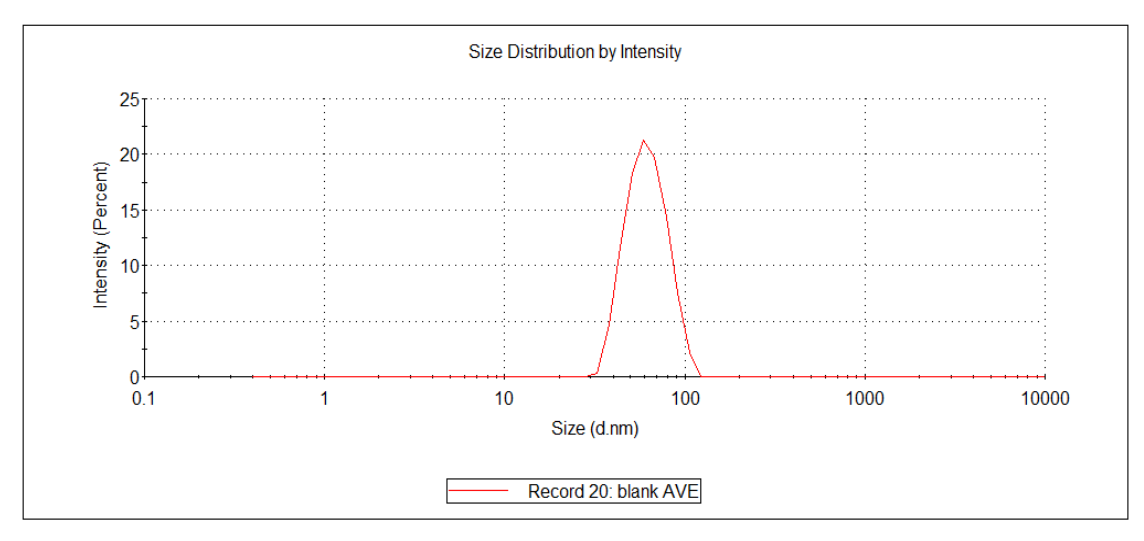
In release studies, 2 cm x 2 cm of electrospun patches including rose bengal in the nanoparticles and curcumin in the nanofibers were placed in dialysis capsules with a cellulose membrane of 12-14 kDa. The capsules were placed in beakers containing 30 ml of PBS-T (1%) at pH=7.4. They were incubated in a shaking incubator at 37°C. The samples were taken at several time intervals as 1-3-6-12-24-48-72-96-120 hours. Rose bengal and curcumin amounts in the samples were determined via UV-Vis analysis using calibration curves prepared in identical conditions. The drug release profile was plotted as cumulative drug release (%) versus time. The resulting release profiles were fitted on Korsmeyer Peppas Model.

#### 6.3 Results and Discussion

# 6.3.1 Characterization of the Chitosan Nanoparticles and PCL Nanofibers DLS Analysis of the Chitosan Nanoparticles

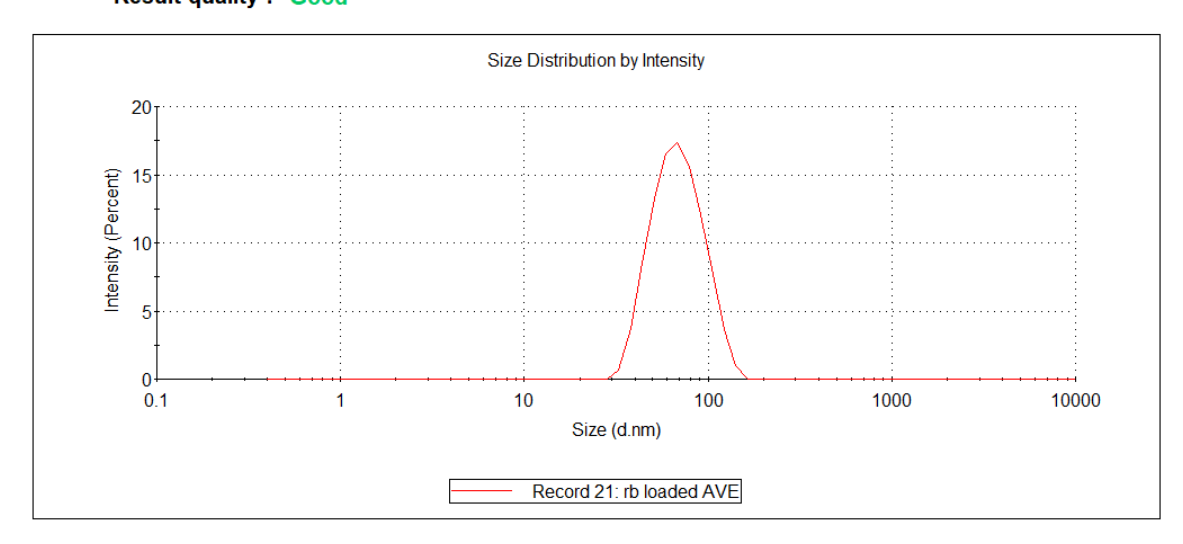
Dynamic light scattering (DLS) is one of the most common characterization techniques to determine the hydrodynamic size of the nanoparticles together with their dispersion behavior in the solution. In our study, bare chitosan nanoparticles have 59,05 nm average particle size and 0,052 polydispersity index (PDI) value. On the other hand, rose bengal loaded chitosan nanoparticles are with 64,58 nm average particle size and 0,090 PDI. (Figure 6-2). Moreover, the zeta potential values of bare and RB loaded nanoparticles were found as 15,6 mV and 13,5 mV, respectively. (Figure 6-3) In rose bengal loaded chitosan nanoparticles, the encapsulation efficiency was evaluated as 92,24% by using Equation 1 and the loading capacity was calculated as 6,06% by using Equation 2.





A

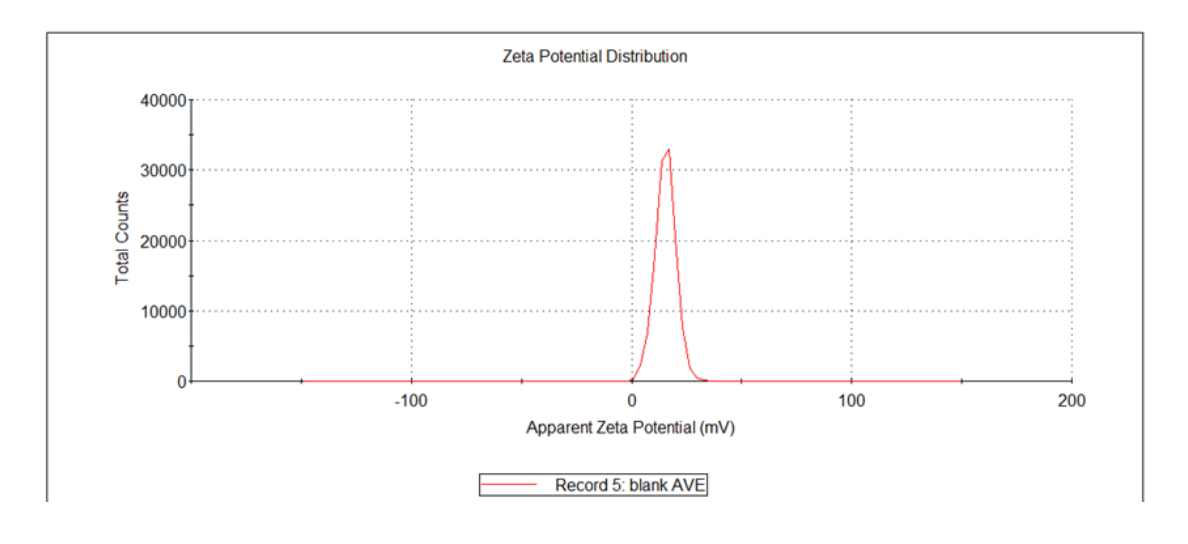
			Size (d.nm):	% Intensity:	St Dev (d.nm):
Z-Average (d.nm):	64,58	Peak 1:	70,97	100,0	22,26
PdI:	0,090	Peak 2:	0,000	0,0	0,000
Intercept:	0,943	Peak 3:	0,000	0,0	0,000
Result quality:	Good				



В

Figure 6-2 : DLS Average Size Analysis of Bare Chitosan Nanoparticles (A) and RB Loaded Chitosan Nanoparticles (B)

			Mean (mV)	Area (%)	St Dev (mV)
Zeta Potential (mV):	15,6	Peak 1:	15,4	100,0	4,75
Zeta Deviation (mV):	4,69	Peak 2:	0,00	0,0	0,00
Conductivity (mS/cm):	1,21	Peak 3:	0,00	0,0	0,00
Result quality :	Good				



 $\mathbf{C}$ 

			Mean (mV)	Area (%)	St Dev (mV)
Zeta Potential (mV):	13,5	Peak 1:	12,9	100,0	5,87
Zeta Deviation (mV):	12,3	Peak 2:	0,00	0,0	0,00
Conductivity (mS/cm):	1,42	Peak 3:	0,00	0,0	0,00
Result quality :	Good				

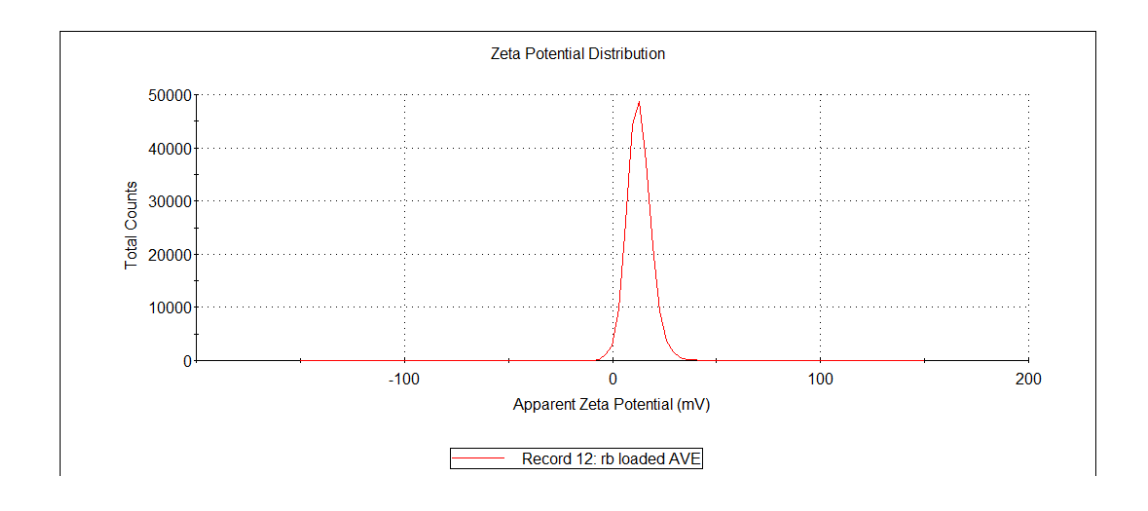


**Figure 6-3 :** Zeta Potential Analysis of Bare Chitosan Nanoparticles (C) and Loaded Chitosan Nanoparticles (D)

D

#### **SEM Analysis of the PCL Nanofibers and Chitosan Nanoparticles**

The morphology of bare and curcumin loaded PCL nanofibers, bare chitosan nanoparticles, rose bengal loaded chitosan nanoparticles and curcumin loaded PCL nanofibers decorated with rose bengal loaded chitosan nanoparticles were analyzed using scanning electron microscopy (SEM). The spherical morphology of the nanoparticles was confirmed by electron microscopy analysis, and it is observed that the size of the nanoparticles is coherent with the DLS results. Here, it is worth emphasizing that the size differences between the DLS and SEM analysis stem from the measurement principles of DLS and SEM techniques. In dynamic light scattering, the measured size is called hydrodynamic size since the technique also includes the ions around the nanoparticles and the size of the nanoparticles is measured as bigger than the actual size. Also, this technique is based on mathematical modeling of the diffusion rate of the nanoparticles that undergo Brownian motion. However, in electron microscopy, the nanoparticles should be prepared in dried form for analysis, and the micrographs are obtained through electron beam-matter interaction. Therefore, smaller size values are observed in electron microscopy. On the other hand, in the electrospun samples, bead-free nanofiber formation below 200 nm in thickness and nanoparticles deposited on the fibers were observed.

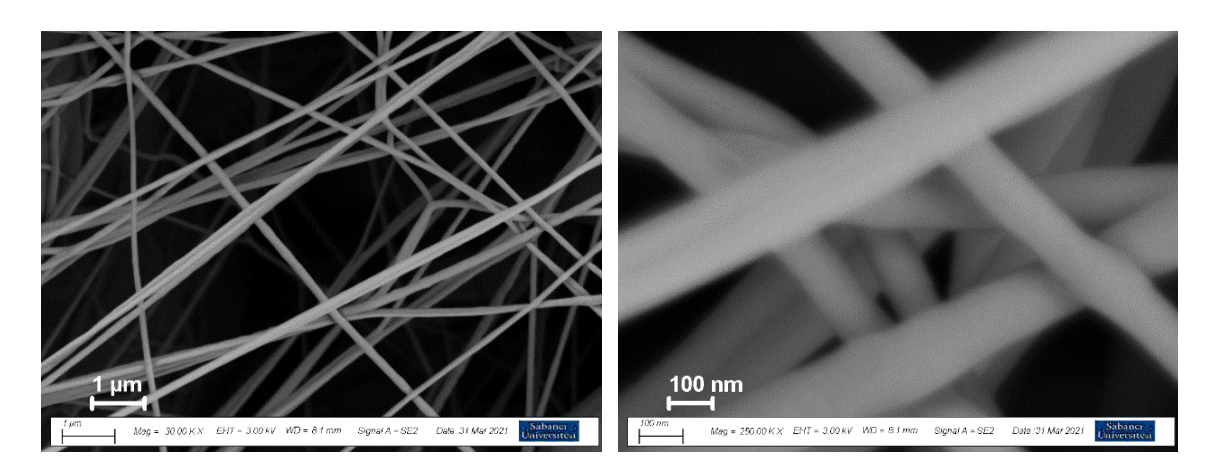


Figure 6-4: SEM Images of Bare PCL Nanofibers

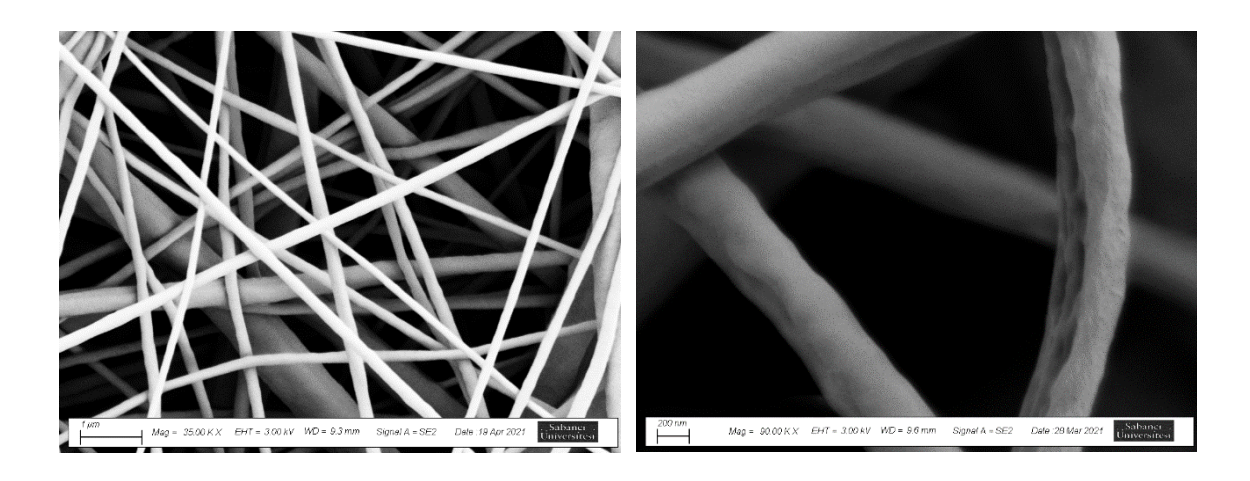
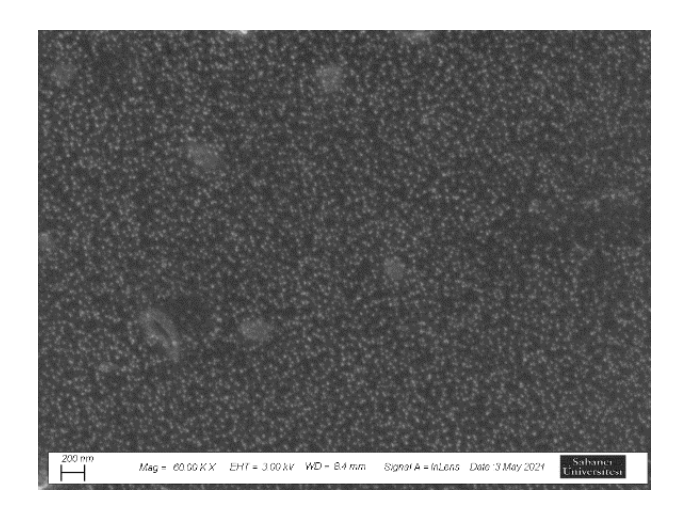
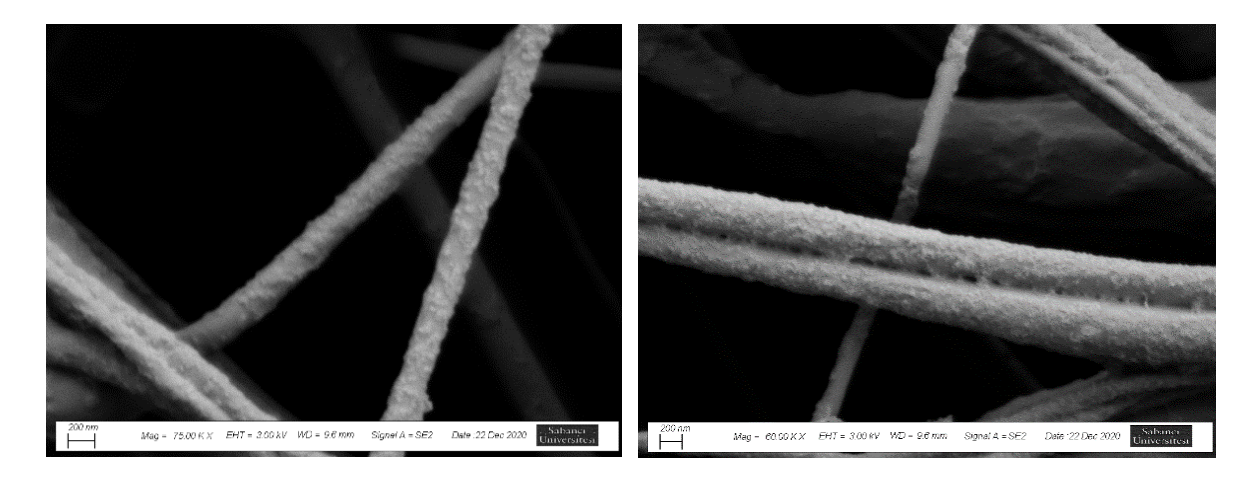


Figure 6-5: SEM Images of Curcumin Loaded PCL Nanofibers



**Figure 6-6 :** SEM Image of Rose Bengal Loaded Chitosan Nanoparticles



**Figure 6-7 :** SEM Images of Curcumin Loaded PCL Nanofibers Decorated with RB loaded Chitosan Nanoparticles

#### FTIR Analysis of the PCL Nanofibers and Chitosan Nanoparticles

The FTIR spectrum including curcumin, bare PCL nanofibers, and curcumin loaded PCL nanofibers is presented in Figure 6-8. Curcumin has the vibration of phenolic O-H bond at 3507 cm<sup>-1</sup> and the peak at 1626 cm<sup>-1</sup> represents C=C stretching in aromatic carbon ring, 1505 cm<sup>-1</sup> indicates C=O vibration. Moreover, the peaks and 1427cm<sup>-1</sup> and 1273cm<sup>-1</sup> correspond to C-H bending and C-O stretching respectively.

In the spectrum of PCL nanofibers, asymmetric and symmetric CH<sub>2</sub> stretchings were detected at 2943 cm<sup>-1</sup> and 2865 cm<sup>-1</sup> respectively. Besides, C-O stretching was identified at, 1721 cm<sup>-1</sup>. Furthermore, 1293 cm<sup>-1</sup> and 1237 cm<sup>-1</sup> in the spectrum indicate C-C stretching and asymmetric C-O-C stretching respectively. The FTIR spectrum of curcumin loaded PCL nanofibers was similar to the bare PCL nanofibers. Only very small shifts were observed.

The FTIR spectrum including rose bengal, chitosan nanoparticles and rose bengal loaded chitosan nanoparticles is shown in Figure 6-9. In the FTIR spectrum of rose bengal dye, the phenolic O-H stretching and bending vibrations were detected at 3282 cm<sup>-1</sup> and 1326cm<sup>-1</sup>. The peaks at 1608 cm<sup>-1</sup> and 1435 cm<sup>-1</sup> correspond to the C=C stretch and C-C stretch in the aromatic moieties. Also, the C-O stretch in the carboxylic acid compound in the rose bengal structure was detected at 1265cm<sup>-1</sup>.

In chitosan nanoparticles, C=O stretching and N-H bending was identified at 1688cm<sup>-1</sup> and 1635 cm<sup>-1</sup> respectively. Besides, at 1537 cm<sup>-1</sup> C-H bending was observed and antisymmetric stretching in the C-O-C compound was detected at 1050 cm<sup>-1</sup>. Also, C-N stretch in the chitosan

structure was identified at 1124cm<sup>-1</sup>. The presence of rose bengal in the chitosan/TPP structure leads to the disappearance of the peak at 1124cm<sup>-1</sup>. Also, it caused some small shiftings such as 1537,77 cm<sup>-1</sup> to 1546,23 cm<sup>-1</sup>. These can be attributed to the possible interactions between chitosan nanoparticle structure and rose bengal molecules.

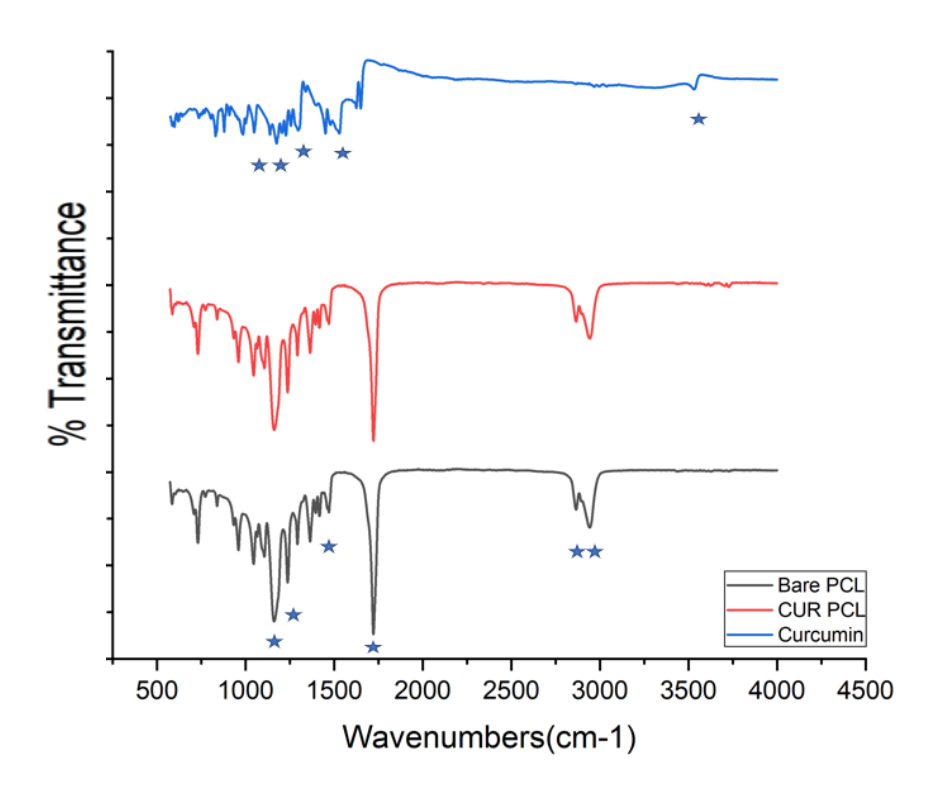


**Figure 6-8 :** FTIR Spectrum of Curcumin, PCL Nanofibers and Curcumin Loaded PCL Nanofibers

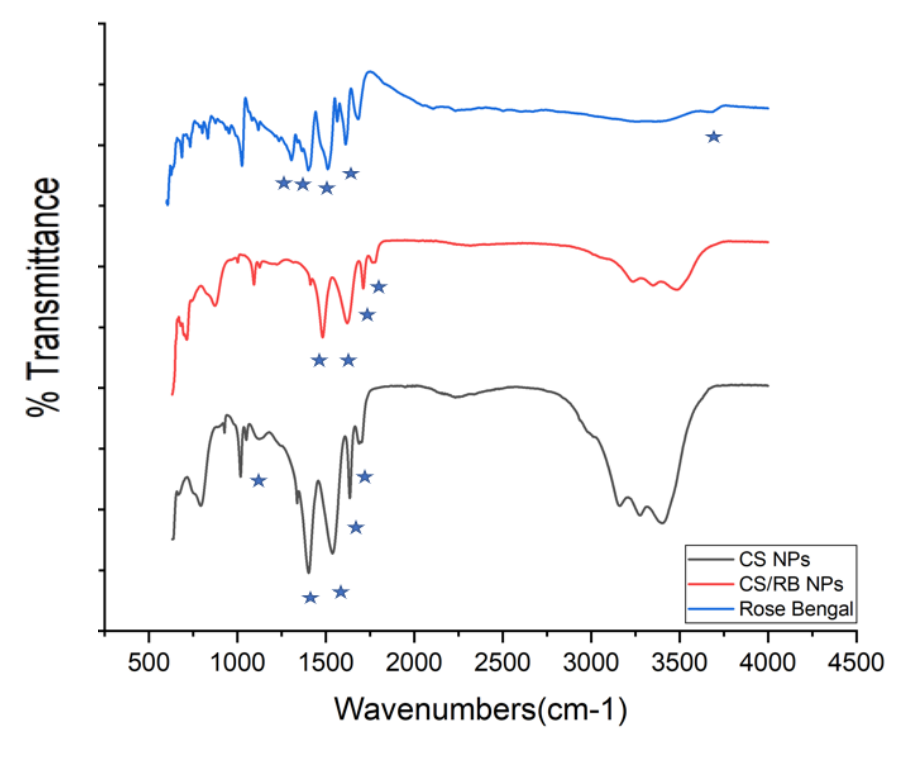


**Figure 6-9 :** FTIR spectrum of Rose Bengal, Chitosan Nanoparticles and Rose Bengal Loaded Chitosan Nanoparticles

## 6.3.2 Drug Release Studies and Kinetic Analysis

Drug release tests were performed for the curcumin loaded PCL nanofibers and curcumin loaded PCL nanofibers with rose bengal loaded chitosan nanoparticles. The release profiles were drawn based on cumulative drug release (%) versus time. Sustained drug release was observed in all release profiles. According to our results, 71% of curcumin was released from the PCL nanofibers that are not integrated with nanoparticles. However, this amount was reduced to 59,34 % in CUR loaded PCL nanofibers decorated with RB loaded chitosan nanoparticles. This deceleration behavior in curcumin release can stem from possible interactions between the curcumin loaded PCL fibers and chitosan nanoparticles. On the other hand, 80,3% of rose bengal was released during the 120 hours. The initial burst release at first 10h might stem from the curcumin and rose bengal molecules on the surface of the nanofibers and nanoparticles.

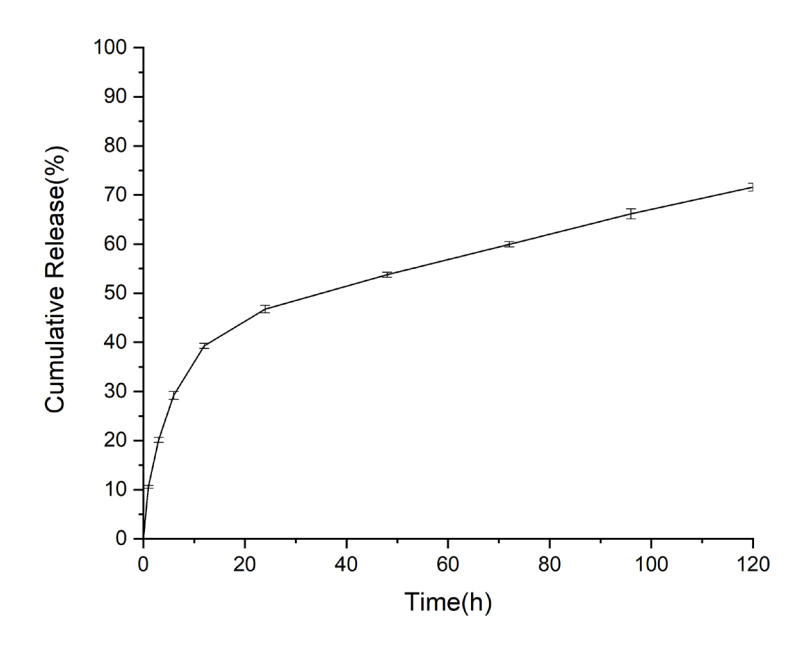
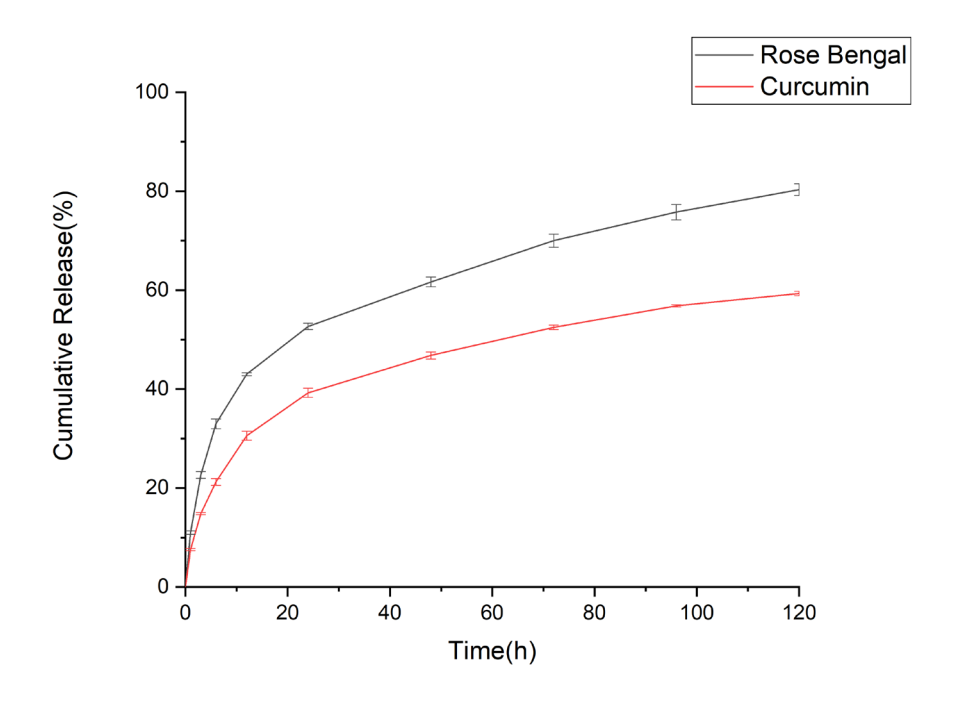
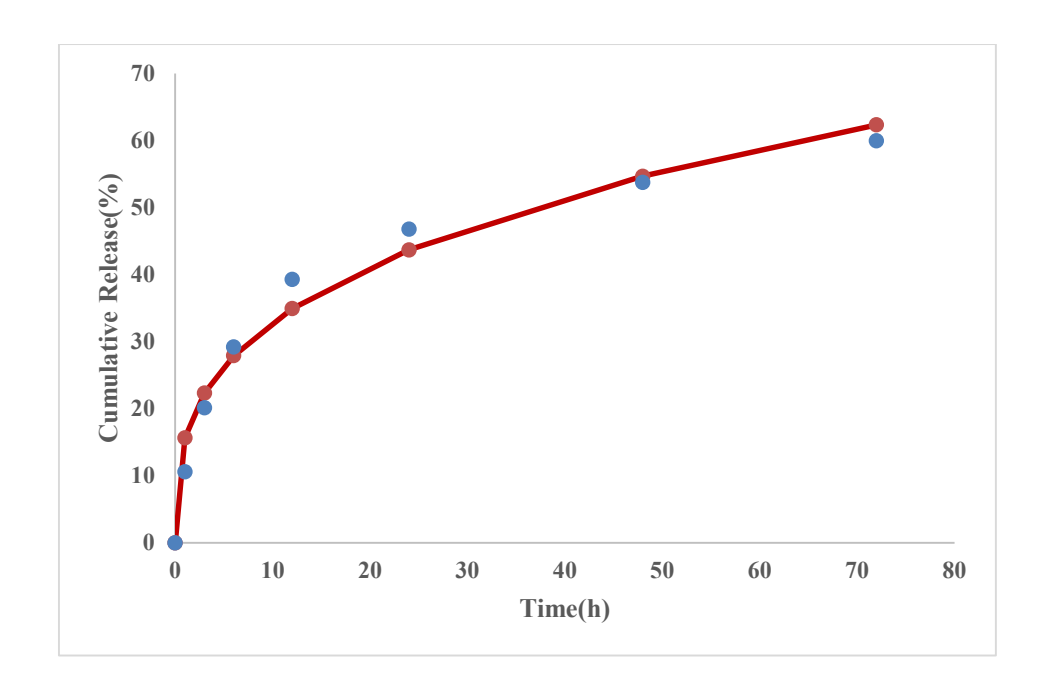


Figure 6-10: Drug Release Profile of Curcumin Loaded PCL Nanofibers



**Figure 6-11:** Drug Release Profiles of CUR Loaded PCL Nanofibers with RB Loaded Chitosan Nanoparticles

Following the curve fitting processes on Korsmeyer Peppas Model, we obtained a great correlation between our experimental release data and fitted data. ( $R^2 > 0.99$ ). In the case of curcumin release, nanofibers were considered cylindrical carrier matrix, and for the rose bengal release, it is considered spherical matrix due to the spherical morphology of the nanoparticles. The n values for each release profile are indicating Fickian diffusion behavior, where n values are below 0.45 for cylindrical morphology and 0.43 for spherical morphology. It can be deduced that Fickian diffusion is dominating drug transportation and polymer chains do not have any significant effect on drug transportation. The coherence of the Korsmeyer Peppas Model to our release profiles can be seen by Figure 6-12, Figure 6-12, Figure 6-14. The model release results are shown as red lines while our release results were presented as blue dots.



**Figure 6-12 :** Curve Fitting Analysis for Curcumin Release from CUR-PCL (R<sup>2</sup>=0.99, n=0.32)

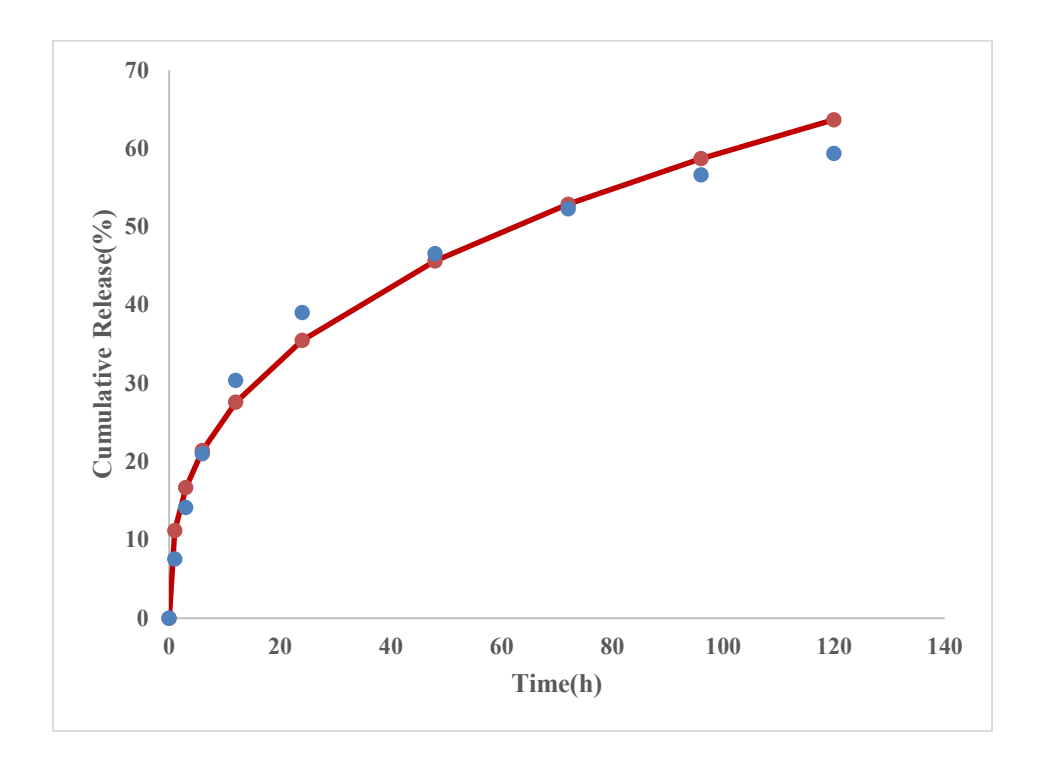


**Figure 6-13 :** Curve Fitting Analysis for Curcumin Release from CUR-PCL/RB-CS ( $R^2$ =0.99, n=0.36)

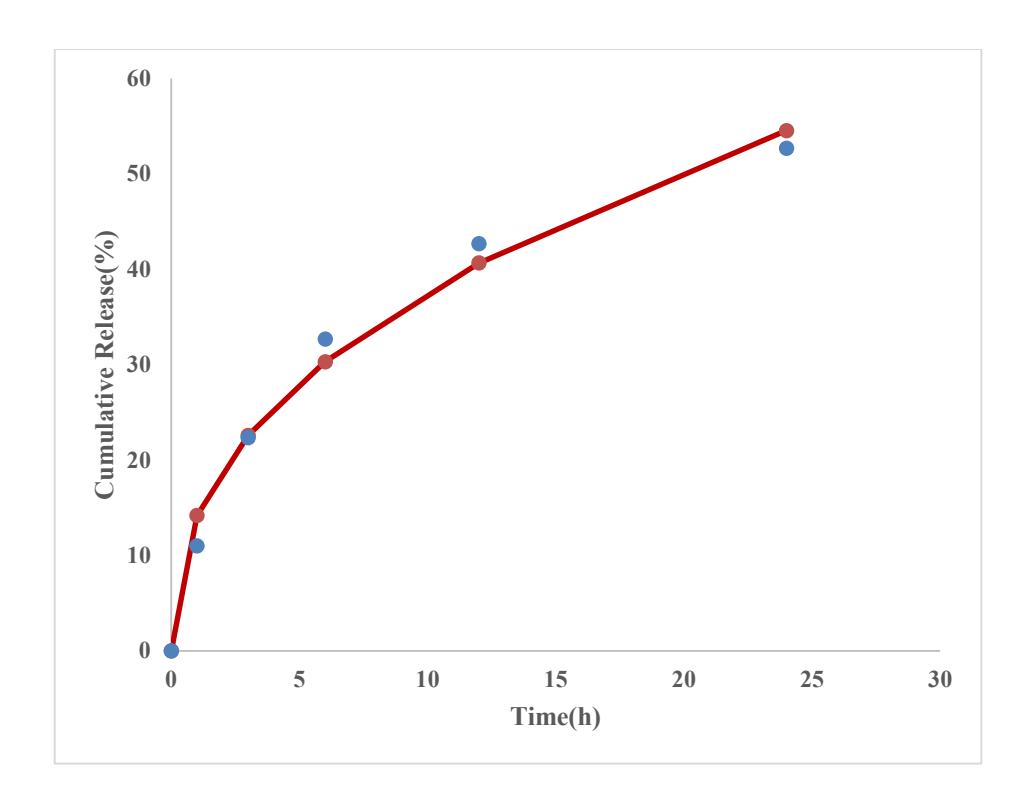


**Figure 6-14 :** Curve Fitting Analysis for Rose Bengal Release from CUR-PCL/RB-CS  $(R^2=0.99, n=0.42)$ 

## 6.4 Conclusion

Nanoparticles associated electrospun patches were fabricated via facile route using a commercial airbrush, for co-delivery of hydrophilic and hydrophobic drugs in nanomedicine applications. In addition to the fundamental characterization tests, electrospun patches also demonstrated the ability to release multiple drugs in different profiles. Curcumin-loaded PCL nanofibers associated with rose bengal loaded chitosan nanoparticles have the potential to be used as implantable drug delivery nanoplatforms that can fulfill the needs of local drug delivery systems.

# **Chapter 7: CONCLUSION**

This thesis focused on the design and synthesis of stimuli-responsive nanostructures for drug delivery applications. Chapter 3 involved the synthesis of pH and temperature-responsive coreshell nanostructures, chitosan/poly (acrylic acid)/poly (n-vinyl caprolactam) nanoparticles for colon-specific drug delivery. The release mechanisms were investigated at different pH and temperature levels that are pH=5.0 and pH=7.4 and 40°C and 25°C. The nanoparticles could provide triggered drug release at elevated temperature and alkali pH level which is coherent with the colon environment. Chapter 4 was about the encapsulation of multiple drugs in single, stimuli-responsive nanocarriers. Here, a hydrophobic drug was encapsulated within niosomes, and encapsulation of the hydrophilic drug was accomplished by CSgPNVCL polymer coating. The ultimate pH and temperature-responsive niosome/polymer hybrid nanoparticles were able to display triggered drug release under acidic pH and elevated temperature conditions, that are corresponding to the tumor environment. In Chapter 5, redox responsive nanocarriers were prepared using albumin nanoparticles. Crosslinker-free synthesis of albumin nanoparticles was achieved via the reducing agent-assisted desolvation method. Here, albumin nanocarriers were able to display triggered drug release in redox environment. Finally, Chapter 6 involved a facile fabrication method for nanoparticles associated with electrospun drug delivery patches. Encapsulation of multiple therapeutic agents was achieved using nanoparticles and nanofibers together. Chitosan nanoparticles synthesized via the ionic gelation method, and they were deposited onto PCL nanofibers, using a commercial airbrush. This work can be considered a facile fabrication route for dual drug-loaded implantable drug delivery patches. All these studies were confirmed that these smart nanostructures have the potential to display triggered release profiles for a specific stimulus and they can be preferred as drug delivery systems.

## **REFERENCES**

- [1] C. L. Ventola, "The nanomedicine revolution: part 1: emerging concepts.," *P T*, vol. 37, no. 9, pp. 512–525, Sep. 2012.
- [2] H. Xiao *et al.*, "Structure-based design of charge-conversional drug self-delivery systems for better targeted cancer therapy," *Biomaterials*, vol. 232, Feb. 2020.
- [3] M. Bil, E. Kijeńska-Gawrońska, E. Głodkowska-Mrówka, A. Manda-Handzlik, and P. Mrówka, "Design and in vitro evaluation of electrospun shape memory polyurethanes for self-fitting tissue engineering grafts and drug delivery systems," *Mater. Sci. Eng. C*, vol. 110, May 2020.
- [4] R. van der Meel, E. Sulheim, Y. Shi, F. Kiessling, W. J. M. Mulder, and T. Lammers, "Smart cancer nanomedicine," *Nat. Nanotechnol.*, vol. 14, no. 11, pp. 1007–1017, 2019.
- [5] Y. Barenholz, "Doxil® The first FDA-approved nano-drug: Lessons learned," *Journal of Controlled Release*, vol. 160, no. 2. Elsevier, pp. 117–134, Jun-2012.
- [6] Y. Dang and J. Guan, "Nanoparticle-based drug delivery systems for cancer therapy," *Smart Mater. Med.*, vol. 1, no. March, pp. 10–19, 2020.
- [7] W. B. Liechty, D. R. Kryscio, B. V Slaughter, and N. A. Peppas, "Polymers for Drug Delivery Systems," *Annu. Rev. Chem. Biomol. Eng.*, vol. 1, no. 1, pp. 149–173, 2010.
- [8] A. Juan, F. J. Cimas, I. Bravo, A. Pandiella, A. Ocaña, and C. Alonso-Moreno, "An Overview of Antibody Conjugated Polymeric Nanoparticles for Breast Cancer Therapy," *Pharmaceutics*, vol. 12, no. 9, 2020.
- [9] H. Kulhari, D. Pooja, S. Shrivastava, N. V.G.M, and R. Sistla, "Peptide conjugated polymeric nanoparticles as a carrier for targeted delivery of docetaxel," *Colloids Surfaces B Biointerfaces*, vol. 117, pp. 166–173, 2014.
- [10] M. Wei, Y. Gao, X. Li, and M. J. Serpe, "Stimuli-responsive polymers and their applications," *Polym. Chem.*, vol. 8, no. 1, pp. 127–143, 2017.
- [11] S. Indermun, M. Govender, P. Kumar, Y. E. Choonara, and V. Pillay, "2 Stimuliresponsive polymers as smart drug delivery systems: Classifications based on carrier

- type and triggered-release mechanism," in *Stimuli Responsive Polymeric Nanocarriers* for Drug Delivery Applications, Volume 1, A. S. H. Makhlouf and N. Y. Abu-Thabit, Eds. Woodhead Publishing, 2018, pp. 43–58.
- [12] M. Kanamala, W. R. Wilson, M. Yang, B. D. Palmer, and Z. Wu, "Mechanisms and biomaterials in pH-responsive tumour targeted drug delivery: A review," *Biomaterials*, vol. 85, pp. 152–167, 2016.
- [13] A. Ghaffar, B. Yameen, M. Latif, and M. I. Malik, "Chapter 14 pH-sensitive drug delivery systems," in *Metal Nanoparticles for Drug Delivery and Diagnostic Applications*, M. R. Shah, M. Imran, and S. Ullah, Eds. Elsevier, 2020, pp. 259–278.
- [14] L. Liu, W. Yao, Y. Rao, X. Lu, and J. Gao, "pH-Responsive carriers for oral drug delivery: challenges and opportunities of current platforms," *Drug Deliv.*, vol. 24, no. 1, pp. 569–581, 2017.
- [15] X. He, J. Li, S. An, and C. Jiang, "pH-sensitive drug-delivery systems for tumor targeting.," *Ther. Deliv.*, vol. 4, no. 12, pp. 1499–1510, Dec. 2013.
- [16] D. Schmaljohann, "Thermo- and pH-responsive polymers in drug delivery," *Adv. Drug Deliv. Rev.*, vol. 58, no. 15, pp. 1655–1670, 2006.
- [17] Y. Guan and Y. Zhang, "PNIPAM microgels for biomedical applications: from dispersed particles to 3D assemblies," *Soft Matter*, vol. 7, no. 14, pp. 6375–6384, 2011.
- [18] J. Ramos, A. Imaz, and J. Forcada, "Temperature-sensitive nanogels: poly(N-vinylcaprolactam) versus poly(N-isopropylacrylamide)," *Polym. Chem.*, vol. 3, no. 4, pp. 852–856, 2012.
- [19] H. Zhang, I. A. Alsarra, and S. H. Neau, "An in vitro evaluation of a chitosan-containing multiparticulate system for macromolecule delivery to the colon," *Int. J. Pharm.*, vol. 239, no. 1, pp. 197–205, 2002.
- [20] A. Raza, T. Rasheed, F. Nabeel, U. Hayat, M. Bilal, and H. M. N. Iqbal, "Endogenous and Exogenous Stimuli-Responsive Drug Delivery Systems for Programmed Site-Specific Release," *Molecules*, vol. 24, no. 6, 2019.
- [21] S. Dash, P. N. Murthy, L. Nath, and P. Chowdhury, "Kinetic modeling on drug release from controlled drug delivery systems.," *Acta Pol. Pharm.*, vol. 67, no. 3, pp. 217–223,

2010.

- [22] P. Costa and J. M. Sousa Lobo, "Modeling and comparison of dissolution profiles," *Eur. J. Pharm. Sci.*, vol. 13, no. 2, pp. 123–133, 2001.
- [23] N. V Mulye and S. J. Turco, "A Simple Model Based on First Order Kinetics to Explain Release of Highly Water Soluble Drugs from Porous Dicalcium Phosphate Dihydrate Matrices," *Drug Dev. Ind. Pharm.*, vol. 21, no. 8, pp. 943–953, 1995.
- [24] M. L. Bruschi, Ed., "5 Mathematical models of drug release," in *Strategies to Modify the Drug Release from Pharmaceutical Systems*, Woodhead Publishing, 2015, pp. 63–86.
- [25] E. Calzoni, A. Cesaretti, A. Polchi, A. Di Michele, B. Tancini, and C. Emiliani, "Biocompatible Polymer Nanoparticles for Drug Delivery Applications in Cancer and Neurodegenerative Disorder Therapies," *J. Funct. Biomater.*, vol. 10, no. 1, p. 4, Jan. 2019.
- [26] X. Hu, S. Liu, G. Zhou, Y. Huang, Z. Xie, and X. Jing, "Electrospinning of polymeric nanofibers for drug delivery applications," *J. Control. Release*, vol. 185, pp. 12–21, 2014.
- [27] S. A. M. Ealia and M. P. Saravanakumar, "A review on the classification, characterisation, synthesis of nanoparticles and their application," *{IOP} Conf. Ser. Mater. Sci. Eng.*, vol. 263, p. 32019, 2017.
- [28] A. V. Rane, K. Kanny, V. K. Abitha, and S. Thomas, "Chapter 5 Methods for Synthesis of Nanoparticles and Fabrication of Nanocomposites," in *Synthesis of Inorganic Nanomaterials*, S. Mohan Bhagyaraj, O. S. Oluwafemi, N. Kalarikkal, and S. Thomas, Eds. Woodhead Publishing, 2018, pp. 121–139.
- [29] G. Zhao, J. Wang, X. Peng, Y. Li, X. Yuan, and Y. Ma, "Facile Solvothermal Synthesis of Mesostructured Fe3O4/Chitosan Nanoparticles as Delivery Vehicles for pH-Responsive Drug Delivery and Magnetic Resonance Imaging Contrast Agents," *Chem. An Asian J.*, vol. 9, no. 2, pp. 546–553, 2014.
- [30] S. Pulavendran, C. Rose, and A. B. Mandal, "Hepatocyte growth factor incorporated chitosan nanoparticles augment the differentiation of stem cell into hepatocytes for the recovery of liver cirrhosis in mice," *J. Nanobiotechnology*, vol. 9, pp. 1–11, 2011.

- [31] S. Esfandiarpour-Boroujeni, S. Bagheri-Khoulenjani, H. Mirzadeh, and S. Amanpour, "Fabrication and study of curcumin loaded nanoparticles based on folate-chitosan for breast cancer therapy application," *Carbohydr. Polym.*, vol. 168, pp. 14–21, 2017.
- [32] M. A. Mohammed, J. T. M. Syeda, K. M. Wasan, and E. K. Wasan, "An Overview of Chitosan Nanoparticles and Its Application in Non-Parenteral Drug Delivery," *Pharmaceutics*, vol. 9, no. 4, 2017.
- [33] S. Kim, K. Kim, and S. Q. Choi, "Controllable one-step double emulsion formation via phase inversion," *Soft Matter*, vol. 14, no. 7, pp. 1094–1099, 2018.
- [34] A. T. Alex, A. Joseph, G. Shavi, J. V. Rao, and N. Udupa, "Development and evaluation of carboplatin-loaded PCL nanoparticles for intranasal delivery," *Drug Deliv.*, vol. 23, no. 7, pp. 2144–2153, 2016.
- [35] S.-B. Sun, P. Liu, F.-M. Shao, and Q.-L. Miao, "Formulation and evaluation of PLGA nanoparticles loaded capecitabine for prostate cancer.," *Int. J. Clin. Exp. Med.*, vol. 8, no. 10, pp. 19670–19681, 2015.
- [36] P. Rafiei and A. Haddadi, "Docetaxel-loaded PLGA and PLGA-PEG nanoparticles for intravenous application: pharmacokinetics and biodistribution profile.," *Int. J. Nanomedicine*, vol. 12, pp. 935–947, 2017.
- [37] P. Grossen, D. Witzigmann, S. Sieber, and J. Huwyler, "PEG-PCL-based nanomedicines: A biodegradable drug delivery system and its application," *J. Control. Release*, vol. 260, pp. 46–60, 2017.
- [38] F. M. Veronese and G. Pasut, "PEGylation, successful approach to drug delivery," *Drug Discov. Today*, vol. 10, no. 21, pp. 1451–1458, 2005.
- [39] A. A. D'souza and R. Shegokar, "Polyethylene glycol (PEG): a versatile polymer for pharmaceutical applications," *Expert Opin. Drug Deliv.*, vol. 13, no. 9, pp. 1257–1275, 2016.
- [40] Y. L. Tan and H. K. Ho, "Navigating albumin-based nanoparticles through various drug delivery routes," *Drug Discov. Today*, vol. 23, no. 5, pp. 1108–1114, 2018.
- [41] T. Lin *et al.*, "Blood–Brain-Barrier-Penetrating Albumin Nanoparticles for Biomimetic Drug Delivery via Albumin-Binding Protein Pathways for Antiglioma Therapy," *ACS Nano*, vol. 10, no. 11, pp. 9999–10012, 2016.

- [42] A. Rudin and P. Choi, "Chapter 10 Dispersion and Emulsion Polymerizations," in *The Elements of Polymer Science & Engineering (Third Edition)*, Third Edit., A. Rudin and P. Choi, Eds. Boston: Academic Press, 2013, pp. 427–447.
- [43] Y.-S. Cho, S. Ji, and Y. S. Kim, "Synthesis of Polymeric Nanoparticles by Emulsion Polymerization for Particle Self-Assembly Applications.," *J. Nanosci. Nanotechnol.*, vol. 19, no. 10, pp. 6398–6407, Oct. 2019.
- [44] Y. Yar *et al.*, "Development of tailored SPION-PNIPAM nanoparticles by ATRP for dually responsive doxorubicin delivery and MR imaging," *J. Mater. Chem. B*, vol. 6, no. 2, pp. 289–300, 2018.
- [45] L. Ahmadkhani, M. Abbasian, and A. Akbarzadeh, "Synthesis of sharply thermo and PH responsive PMA-b-PNIPAM-b-PEG-b-PNIPAM-b-PMA by RAFT radical polymerization and its schizophrenic micellization in aqueous solutions," *Des. Monomers Polym.*, vol. 20, no. 1, pp. 406–418, 2017.
- [46] B. B. Shen, X. C. Gao, S. Y. Yu, Y. Ma, and C. H. Ji, "Fabrication and potential application of a di-functional magnetic system: magnetic hyperthermia therapy and drug delivery," *CrystEngComm*, vol. 18, no. 7, pp. 1133–1138, 2016.
- [47] K. M. Rao, K. S. V. K. Rao, and C.-S. Ha, "Stimuli Responsive Poly(Vinyl Caprolactam) Gels for Biomedical Applications," *Gels*, vol. 2, no. 1, 2016.
- [48] A. Morfin-Gutierrez, J. L. Sánchez-Orozco, L. A. García-Cerda, B. Puente-Urbina, and H. I. Meléndez-Ortiz, "Preparation and characterization of nanocomposites based on poly(N-vinycaprolactam) and magnetic nanoparticles for using as drug delivery system," *J. Drug Deliv. Sci. Technol.*, vol. 60, p. 102028, 2020.
- [49] A. Pardakhty, "Non-Ionic Surfactant Vesicles (Niosomes) as New Drug Delivery Systems." pp. 89–119, 2017.
- [50] V. Sharma, S. Anandhakumar, and M. Sasidharan, "Self-degrading niosomes for encapsulation of hydrophilic and hydrophobic drugs: An efficient carrier for cancer multi-drug delivery.," *Mater. Sci. Eng. C. Mater. Biol. Appl.*, vol. 56, pp. 393–400, Nov. 2015.
- [51] S. Durak *et al.*, "Niosomal Drug Delivery Systems for Ocular Disease-Recent Advances and Future Prospects.," *Nanomater. (Basel, Switzerland)*, vol. 10, no. 6,

- Jun. 2020.
- [52] S. Liu *et al.*, "Inhibition of orthotopic secondary hepatic carcinoma in mice by doxorubicin-loaded electrospun polylactide nanofibers," *J. Mater. Chem. B*, vol. 1, no. 1, pp. 101–109, 2013.
- [53] S. Sayin *et al.*, "Electrospun Nanofibers With pH-Responsive Coatings for Control of Release Kinetics," *Front. Bioeng. Biotechnol.*, vol. 7, p. 309, 2019.
- [54] Y. Wang, B. Wang, W. Qiao, and T. Yin, "A Novel Controlled Release Drug Delivery System for Multiple Drugs Based on Electrospun Nanofibers Containing Nanoparticles," *J. Pharm. Sci.*, vol. 99, no. 12, pp. 4805–4811, 2010.
- [55] J. Jalvandi, M. White, Y. Gao, Y. B. Truong, R. Padhye, and I. L. Kyratzis, "Slow release of levofloxacin conjugated on silica nanoparticles from poly(ε-caprolactone) nanofibers," *Int. J. Polym. Mater. Polym. Biomater.*, vol. 66, no. 10, pp. 507–513, 2017.
- [56] L. Li, G. Zhou, Y. Wang, G. Yang, S. Ding, and S. Zhou, "Controlled dual delivery of BMP-2 and dexamethasone by nanoparticle-embedded electrospun nanofibers for the efficient repair of critical-sized rat calvarial defect," *Biomaterials*, vol. 37, pp. 218–229, 2015.
- [57] N. Bhardwaj and S. C. Kundu, "Electrospinning: A fascinating fiber fabrication technique," *Biotechnol. Adv.*, vol. 28, no. 3, pp. 325–347, 2010.
- [58] X. Shi *et al.*, "Electrospinning of Nanofibers and Their Applications for Energy Devices," *J. Nanomater.*, vol. 2015, p. 140716, 2015.
- [59] A. Haider, S. Haider, and I.-K. Kang, "A comprehensive review summarizing the effect of electrospinning parameters and potential applications of nanofibers in biomedical and biotechnology," *Arab. J. Chem.*, vol. 11, no. 8, pp. 1165–1188, 2018.
- [60] V. Beachley and X. Wen, "Effect of electrospinning parameters on the nanofiber diameter and length," *Mater. Sci. Eng. C*, vol. 29, no. 3, pp. 663–668, 2009.
- [61] D. Choudhary, L., Jain, A., & Agarwal, "Colon-Targeted Oral Drug Delivery Systems: A Review," *Asian J. Pharm. Res. Dev.*, vol. 8, no. 4, pp. 186-193., 2020.
- [62] S. Amidon, J. E. Brown, and V. S. Dave, "Colon-Targeted Oral Drug Delivery Systems: Design Trends and Approaches," *AAPS PharmSciTech*, vol. 16, no. 4, pp.

- 731–741, 2015.
- [63] S. Thakral, N. K. Thakral, and D. K. Majumdar, "Eudragit®: A technology evaluation," *Expert Opin. Drug Deliv.*, vol. 10, no. 1, pp. 131–149, 2013.
- [64] M. G. Li *et al.*, "Preparation and characterization of insulin nanoparticles employing Chitosan and poly(methylmethacrylate/methylmethacrylic acid) copolymer," *J. Nanosci. Nanotechnol.*, vol. 6, no. 9–10, pp. 2874–2886, 2006.
- [65] C. T. H. Nguyen *et al.*, "Bifunctional Succinylated ε-Polylysine-Coated Mesoporous Silica Nanoparticles for pH-Responsive and Intracellular Drug Delivery Targeting the Colon," *ACS Appl. Mater. Interfaces*, vol. 9, no. 11, pp. 9470–9483, 2017.
- [66] Q. Song *et al.*, "An oral drug delivery system with programmed drug release and imaging properties for orthotopic colon cancer therapy," *Nanoscale*, vol. 11, no. 34, pp. 15958–15970, 2019.
- [67] N. J. N. Daniel E Shumer Norman P Spack, "Temperature-Responsive Smart Nanocarriers for Delivery Of Therapeutic Agents: Applications and Recent Advances," *Physiol. Behav.*, vol. 176, no. 12, pp. 139–148, 2017.
- [68] R. Cheng, F. Meng, C. Deng, H.-A. Klok, and Z. Zhong, "Dual and multi-stimuli responsive polymeric nanoparticles for programmed site-specific drug delivery," *Biomaterials*, vol. 34, no. 14, pp. 3647–3657, 2013.
- [69] S. K. Joseph, M. Sabitha, and S. C. Nair, "Stimuli-responsive polymeric nanosystem for colon specific drug delivery," *Adv. Pharm. Bull.*, vol. 10, no. 1, pp. 1–12, 2020.
- [70] W.-Y. C. CHUNG-YANG CHUANG, TRONG-MING DON, "Synthesis and Properties of Chitosan-Based Thermo- and pH-Responsive Nanoparticles and Application in Drug Release," *J. Polym. Sci. Part A Polym. Chem. Vol. 47*, vol. 47, pp. 2798–2810, 2009.
- [71] Y. K. Kim *et al.*, "Dual Stimuli-Triggered Nanogels in Response to Temperature and pH Changes for Controlled Drug Release," *Nanoscale Res. Lett.*, vol. 14, 2019.
- [72] J. Ramos, A. Imaz, and J. Forcada, "Temperature-sensitive nanogels: Poly(N-vinylcaprolactam) versus poly(N-isopropylacrylamide)," *Polym. Chem.*, vol. 3, no. 4, pp. 852–856, 2012.
- [73] N. A. Cortez-Lemus and A. Licea-Claverie, "Poly(N-vinylcaprolactam), a

- comprehensive review on a thermoresponsive polymer becoming popular," *Prog. Polym. Sci.*, vol. 53, pp. 1–51, 2016.
- [74] N. Wang, X. Cheng, N. Li, H. Wang, and H. Chen, "Nanocarriers and Their Loading Strategies," *Adv. Healthc. Mater.*, vol. 8, no. 6, p. 1801002, 2019.
- [75] "IR Spectrum Table by Frequency Range." [Online]. Available: https://www.sigmaaldrich.com/technical-documents/articles/biology/ir-spectrum-table.html.
- [76] S. Kozanoğlu, T. Özdemir, and A. Usanmaz, "Polymerization of N-Vinylcaprolactam and Characterization of Poly(N-Vinylcaprolactam)," *J. Macromol. Sci. Part A*, vol. 48, no. 6, pp. 467–477, 2011.
- [77] C. Duan *et al.*, "Chitosan-g-poly(N-isopropylacrylamide) based nanogels for tumor extracellular targeting," *Int. J. Pharm.*, vol. 409, no. 1, pp. 252–259, 2011.
- [78] S. Tran, P. DeGiovanni, B. Piel, and P. Rai, "Cancer nanomedicine: a review of recent success in drug delivery," *Clin. Transl. Med.*, vol. 6, no. 1, 2017.
- [79] B. Kumar, K. Jalodia, P. Kumar, and H. K. Gautam, "Recent advances in nanoparticle-mediated drug delivery," *J. Drug Deliv. Sci. Technol.*, vol. 41, pp. 260–268, 2017.
- [80] C. Marianecci, S. Petralito, F. Rinaldi, P. N. Hanieh, and M. Carafa, "Some recent advances on liposomal and niosomal vesicular carriers," *J. Drug Deliv. Sci. Technol.*, vol. 32, pp. 256–269, 2016.
- [81] D. Tila, S. N. Yazdani-Arazi, S. Ghanbarzadeh, S. Arami, and Z. Pourmoazzen, "PH-sensitive, polymer modified, plasma stable niosomes: promising carriers for anticancer drugs," *EXCLI J.*, vol. 14, pp. 21–32, 2015.
- [82] F. Marzoli *et al.*, "Long-lasting, antinociceptive effects of pH-sensitive niosomes loaded with ibuprofen in acute and chronic models of pain," *Pharmaceutics*, vol. 11, no. 2, 2019.
- [83] L. Tavano, C. Oliviero Rossi, N. Picci, and R. Muzzalupo, "Spontaneous temperature-sensitive Pluronic® based niosomes: Triggered drug release using mild hyperthermia," *Int. J. Pharm.*, vol. 511, no. 2, pp. 703–708, 2016.
- [84] M. Baranei *et al.*, "Anticancer effect of green tea extract (GTE)-Loaded pH-responsive niosome Coated with PEG against different cell lines," *Mater. Today Commun.*, p.

- 101751, 2020.
- [85] F. Rinaldi *et al.*, "Chitosan glutamate-coated niosomes: A proposal for nose-to-brain delivery," *Pharmaceutics*, vol. 10, no. 2, pp. 1–16, 2018.
- [86] W. Zeng *et al.*, "Hyaluronic acid-coated niosomes facilitate tacrolimus ocular delivery: Mucoadhesion, precorneal retention, aqueous humor pharmacokinetics, and transcorneal permeability," *Colloids Surfaces B Biointerfaces*, vol. 141, pp. 28–35, 2016.
- [87] E. Mazzotta, L. Tavano, and R. Muzzalupo, "Thermo-sensitive vesicles in controlled drug delivery for chemotherapy," *Pharmaceutics*, vol. 10, no. 3, 2018.
- [88] C. Duan *et al.*, "Chitosan- g -poly (N -isopropylacrylamide) based nanogels for tumor extracellular targeting," *Int. J. Pharm.*, vol. 409, no. 1–2, pp. 252–259, 2015.
- [89] A. Imaz, J. I. Miranda, J. Ramos, and J. Forcada, "Evidences of a hydrolysis process in the synthesis of N-vinylcaprolactam-based microgels," *Eur. Polym. J.*, vol. 44, no. 12, pp. 4002–4011, 2008.
- [90] M. M. Mady and M. M. Darwish, "Effect of chitosan coating on the characteristics of DPPC liposomes," *J. Adv. Res.*, vol. 1, no. 3, pp. 187–191, 2010.
- [91] E. Joseph and G. Singhvi, *Multifunctional nanocrystals for cancer therapy: A potential nanocarrier*. Elsevier Inc., 2019.
- [92] A. Bootz, V. Vogel, D. Schubert, and J. Kreuter, "Comparison of scanning electron microscopy, dynamic light scattering and analytical ultracentrifugation for the sizing of poly(butyl cyanoacrylate) nanoparticles," *Eur. J. Pharm. Biopharm.*, vol. 57, no. 2, pp. 369–375, 2004.
- [93] P. Eaton *et al.*, "A direct comparison of experimental methods to measure dimensions of synthetic nanoparticles," *Ultramicroscopy*, vol. 182, pp. 179–190, 2017.
- [94] Y. Xie *et al.*, "Stimuli-responsive polymeric nanomaterials for rheumatoid arthritis therapy," *Biophys. Reports*, vol. 6, no. 5, pp. 193–210, 2020.
- [95] S. S. Das *et al.*, "Stimuli-Responsive Polymeric Nanocarriers for Drug," *Polymers* (*Basel*)., vol. 12, pp. 1–45, 2020.
- [96] "Mathematical models of drug release," Strateg. to Modify Drug Release from Pharm.

- Syst., pp. 63–86, 2015.
- [97] D. R. Paul, "Elaborations on the Higuchi model for drug delivery," *Int. J. Pharm.*, vol. 418, no. 1, pp. 13–17, 2011.
- [98] M. P. Paarakh, P. A. N. I. Jose, C. M. Setty, and G. V Peter, "Release Kinetics Concepts and Applications," *Int. J. Pharm. Res. Technol.*, vol. 8, no. 1, pp. 12–20, 2019.
- [99] A. Parodi, J. Miao, S. M. Soond, M. Rudzińska, and A. A. Zamyatnin, "Albumin nanovectors in cancer therapy and imaging," *Biomolecules*, vol. 9, no. 6, pp. 1–23, 2019.
- [100] J. S. Choi and N. Meghani, "Impact of surface modification in BSA nanoparticles for uptake in cancer cells," *Colloids Surfaces B Biointerfaces*, vol. 145, pp. 653–661, 2016.
- [101] E. Karami, M. Behdani, and F. Kazemi-Lomedasht, "Albumin nanoparticles as nanocarriers for drug delivery: Focusing on antibody and nanobody delivery and albumin-based drugs," *J. Drug Deliv. Sci. Technol.*, vol. 55, p. 101471, 2020.
- [102] A. Bansal, D. Kapoor, R. Kapil, N. Chhabra, and S. Dhawan, "Design and development of paclitaxel-loaded bovine serum albumin nanoparticles for brain targeting," *Acta Pharm.*, vol. 61, no. 2, pp. 141–156, 2011.
- [103] J. Lou *et al.*, "Optimization and evaluation of a thermoresponsive ophthalmic in situ gel containing curcumin-loaded albumin nanoparticles.," *Int. J. Nanomedicine*, vol. 9, pp. 2517–2525, 2014.
- [104] R. R. Kudarha and K. K. Sawant, "Hyaluronic acid conjugated albumin nanoparticles for efficient receptor mediated brain targeted delivery of temozolomide," *J. Drug Deliv. Sci. Technol.*, vol. 61, p. 102129, 2021.
- [105] M. B. St Clair, E. Bermudez, E. A. Gross, B. E. Butterworth, and L. Recio, "Evaluation of the genotoxic potential of glutaraldehyde.," *Environ. Mol. Mutagen.*, vol. 18, no. 2, pp. 113–119, 1991.
- [106] W. Fürst and A. Banerjee, "Release of glutaraldehyde from an albumin-glutaraldehyde tissue adhesive causes significant in vitro and in vivo toxicity.," *Ann. Thorac. Surg.*, vol. 79, no. 5, pp. 1522–8; discussion 1529, May 2005.

- [107] W. Wang, Y. Huang, S. Zhao, T. Shao, and Y. Cheng, "Human serum albumin (HSA) nanoparticles stabilized with intermolecular disulfide bonds," *Chem. Commun.*, vol. 49, no. 22, pp. 2234–2236, 2013.
- [108] G. Ilangovan, H. Li, J. L. Zweier, and P. Kuppusamy, "In vivo measurement of tumor redox environment using EPR spectroscopy.," *Mol. Cell. Biochem.*, vol. 234–235, no. 1–2, pp. 393–398, 2002.
- [109] S. Zhao, W. Wang, Y. Huang, Y. Fu, and Y. Cheng, "Paclitaxel loaded human serum albumin nanoparticles stabilized with intermolecular disulfide bonds," *Med. Chem. Commun.*, vol. 5, no. 11, pp. 1658–1663, 2014.
- [110] A. Martínez, I. Iglesias, R. Lozano, J. M. Teijón, and M. D. Blanco, "Synthesis and characterization of thiolated alginate-albumin nanoparticles stabilized by disulfide bonds. Evaluation as drug delivery systems," *Carbohydr. Polym.*, vol. 83, no. 3, pp. 1311–1321, 2011.
- [111] M. S. Safavi *et al.*, "Reducing agent-free synthesis of curcumin-loaded albumin nanoparticles by self-assembly at room temperature," *Int. J. Pharm.*, vol. 529, no. 1, pp. 303–309, 2017.
- [112] J. H. Lee and A. Nan, "Combination Drug Delivery Approaches in Metastatic Breast Cancer," *J. Drug Deliv.*, vol. 2012, p. 915375, 2012.
- [113] L. Ma, M. Kohli, and A. Smith, "Nanoparticles for Combination Drug Therapy," *ACS Nano*, vol. 7, no. 11, pp. 9518–9525, 2013.
- [114] Y. Feng, N. Li, H. Yin, T. Chen, Q. Yang, and M. Wu, "Thermo- and pH-responsive, Lipid-coated, Mesoporous Silica Nanoparticle-based Dual Drug Delivery System To Improve the Antitumor Effect of Hydrophobic Drugs," *Mol. Pharm.*, vol. 16, no. 1, pp. 422–436, 2019.
- [115] P. Soni, J. Kaur, and K. Tikoo, "Dual drug-loaded paclitaxel-thymoquinone nanoparticles for effective breast cancer therapy," *J. Nanoparticle Res.*, vol. 17, no. 1, 2015.
- [116] S. Talebian *et al.*, "Biopolymers for Antitumor Implantable Drug Delivery Systems: Recent Advances and Future Outlook," *Adv. Mater.*, vol. 30, no. 31, pp. 1–31, 2018.
- [117] F. Davani, M. Alishahi, M. Sabzi, M. Khorram, A. Arastehfar, and K. Zomorodian,

- "Dual drug delivery of vancomycin and imipenem/cilastatin by coaxial nanofibers for treatment of diabetic foot ulcer infections," *Mater. Sci. Eng. C*, vol. 123, p. 111975, 2021.
- [118] P. McClellan and W. J. Landis, "Recent Applications of Coaxial and Emulsion Electrospinning Methods in the Field of Tissue Engineering.," *Biores. Open Access*, vol. 5, no. 1, pp. 212–227, 2016.
- [119] C. Günday *et al.*, "Ciprofloxacin-loaded polymeric nanoparticles incorporated electrospun fibers for drug delivery in tissue engineering applications," *Drug Deliv. Transl. Res.*, vol. 10, no. 3, pp. 706–720, 2020.
- [120] I. H. Ali, I. A. Khalil, and I. M. El-Sherbiny, "Single-Dose Electrospun Nanoparticles-in-Nanofibers Wound Dressings with Enhanced Epithelialization, Collagen Deposition, and Granulation Properties," ACS Appl. Mater. Interfaces, vol. 8, no. 23, pp. 14453–14469, 2016.
- [121] S. Fathollahipour, A. Abouei Mehrizi, A. Ghaee, and M. Koosha, "Electrospinning of PVA/chitosan nanocomposite nanofibers containing gelatin nanoparticles as a dual drug delivery system," *J. Biomed. Mater. Res. Part A*, vol. 103, no. 12, pp. 3852–3862, 2015.
- [122] S. Sydow *et al.*, "Layer-by-layer deposition of chitosan nanoparticles as drug-release coatings for PCL nanofibers," *Biomater. Sci.*, vol. 7, no. 1, pp. 233–246, 2019.
- [123] C. J. Tsao et al., "Electrospun Patch Functionalized with Nanoparticles Allows for Spatiotemporal Release of VEGF and PDGF-BB Promoting in Vivo Neovascularization," ACS Appl. Mater. Interfaces, vol. 10, no. 51, pp. 44344–44353, 2018.